Università degli Studi di Ferrara

DOTTORATO DI RICERCA IN
SCIENZE FARMACEUTICHE

CICLO XXI

COORDINATORE Prof. Stefano Manfredini

NOVEL ANTITUMOR AGENTS STRUCTURALLY RELATED TO AMINOBISPHOSPHONATES AND STILBENES

Settore Scientifico Disciplinare CHIM/08

Dottorando	**Tutore**
Dott. Marco Eleopra	Prof. Daniele Simoni
_____	_____

Anni 2006/2008

Contents

Introduction

Cancer is one of the principal causes of death in the world, and the discover of compounds able to kill selectively the affected cells is the main goal for medicinal chemists. The treatment given for cancer is highly variable and dependent on a number of factors including the type, location and amount of disease and the health status of the patient. The treatments are designed to either directly kill/remove the cancer cells or to lead to their eventual death by depriving them of signals needed for cell division. Other treatments work by stimulating the body's own defenses. The treatments may be divided into different categories based on their goal and mode of action. Often the different types of treatment are used in combination, either simultaneously or sequentially: surgery, radiation, chemotherapy, hormonal treatment, targeted therapy, antibodies, immunotherapy, vaccines.

The research group where I stayed during my PhD have a great and internationally recognized experience in the chemotherapy fields, and in the lastest years was interested in many different projects: stilbene and rethinoids derivatives, antiangiogenic compounds, curcumin analogues, hemiasterlin derivatives.

In this thesis, two research projects are described. The first is the design and synthesis of novel geminal Bisphosphonates to use in the field of immunotherapy; the second is the study of new stilbene relates compounds to enhance the antiproliferative activity of natural compounds, such as Combretastatin and Resveratrol.

Hence, in these projects we focused our attention in the development of new molecules with the aim to discover new potent and no toxic leads to improve anticancer therapy.

1. Bisphosphonates as inductor of γδ T lymphocytes

Geminal bisphosphonates (BPs) are analogues of endogenous pyrophosphate with P-C-P backbone instead of P-O-P motif. This substitution makes BPs resistant to hydrolysis and allows two additional chains of variable structure. The ability of BPs to act with specific molecular targets strictly depends on the BPs structural properties. It is well-known that acid phosphonic groups are essential for bone mineral, for the capacity to chelate calcium ion, which is further increased by the hydroxyl group at side chain on central carbon atom position ("bone hook")[1] (e.g. Zolendronate, etc.)

So far are known three generations of BPs (**Figure 1**): non-N-containing, N-containing, and aromatic N-containing bisphosphonates which differ according to structure and mechanism of action.

Clodronic Acid   Pamidronic Acid   Zoledronic Acid
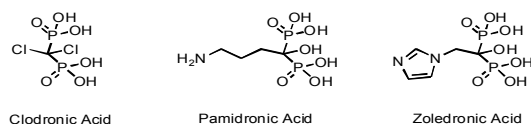
Fig 1. The three generation of Bisphosphonates

The first generation of BPs consists of molecules with an halogens or linear or non-linear alkyl in side chain (e.g. Clodronate). These compounds are very similar to bone tissue and their mechanism of action consists in the accumulation of cytotoxic analogues of ATP in the cells.[2]

The second (e.g. Pamidronate) and third (e.g. Zoledronate) generations consist of compound with linear or cyclic side chain N-containing (N-BPs). The mechanism of

action of these molecules consists in the inhibitions of Farnesyl pyrophosphate synthase, an enzyme in the mevalonate pathway.[3] The introduction of an aromatic N-containing group in side chain (third generation) strongly increases the potency of these products, which are the most used BPs in therapy.[4]

5

1.1 N-containing Bisphosphonates (N-BPs)

Nitrogen-containing bisphosphonates (N-BPs) are important drugs widely used in a variety of bone resorption diseases, such osteoporosis, Paget's disease, and hypercalcemya. Some also have antiparasitic and antibacterial activity[5]. They act by inhibiting the enzyme Farnesyl Pyrophosphate Synthase (FPPS), which plays an important role in the mevalonate pathway and in protein prenylation.

Recently, N-BPs have gained an additional importance as they have shown to inhibit tumor cell adhesion, invasion, and proliferation and to induce apoptosis of a variety of human tumor cell lines in vitro. More importantly, N-BPs also have shown to exhibit direct antitumor activity in vivo by inhibiting cancer growth through antiangiogenic, anti-invasive, and immunomodulatory actions.[6] Although several mechanisms have been proposed to explain the N-BPs' antitumor effect, the inhibition of FPPS surely plays an important role in the reduce prenylation of a variety of proteins with mediator functions in signalling cascades such as Ras2 or Rho. It also results in the accumulation of isoprenoids, such as IPP (isopentenyl pyrophosphate) which induce the expansion of γδ-T cells. Nowadays, there is substantial evidence that γδ-T cells possess potent antitumor activity.

1.13Immunotherapy

Immunotherapy is a modern therapy based on the stimulation of immune system to treat diseases, especially cancer. The enhanced activity of endogenous molecules can be a more efficient and less toxic approach to fight cancer cells.

Classical immunotherapy consists in the use of monoclonal antibodies.[7] Antibodies are a key component of the adaptive immune response, playing a central role in both in the recognition of foreign antigens and the stimulation of an immune response to them. It is not surprising therefore, that many immunotherapeutic approaches involve the use of antibodies. The advent of monoclonal antibody technology has made it possible to raise antibodies against specific antigens such as the unusual antigens that are presented on the surfaces of tumors. A number of therapeutic monoclonal antibodies have been approved for use in humans like Bevacizumab, Alemtuzumab, Cetuximab, Retuximab, used to treat several kind of tumors such as leukaemia, breast, head, neck, colorectal and colon cancer[8].

Radioimmunotherapy involves the use of radioactively conjugated murine antibodies against cellular antigens. Most research currently involved their application to lymphomas, as these are highly radio-sensitive malignancies. To limit radiation exposure, murine antibodies were especially chosen (Ibritumomab tiuxetan, Tositumomab) as their high immunogenicity promotes rapid clearance from the body[9].

The development and testing of second generation immunotherapies are already under way. While antibodies targeted to disease-causing antigens can be effective under certain circumstances, in many cases, their efficacy may be limited by other factors. In the case of cancer tumors, the microenvironment is immunosuppressive, allowing even the tumors that present unusual antigens to survive and flourish in spite of the immune response generated by the cancer patient, against his or her own tumor tissue. Certain members of a group of molecules known as cytokines, such as Interleukin-2 (IL 2) also play a key role in modulating the immune response, and have been tried in conjunction with antibodies in order to generate an even more

devastating immune response against the tumor[10]. While the therapeutic administration of such cytokines may cause systemic inflammation, resulting in serious side effects and toxicity, a new generation of chimeric molecules consisting of an immune-stimulatory cytokine attached to an antibody that targets the cytokine's activity to a specific environment such as a tumor, are able to generate a very effective yet localized immune response against the tumor tissue, destroying the cancer-causing cells without the unwanted side-effects.

In this contest, BPs with an immunostimulatory effect could provide an efficient and no toxic alternative to classical imunotherapies.

8

1.14 Farnesyl Pyrophosphate Synthase (FPPS)

The isoprenoid biosynthetic pathway, with over 23000 metabolites, is unrivaled elsewhere in nature for the chemical diversity of the compounds it produces.

Farnesyl pyrophosphate synthase (FPPS) is a key regulatory enzyme in the mevalonate pathway[11]. This pathway, ubiquitous in mammalian cells, provides essential lipid molecules, such as cholesterol and isoprenoids, with the latter necessary for posttranslational prenylation of small GTPases. In human, Farnesyl pyrophosphate is required for the first committed steps in the biosynthesis of cholesterol, farnesylated proteins, geranylgeranylated proteins, ubiquinones, dolichols, and heme α.[12] FPPS catalyzes the sequential condensation of isopentenyl pyrophosphate (IPP), first with dimethylallyl pyrophosphate (DMAPP) and then with the resultant geranyl pyrophosphate (GPP) to produce the C_{15} farnesyl pyrophosphate (FPP). FPP is a substrate for geranylgeranyl pyrophosphate synthase, which produces the C_{20} isoprenoid geranylgeranyl pyrophosphate (GGPP).

Posttranslational prenylation of small GTPases with FPP or GGPP is crucial for their correct subcellular localization and function.
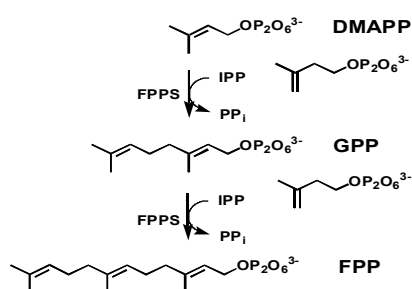
Human FPPS exhibits the all α-helical prenyltransferase fold described earlier for the avian form of FPPS [13]. FPPS is a dimmer with 13 α-helices and connecting loops per subunit (**Figure 2**).
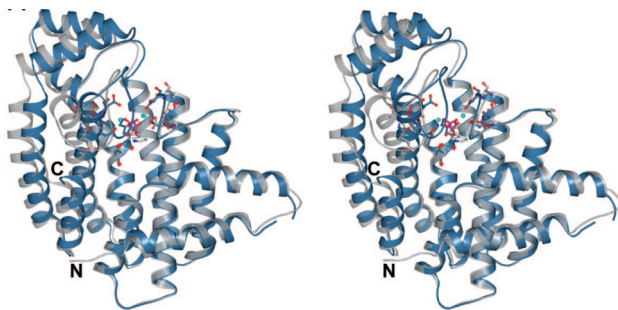
Fig 2. Farnesyl pyrophosphate structure.

Extended loop regions on the top of the protein include those connecting α4–α5 (residues 107–127) and α8–α9 (residues 249–268). A large central cavity located within the helical bundle forms an elongated partly hydrophobic ligand-binding site. The bottom of this cavity is delimited by the side chain of Phe-113. Conserved aspartate-rich motifs found in helices α4 ($_{103}$DDIMD$_{107}$) and α8($_{243}$DDYLD$_{247}$) face the central cavity, and a pronounced kink in helix α7 directs the carbonyl of Lys-200 toward the cavity as well.

It is now clear that FPPS is the major enzyme target of N-BPs, such as risedronate (RIS) and zoledronate (ZOL).

1.4 γδ-T cells

γδ T cells represent a minor subset (5-10%) of human peripheral T cells, differing from αβ T cells in cell surface phenotype, in limited combinatorial diversity TCR, and in human leukocyte antigen-unrestricted antigen recognition. The antigenic molecules that activate γδ T cells are still largely unknown. However, γδ T cells are peculiar in that they do not seem to require antigen processing and MHC presentation of peptide epitopes although some recognize MHC class IB molecules[14]. Furthermore, γδ T cells are believed to have a prominent role in recognition of lipid antigens.

The physiologic function of γδ-T cells remains elusive, though some evidence has been accumulated indicating that γδ-T cells play a role in the "first line of defense" against a broad spectrum of invasive microorganisms such as mycobacteria. In addition, certain hematopoietic tumor cells (eg. Burkitt lymphoma cell line, Daudi or myeloma cell line RPMI 8226) are specifically recognized and lysed by these T cells in vitro. In contrast to αβ-T cells, γδ-T cells (Vγ9Vδ2[+] subset) recognized nonpeptide compounds of low molecular weight (100-600 d) with an essential phosphate residue. So far, only one natural ligand has been isolated and characterized as isopentenyl-pyrophosphate (IPP). However, γδ-T cells exhibit a broad cross-reactivity with a variety of phosphorylated metabolites, such as nucleotidic phosphates, phosphorylated sugars, and synthetic pyrophosphates. The recognition of ubiquitous nonpeptide antigens by γδ-T cells suggest a surveillance function of these T cells for infected or transformed cells. Thus, BPs stimulating γδ T cells could strongly improve their immune response effect against tumor and infective diseases.[15]

Other subsets of γδ-T cells are known as non-Vδ2 T cells and show several differences. The extensive structural diversity of Vδ1 and Vδ3 TCRs and the existence of Vδ1[+] clones reactive against MHC, MHC-like, or non-MHC molecules suggest recognition of a highly diverse and heterogeneous set of antigens by non-

Vδ2 cells, although cognate interactions between non-Vδ2 TCRs and any of these antigens have not been shown yet. MHC class-I-chain-related gene A (MICA) has also been proposed as an important tumor antigen recognized by Vδ1$^+$ T cells. However, the very low affinity of MICA–Vδ1 TCR interactions estimated by surface plasmon resonance analyses raises doubts about the functional relevance of MICA or MHC class-I-chain-related gene B (MICB) recognition by Vδ1$^+$ TCRs. Non-Vδ2 γδ T cells are expanded in various infectious contexts involving intracellular bacteria (Mycobacteria and Listeria) as well as extracellular bacteria, such as *Borrelia burgdorferi* and viruses (HIV, cytomegalovirus). In most instances, the stimuli that trigger Vδ1 expansion are not derived from pathogens but instead correspond to endogenous gene products presumably upregulated on infection. The antigens recognized by non-Vδ2 T cells expanded in the above infectious contexts have not been characterized, but the fact that Vδ1$^+$ T-cell responses are not blocked by monoclonal antibody directed against known classical or non-classical MHC molecules suggests recognition of a new class of conserved stress-induced antigens.

1.5. Mechanism of action

Bisphosphonates, in particular nitrogen-containing compounds, are importantly drugs widely used in a variety of bone resorption diseases, such as osteoporosis, Paget's disease, and hypercalcemia. Some also have antiparasitic and antibacterial activity.

Geminal bisphosphonates are divided in three generations under structure and mechanism of action.

The first generation of BPs have an halogen or linear/cyclic alkyl on the side chain and act by accumulating a toxic analogue of adenosine triphosphate. The resulting metabolites contained the P—C—P moiety in place of the β,γ phosphate groups of ATP, thus resulting in nonhydrolyzable analogs.

The second and especially the third generation, nitrogen-containing bisphosphonates (N-BPs), act by inhibiting the FPPS. The catalytic site of the enzyme consists of a large central cavity formed by mostly antiparallel R-helices with two aspartate-rich regions (DDXX(XX)D) located on opposite walls. The aspartates mediate the binding of prenyl phosphates to the protein via bridging three Mg^{2+} ions. On the basis of crystallographic and kinetic evidence, two types of mechanisms have been proposed, those in which condensation is initiated by heterolytic cleavage of the carbon-oxygen bond of the allylic pyrophosphate, yielding a cationic intermediate, and those where the formation of the Cl-C4 bond between the two substrates and rupture of the C1-oxygen bond is simultaneous through a transition state (TS) with a carbocation character (**Figure 3**). Three conserved residues among different species, Thr203, Gln241, and Lys202 have been proposed to stabilize the possible carbocation intermediate or transition state.
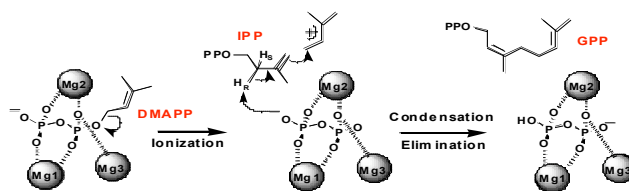
Fig 3. Mechanism of action of N-BPs.

Indeed, the protonated-nitrogen forms of N-BPs closely resemble the cationic transition state/reactive intermediate formed during the FPPS catalytic state. This inhibition results in the reduced prenylation of a variety of proteins with mediator functions in signaling cascades such as Ras2 or Rho. It also results in the accumulation of isoprenoids, such as IPP (isopentenyl pyrophosphate), which is the only natural ligand isolated inducing expansion of $\gamma\delta$ T cells. Different biological studies have demonstrated that $\gamma\delta$ T cells are effective against different types of cancer such as melanomas, renal carcinoma, lymphoma, and multiple myeloma. Thus, $\gamma\delta$ T cells, or $\gamma\delta$ T cells agonists, such as N-BPs, could play a major role in controlling human malignancy and could be used therapeutically in combination with other anticancer agents. Indeed, clinical studies have recently shown that adding immune therapy to classical chemotherapy has survival benefits when compared to chemotherapy alone. There is, therefore, major interest in the development of novel N-BPs as new promising anticancer agents.

14

1.6. Novel Aminobisphosphonates

Bisphosphonates are the treatment of choice for diseases that involve excessive bone resorption and have been shown to be effective in preventing osteolytic bone disease in several different malignancies, including multiple myeloma (MM). Recent animal studies have shown that the aminobisphosphonates also have potent antiangiogenic activity that may contribute to these drugs' antibone resorptive effect as well as provide additional mechanism by which these drugs may have antimyeloma effects as well.

These drugs were shown to induce expansion of Vγ9Vδ2 T cells in peripheral blood mononuclear cell cultures and enhance cytotoxicity of malignant plasma cells in bone marrow cultures by these Vγ9Vδ2 T lymphocytes. Thus, there is increasing evidence that N-BPs can lead direct and indirect effects that result not only in less bone loss but also in less tumor mass.

Confirm this, Wilhem et al. reported of a pilot study of low-dose of interleukin-2 (IL-2) in combination with pamidronate in patients with low-grade non-Hodgkin lymphoma or multiple myeloma.[16] They selected 9 patients by positive in vitro proliferation of Vγ9Vδ2 T cells in response to pamidronate and IL-2, and show that 5 of the patients had significant in vivo activation/proliferation of Vγ9Vδ2 T cells. Three patients also achieved objective response, indicating that Vγ9Vδ2 T cells might contribute to this antilymphoma effect.

Some of use reported another pilot study of low-dose zoledronic acid in 9 cancer patients with bone metastases (3 females affected by breast cancer, 6 males affected by prostate cancer; median age, 66 years (54-83 years)[17]. The aim of this study was to evaluate the activity of zoledronic acid (the most representative N-BPs in therapy) on identified subsets of Vγ9Vδ2 T cells that display different functional activities: $CD45RA^+CD27^+$,$CD45RA^-CD27^+$ and $CD45RA^-CD27^-$. The first and the second subset, respectively naive and memory cells, strongly proliferate but lack immediate effector functions; $CD45RA^-CD27^-$, instead, proliferate poorly but produce interferon γ (INFγ) and exert cytotoxicity. Both of these functions are strictly

involved in their antitumor efficacy. Patients were treated with 4 mg of zoledronic acid via 15-minute intravenous infusion every 3 weeks. Peripheral blood mononuclear cells (PMBC) were collected before treatment (time 0) and 1 month (time 1) and 3 months (time 2) after this administration. The experiment showed that zoledronic acid was able as IPP to stimulate Vγ9Vδ2 T cells upon culture in vitro in presence of IL2. Treatment with zoledronic acid caused a decrease in the percentage of naive and memory cells compared with the control: in the treated cells the percentage of these two subsets was 10% of the whole Vγ9Vδ2 population, while in control cell was 70%. The decrease in the percentage of these subsets was accompanied by increase of the effector subset, which accounted about 80% of the whole Vγ9Vδ2 population after 3 months from the initial treatment with zoledronic acid. These results indicated that zoledronic acid in vivo expands the effector subset while decreasing the naive and memory subsets with the consequent increase of the release of IFNγ and effective antitumor response.

With these results and consideration in hand we thought to design and synthesize a novel class of nitrogen-containing bisphosphonates with the aim to increase the immunomodulatory and the antitumoral properties of these compounds.
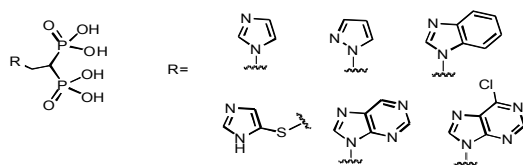
Fig 4. Structure of new N-BPs synthesized.

Since zoledronic acid had shown excellent evidences of its properties as Vγ9Vδ2 T cells activator and since the administration of zoledronate together IL2 represent a

16

novel, safe, and feasible approach to inducing immunological responses in patients with metastatic carcinomas, we thought to develop our new molecules structurally related to zoledronic acid. Specifically, we synthesized a small series of new dehydroxy-aminobisphosphonates (**Figure 4**), to verify if the absence of the OH group on the central carbon atom were indispensable for biological activity, and if these new compounds had less affinity for the bone tissue and were more bioavailable.

1.7 Chemistry

Bisphosphonates are known by several years, and in literature there are different synthesis for the preparation of the various type of compounds (eg. alkylic, cyclic, linear, amino, thio-BPs)[18].

For the preparation of our compounds we used a simple and efficient synthetic route as shown in **Scheme 1**. A common starting material, the methylenebisphosphonate **2**, react with the proper heterocyclic nucleophile **a-f** in THF at reflux. TBD (1,5,7-triazabicyclo[4.4.0]dec-5-ene) was used as catalyst, but experimental proofs demonstrated that the reaction occurs also without the base in good yields. Additionally, bisphosphonate derivatives were also prepared heating the solution at 120°C in a scientific microwave oven for 10 min. The starting material **2** was prepared treating paraformaldehyde with diethylamine, and then with commercial tetraethyl methylenebisphosphonate **1**. The bisphosphonate acid derivatives **4a-f** were obtained, starting from the correspondent tetraethyl ester **3a-f**, by hydrolysis with hydrochloric acid or with iodotrimethylsilane.
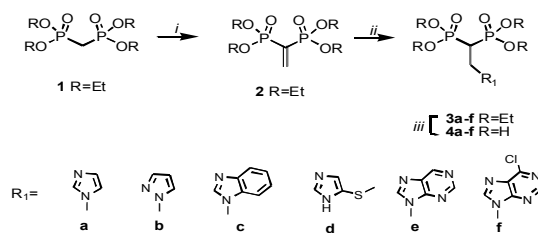
Scheme 1. Reagent and conditions: (i) Et$_2$NH, (CHO)n, pTSA; (ii) Het(a-f), TBD or not; (iii) HCl conc.or TMSI.

18

Interesting, compounds 6e-6f, could be in two regioisomeric forms. To establish if the reaction was regioselective, and the ratio of the two isomers, these compounds had been fully studied by means of NMR techniques by the Department of Analytical Chemistry at GlaxoSmithKline in Verona (Italy).
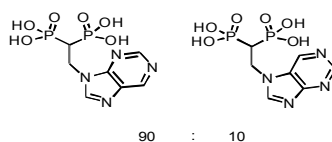

90 : 10

Fig 5. Two regioisomers ratio.

Peaks assignments were achieved for both isomers, directly on the 90:10 mixture, using gHMQC and gHMBC experiments, while gROESY experiments allowed the determination of the chain position (**Figure 5**).

19

1.8. Molecular modeling

To design novel compounds, to understand their structure-activity relationship (SAR) and confirm their mechanism of action, we conducted some molecular modeling studies in collaboration with the Università degli Studi di Napoli Federico II (Napoli, Italy).

In last years, several molecular modeling works had published, about the FPPS, its catalytic site, and the interactions of more important BPs, such zoledronate and risedronate, with the enzyme.

Oldfield et al. identified some indispensable features for the activity of BPs on FPPS catalytic site: hydrophobic, aromatic, and cationic moieties, together two metal-binding groups are very important for a bisphosphonate with antitumor activity.[19]

We also began with the knowledge of how our lead (zoledronate) binds to the FPPS catalytic site. In analyzing the details of the interactions between zoledronate and the FPPS catalytic site (PDB codes of the X-ray structures: 1ZW5, 2F8Z, 2F9K), it emerges that the two phosphonate groups are highly important for the binding of zoledronate to the enzyme. The phosphonate groups in N-BPs coordinate via Mg ions with the aspartate-rich motifs of the enzyme, which are associated with binding the pyrophosphate groups of the allylic (DMAP/GPP) substrate. The loss of these interactions either by removal or replacement of a phosphonate with other groups leads a huge loss in potency and a total abrogation of the ability to hold the enzyme-inhibitor in an isomerized state. The anchoring of the bisphosphonate in the active site by the magnesium-dependent aspartate-phosphonate interaction is thus a vital component in the inhibitor binding and the subsequent isomerisation of the enzyme-inhibitor complex.

Even the imidazole moiety of zoledronate plays an important role in the binding to the enzyme (**Figure 6**). Indeed, the imidazole in its protonated state mimics the carbocation intermediate formed during the catalysis, and the protonated

20

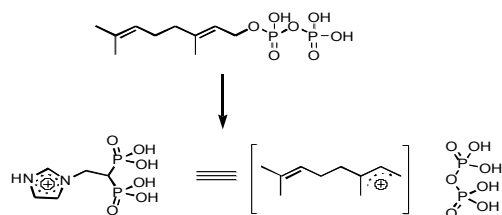nitrogen makes a double H-bond with the Lys200 carbonyl oxygen and the Thr201 side chain (Oγ1).

Fig 6. The protonated state of imidazole mimics the carbocation intermediate in catalytic site.

As a consequence, the only group that could be substituted without a dramatic decrease of the FPPS inhibition would be the 1-OH group, which, in the binary complex FPPS-zoledronate, forms a water-mediated interaction with Gln240 and is also in close proximity to Asp243, which coordinates with magnesium. In previous work[ref], has been shown that the absence of the hydroxyl group at R_1 would therefore appear to initially make the N-BPs better competitive inhibitors, able to fit into the open active site more easily. Invariably, the N-BPs with a hydroxyl are the better final inhibitors, which suggests that interactions perhaps mediated by the hydroxyl further stabilize the isomerized state. Also, inspection of the FPPS/ZOL-IPP crystal structure suggests that the presence of the hydroxyl group may prove the packing with IPP and that compounds lacking a hydroxyl may form a looser ternary complex (eg., would be destabilized).

To test our hypothesis, we performed molecular docking studies of zoledronate and 1-deshydroxyzoledronate **4a** using the FPPS (PDB code: 2F8Z) as receptor (**Figure 7**).
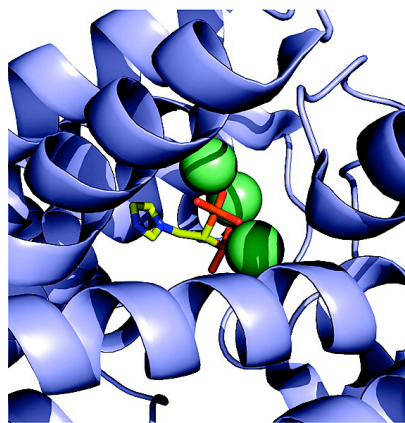
Fig 7. Docking simulation of compound **4a**

As expected, docking calculations provided a binding mode of **4a** largely overlapping with that of zoledronate. Furthermore, the computed binding free energy of **4a**, -10.8 kcal/mol, is comparable to that of zoledronate, -9.8 kcal/mol, within the statistical error of the algorithm used for docking. The only difference in the binding mode of **4a** with respect to zoledronate resides in the lack of the interaction established by the hydroxyl group, which is absent in our compound.

If the removal of the C1 hydroxyl group does not substantially influence the inhibition of FPPS, it have an important effect of BPs activity in vitro, and especially in vivo. In fact, removal of this group should reduce the bone and the skeletal retention and should increase exposure of the drug in the peripheral blood and in the soft tissue with an increase in the in vitro/vivo antitumor activity.

22

1.9. Biological Results

The goal of this work is to develop a new series of N-BPs with less bone affinity and an increase of efficacy as inductors of γδ T cells compared to bisphosphonates drugs in therapy. As seeing above, this stimulation, improving the CD45RA⁻CD27⁻ subset of Vγ9Vδ2 T cells, can increase the concentration in circulating system of IFNγ improving the response of these lymphocytes to infections and cancer. Indeed, these bioactive compounds can used in immunotherapy, a modern and very important branch of antitumor therapy.

All the synthesized compounds have been tested in a preliminary assay for their in vitro bioactivity toward activation-expansion of γδ T lymphocytes. The capacity of bisphosphonates to activate, in vitro, human γδ T lymphocytes was studied in comparison to zoledronic acid and phosphostim (**3**), the bromohydrin derivative of isopentenyl pyrophosphate, which strongly activates γδ T lymphocytes.

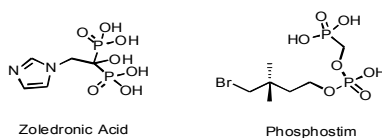**Fig 8**. Zoledronic acid and Phosphostim are strong γδ T lymphocytes activators.

Firstly, we conducted a typical dose-response experiment out of seven in which peripheral blood mononuclear cells were stimulated in vitro with different concentrations of compounds and low doses of IL2 for 7 days. The expansion of γδ T cells was calculated and expressed as an expansion factor.

At first glance, it is evident that the activity of the compounds is strongly influenced by the nitrogens positions in aromatic system. In fact, compound **4b** results about 5000 times less active that **6a.** This is completely in line with the theory that protonable nitrogen must have a certain distance to geminal carbon atom to properly mimic the transition state in the FPPS catalytic cycle (**Figure 9**).
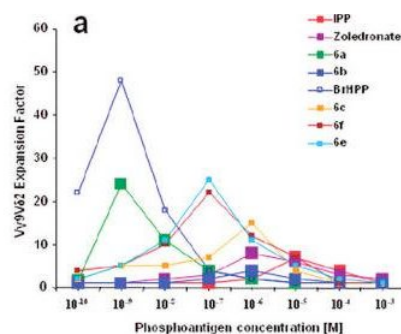
Fig 9. Ability of different N-BPs derivatives to expand in vitro human $\gamma\delta$ T cells. Peripheral blood mononuclear cells were incubated in vitro with different N-BPs derivatives at the indicated final concentrations and 20 U/mL final concentration of rIL-2, for 7 days at 37 °C. At the end of the incubation period, cells were collected and the $\gamma\delta$ T cell expansion factor calculated as described in Experimental Section.

In the in vitro FPPS assay, test conducted at the University of Oxford, it becomes apparent that the movement of the nitrogen away by the position in zoledronate caused a large decrease in potency. Furthermore, the basicity of the nitrogens present in the ring also plays a pivotal role in determining the different pharmacological profiles of the compounds under study, influencing their strength of binding to the enzyme as well as their ability to pass through the cellular membrane. In fact, from the enzyme inhibition assays (**Table 1**), it clearly emerges that compounds presenting a more basic nitrogen such as **4a**, **4c**, and **4d**, show lower IC50 values. This is probably due to a stronger interaction of the protonable nitrogen with the nearby Lys200 and Thr201.

24

Compounds	$IC_{50} \pm SEM$ (nm)
Zoledronate	4.1 ± 0.22[29]
4a	9.03 ± 1.8
4b	3069 ± 264
4c	16.1 ± 1.4
4d	28.1 ± 2.8
4e	388.2 ± 16.2
4f	883.1 ± 71.9

Table 1. In vitro activity of new N-BPs compared to zoledronate on human FPPS.

However, although the introduction of the purine system in the compounds **4e,f**, decreases by-around 500 folds the affinity to the enzyme, but the activity on the induction of Vγ9Vδ2 T cells is similar to zoledronic acid. These results suggest that the introduction of the more lipophilic substituent on the side chain, even if decrease the potency to inhibit FPPS of studied N-BPs, enhance their ability to pass cell membrane (**Table 2**).

Compounds	T lymphocytes stimulation (μM)
BrHPP	0.015-0.001
IPP	1-3
Zoledronate	0.1-0.3
4a	0.001-0.003
4b	>10
4c	1-2
4d	>10
4e	0.2-0.4
4f	0.1-0.3

Table 2. Vγ9Vδ2 T cells stimulation.

However, as summarized in **Table 2**, the most surprising finding is that the deshydroxyzoledronate **4a** is approximately 100 times more capable of activating γδ T lymphocytes with respect to zoledronate, considering that the IC50 for FPPS inhibition for **4a** is twice that of zoledronate (**Table 1**). In fact, derivative **4a** was extremely active in inducing activation of human γδ T lymphocytes upon culture of peripheral blood mononuclear cells (PBMC) in the presence of a low dose (20 U/mL final concentration) of interleukin (IL)-2. Dose response analysis revealed that optimal stimulation and expansion of human γδ T cells occurs at the final concentration of 1 nM. In addition, **4a** produced a phenotypic switch from naive and central memory to effector memory cells, the latter exerting important effector functions (such as production of TNF-R and IFNγ and cytotoxicity) against tumor cell lines in vitro (data not shown).

By these experiments, we can defined the mechanism of action of compound **4a**. In fact, from our initial studies in vitro, we found that activity of compound **4a** in PMBC cellular line, in association with IL2, was blocked by the presence of Mevastatin or Lovastatin (**Figure 10**).
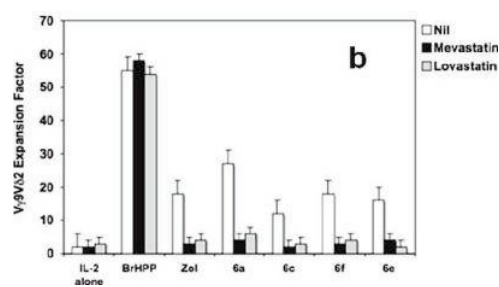

Fig 10. Mechanism of action of different N-BPs derivatives on human γδ T cell activation. expansion in vitro of γδ T cells was carried out in the presence or absence of mevastatin or lovastatin, both used at 1 μM final concentration.

26

In addition, when the above-described in vitro assay is carried out with PBMCs depleted of monocytes, the drugs' effects again disappear (data not shown). With these results in hand, we can indicate that compound **4a** don't stimulate directly γδ T cells, acting on lymphocytes receptors, but it inhibit the FPPS of macrophages and monocytes, that, accumulating and releasing substrates as IPP, induce proliferation of Vγ9Vδ2 T cells effector subset and enhance antitumor response. Indeed, compound **4a** act as a "third generation" bisphosphonate, although it proved considerably more potent that zoledronic acid, the most studied and potent N-BP today in therapy.

To gain better the antitumor activity of our compound **4a**, we further investigated the antiapoptotic activity on different cell lines and its toxicity on normal and bone marrow-derived hematopoietic cells.

The cytotoxic activity of **4a** and of zoledronate was tested on the HUT78 (human T-lymphoma), K562 (chronic myeloid leukemia expressing the antiapoptotic oncogene Bcr-Abl), CCRF-CEM (acute lymphoblastic), CCRFCEM VBL300 (P-glycoprotein, multiple drug resistant (MDR) protein expressing acute lymphoblastic) cell lines.

As shows in **Figure 11** our compound **4a** was endowed with antiproliferative effects and pro-apoptotic activity higher than that of zoledronic acid in both human lymphoma HUT78 cells and P-glycoprotein expressing CCRF-CEM VBL300, while no significant differences were observed in K562 and CCRF-CEM cells.
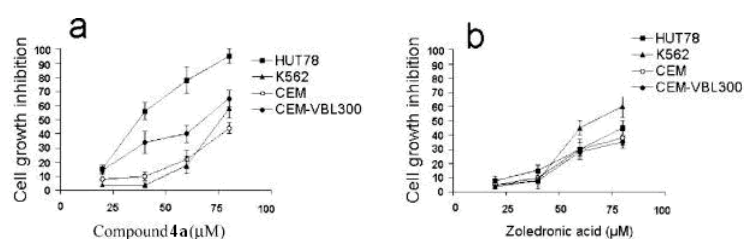

Fig 11. (a) Cell growth inhibition induced by different concentration of compound **4a**. (b) Cell growth inhibition induced by different concentration of zoledronic acid.

27

Moreover, in **Table 3**, we can see the higher proapoptotic activity of **4a** in HUT78 and CCRF-CEM VBL300 cells, compares to zoledronic acid. We can also note that compound **4a** was more active than zoledronic acid in the MDRexpressing cells than in the parental CCRF-CEM line. As shown in **Figure 11a,b** and **Table 3**, zoledronic acid and **4a** were barely active on Bcr-Abl, expressing K562 cells when used at concentrations lower than 50 μM.

Cells	4a	Zoledronate
HUT78	40 ± 5.3	24 ± 4.6
K562	15 ± 3.2	16 ± 5.1
CEM	22 ± 3.1	20 ± 4.4
CEMVBL300	37 ± 6.0	22 ± 3.2
CFU-GM	15 ± 2.2	18 ± 2.7

Table 3. Percentage (±SE=standard error) of Apoptosis Induced by 100 μM compound **4a** and 100 μM Zoledronic Acid.

Recent reports indicated that Imatinib mesilate (Gleevec), the reference compound for anticancer studies, have a synergistic effect in association to zoledronic acid on Bcr-Abl expressing cells.[20] With these results in hand, we though to investigate if our compound **4a** keep this activity. K562 cells were exposed to different concentrations of imatinib in combination with 30 μM **4a** or zoledronic acid. We was pleasantly affected to see that activity of combination of Imatinib with our bisphosphonate was higher than combination with zoledronic acid.

28
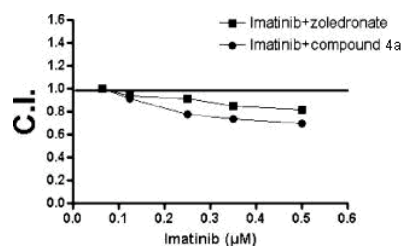
Fig 12. Effects of imatinib-zoledronic acid and imatinib-compound **6a** combinations in K562 cells. Cells were incubated with 30 μM zoledronic acid or 30 μM compound **6a** in combination with concentrations of imatinib ranging from 0.065 to 0.5 μM. After 48 h, the number of living cells was determined and expressed as percentage of control.

Additionally, we tested compound 6a and zoledronic acid on normal hematopoietic cells CFU-GM proving their absence of toxicity (**Figure 13**).
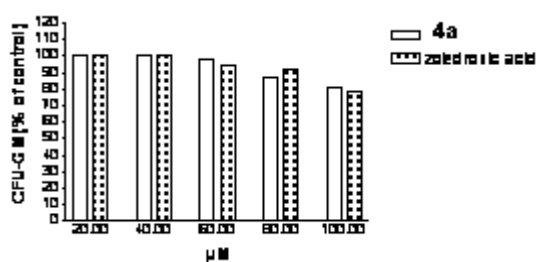
Fig 13. Cytotoxic concentrations of 6a and zoledronic acid don't change the number of CFU-GM.

With these good results in hand, we decided to test the antitumor effect of **4a** in vivo. We investigated the in vivo tumor reactivity of human γδ T cells activated and expanded in vitro and then adoptively transferred into SCID mice, according to the experimental protocol described by Kabelitz et al.,[21]analyzing the optimal therapeutic efficacy against the breast cancer BT459 cell line. SCID mice were conditioned by irradiation and antiasialo-GM1 monoclonal antibody treatment, and received at day 0 a single intraperitoneal injection of the breast cancer cell line

BT549 (2 × 106/mouse). The high numbers of tumor cells were inoculated to allow for fully fledged tumor growth within the period before graft-vs-host reactions developed in the SCID mouse reconstituted with human lymphocytes. Mice received concomitantly, with the tumor cells, an intraperitoneal injection of human recombinant (r)IL-2 (300 ng), or 6a (2 μg), or zoledronate (5 μg), or **4a** (2 μg) plus rIL-2 (300 ng), or zoledronate (5 μg) plus rIL-2 (300 ng). In addition, mice received highly purified human γδ T cells (2 × 107/mouse) where indicated. γδ T cells (2 × 107/mouse) and zoledronate (5 μg), or **6a** (2 μg), were injected every 15 days, while (r)IL-2 (300 ng) was given on the same day and at 3 and 6 days after each injection of γδ T cells.
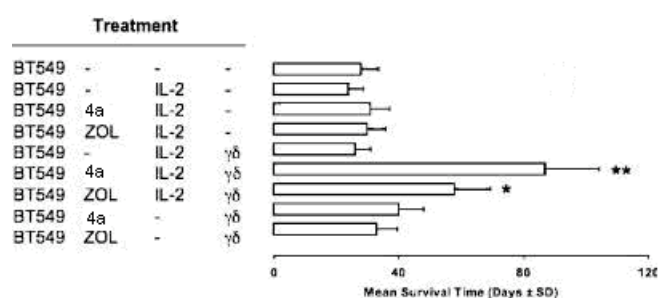
Fig 14. Antitumor effect of **4a** and γδ T cells in SCID mice in vivo. SCID mice received a single intraperitoneal injection of the breast cancer cell line BT549. Mice concomitantlyreceived with the tumor cells an intraperitoneal injection of human recombinant (r)IL-2, or **4a**, or zoledronate, or **4a** plus rIL-2, or zoledronate plus rIL-2. Where indicated, mice received highly purified human γδ T cells.

As shown in **Figure 14**, neither compound **4a** nor zoledronic acid or IL 2 alone or in combination increase survival time of the mice. This increase when γδ T cells were given in association with **4a** but not with zoledronic acid or IL 2, however, the improvement of survival is not statistically relevant (40 ± 10 versus 28 ± 6). The best result was obtained when compound **4a** was given together γδ cells and IL2, and compares to zoledronic acid in the same association, the increase of survival

time was statistically significant ($p < 0.05$), indicating that **4a** is more potent than zoledronate in activating and sustaining the antitumor activity of human γδ T cells.

1.10. Conclusions

In this work, we have synthesized a small series of novel geminal bisphosphonates with the aim to develop new leads for immunotherapy against cancer.

Recent data literature showed that N-bisphosphonates, drugs commonly used in bone and calcium-correlate diseases for their antiresorptive effect, had an stimulating effect on γδ T cells. These lymphocytes subset plays an important role in natural immunomodulatory response to infections and, in particular, cancer. To confirm this N-BPs activity, recent in vivo tests demonstrated that zoledronic acid, the most used N-bisphosphonate, is able to enhance the effector γδ T cells subset and, as consequence, their activity.

Starting by these results we synthesized our compounds with the aim to increase the immunomodulatory effect and, at the same time, to decrease their bone affinity. Our synthetic strategy, based on molecular modelling studies, focused on elimination of the hydroxyl moiety on central C carbon and insertion of an N-aromatic cyclic side chain.

Hence, our small N-BPs set was tested for its in vitro and in vivo activity. Interestingly, one of our compounds, simply the deshydroxy-zoledronic acid (**4a**) showed very exciting results compares to zoledronic acid. In fact, although **4a** is less affine to target enzyme farnesyl pyrophosphate synthase, demonstrated better γδ T cells induction, better cells growth inhibition and apoptotic affect itself and in association with Imatinib mesylate (Gleevec), than zoledronic acid. Probably, it is due by the absence of the hydroxyl moiety that give zoledronic acid more able to interact with FPPS and bone tissue, but at the same time less disposable to peripheral blood and soft tissues.

Also in vivo tests was very interesting, showing that **4a**, more than zoledronic acid, in association with γδ T cells and IL 2, sensibly enhance the survival time of mice after injection of cancer cells. Finally, these very good biological results are followed by an important absence of toxicity on normal hematopoietic cells at cytotoxic concentration.

32

Thus, taking into account of the unique pharmacological profile of **4a**, with a potent γδ T cells activation, a remarkable proapoptotic effect both in vitro and in vivo and an absolute absence of toxicity, it may be a very interesting anti-cancer drug which can be added to immuno-chemotherapy against a wide range of tumor types.

1.11. Experimental Section

Molecular Modeling. Docking Simulations.

Molecular docking of zoledronate and **6a** into the three-dimensional X-ray structure of FPPS (PDB code: 2F8Z) was carried out using the AutoDock software package (version 4.0) as implemented through the graphical user interface AutoDockTools (ADT 1.4.6).[20]

Ligands and Protein Setup.

The structures of the inhibitors were first generated from the standard fragment library of the SYBYL software version 7.3.[21] The docking parametrization of ligands, the cofactor isopentenyl pyrophosphate (IPP), and the region of the enzyme including the metals and its coordinating ligands (Mg subsite) were performed by using the Gaussian03 package[22] by applying a full geometry optimization at Hartree-Fock level of theory and then calculating the charges using the restrained electrostatic potential (RESP) fitting procedure.[23,24] For both the optimization and the electrostatic potential (ESP) calculation, the locally dense 6-31G* basis set was used. The starting geometry of the Mg subsite for ab initio calculations was derived by a crystallographic template (PDB code: 2F8Z) including the cocrystallized zoledronic acid necessary to get an octahedral coordination of the ions. We treated the three magnesium as ions in the +2 oxidation state and with a low spin state (S) 0). To properly describe the electrostatic protein environment, the N and C termini of the coordinating aspartates were capped with NME and ACE residues, respectively. Hence, the system was geometrically optimized by constraining the atoms of the backbone of the aspartates and using the previously reported locally dense basis set. The model system was then optimized until reaching the default Gaussian03 convergence criterion. The RESP charges were then calculated on the geometrically minimized ligands, cofactor, and Mg subsite. First, the ESP were calculated again by means of the Gaussian package and then the RESP charges were obtained by a two-stages fitting procedure,[25] fitting first the polar areas by using

34

weak hyperbolic restraints (0.0005 au) and then fitting the remaining areas, imposing equivalencies, and by using a stronger hyperbolic restraint (0.001 au). In each step, the charges of the standard residues ACE and NME were constrained to their AMBER force field value.25 The electrostatic potential used as an input by the RESP program was sampled by adapting the Merz-Singh-Kollman scheme,26 namely using 10 concentric layers at the default level of spacing, a surface density of 6 points/Å2, and adopting the covalent radius of 0.86 Å for magnesium as reported on the WebElements server (Winter M. WebElements Periodic Table; United Kingdom: University of Sheffield. http://www.webelements.com/). Hence, the computed charges for ligands, cofactor, and Mg subsite were used for further docking calculations.

Docking Setup.

The docking area has been defined by a box, centered on the mass center of the cocrystallized zoledronate. Grids points of $40 \times 40 \times 40$ with 0.375 Å spacing were calculated around the docking area for all the ligand atom types using AutoGrid4. For each ligand, 100 separate docking calculations were performed. Each docking calculation consisted of 2.5×106 energy evaluations using the Lamarckian genetic algorithm local search (GALS) method. A low-frequency local search according to the method of Solis and Wets was applied to docking trials to ensure that the final solution represents a local minimum. Each docking run was performed with a population size of 150, and 300 rounds of Solis and Wets local search were applied with a probability of 0.06. A mutation rate of 0.02 and a crossover rate of 0.8 were used to generate new docking trials for subsequent generations. The GALS method evaluates a population of possible docking solutions and propagates the most successful individuals from each generation into the next one. The docking results from each of the 100 calculations were clustered on the basis of root-mean square deviation (rmsd) 1.5 Å) between the Cartesian coordinates of the ligand atoms and were ranked on the basis of the free energy of binding.

Chemistry.

General Methods and Materials.

Melting points were obtained in open capillary tubes and are uncorrected. Reactions and product mixtures were routinely monitored by thin-layer chromatography (TLC) on Merck silica gel precoated F254 plates. Nuclear magnetic resonance (^{1}H NMR, ^{13}C NMR) spectra were determined in CDCl$_3$ solution unless otherwise indicated with a Bruker AC-200 or with Varian Mercury Plus 400 spectrometer, and peak positions are given in parts per million downfield from tetramethylsilane as the internal standard; J values are expressed in hertz. Compound **4a** has been studied using a Varian Inova 600 MHz spectrometer in D$_2$O solution. Light petroleum ether refers to the 40-60 °C boiling range fractions. Column chromatography was performed with Merck 60-200 mesh silica gel. All drying operations were performed over anhydrous sodium sulphate. Column chromatography (medium pressure) was carried out using the "flash" technique. Microanalysis of all new synthesized compounds agreed within ±0.4% of calculated values. The microwave reactions were performed in a Discover CEM, which produced controlled irradiation with a power of 0-300 W.

Tetraethyl-ethenylidenebisphosphonate. (2). Paraformaldehyde (520 mg, 17.3 mmol) and diethyl amine (0.36 mL, 3.46 mmol) were combined in 10 mL of methanol, warmed until clear, then treated with tetraethylmethylene bisphosphonate (0.86 mL, 3.46 mmol) and refluxed for 18 h. The mixture was concentrated in vacuo, toluene was then added, and the solvent was evaporated again (2 × 5 mL). The residue was dissolved in toluene (20 mL), treated with p-toluensulphonic acid (cat.), and refluxed through a Dean-Stark trap for 18 h. The sample was concentrated in vacuo, dissolved in chloroform (20 mL), washed with water (10 mL), dried, and concentrated in vacuo. The residue oil was used without further purifications for the next reaction. Yellow oil; yield: 90%.

^{1}H NMR δ: 1.17 (t, J=7.2, 12H), 3.90-4.03 (m, 8H), 6.63 (s, 1H), 6.70 (d, J=38, 1H), 7.10 (d, J=38, 1H).^{13}C NMR δ: 14.5, 62.4, 121.8, 148.2.

General Procedures for the Synthesis of Tetraethyl Bisphosphonate 3a-f.

Method A. A solution of compounds **a-f** (0.66 mmol) and **2** (200 mg, 0.66 mmol) in THF (10 mL) was kept in a microwave vial and heated to 150-160 °C for 15 min in a scientific microwave oven. After cooling at room temperature, the solvent was evaporated in vacuo, the crude material was dissolved in water (10 mL) and extracted with dichloromethane (2 × 15 mL). The organic layers were collected, dried, filtered, and evaporated. The crude material was purified by flash chromatography on silica gel with dichloromethane-methanol as eluent.

Method B. A mixture of compounds **a-f** (0.66 mmol), **2** (200 mg, 0.66 mmol), and TBD (88 mg, 0.066 mmol) in THF (15 mL) was stirred under reflux for 4 h, the solvent was evaporated in vacuo, and the crude material was dissolved in water (10 mL) and extracted with dichloromethane (2 × 10 mL). The organic layers were collected, dried, filtered, and evaporated. The crude material was purified by flash chromatography on silica gel with dichloromethane- methanol as eluent.

Tetraethyl-[2-(imidazol-1-yl)ethyl]-bisphosphonate (3a). Yield 90%; yellow oil. ^{1}H NMR δ 1.25-1.34 (m, 12H), 2.40-2.85 (m, 1H), 4.05-4.21 (m, 8H), 4.41-4.59 (m, 2H), 6.90 (s, 1H), 7.21 (s, 1H), 7.57 (s, 1H). ^{13}C NMR δ 13.4, 45.3, 48.2, 61.3, 121.7, 126.9, 141.6.

Tetraethyl-[2-(pyrazol-1-yl)ethyl]-bisphosphonate (3b). Yield 79%; yellow oil. ^{1}H NMR δ 1.25-1.32 (m, 12H), 3.16-3.43 (m, 1H), 4.02-4.20 (m, 8H), 4.56-4.73 (m, 2H), 6.17-6.19 (m, 1H), 7.48 (d, J=2.0, 1H), 7.52 (d, J =2.0, 1H). ^{13}C NMR: δ 16.4, 30.5, 33.8, 37.0, 46.0, 60.4, 105.1, 126.6, 138.8.

Tetraethyl-[2-(benzoimidazol-1-yl)ethyl]-bisphosphonate (3c). Yield 71%; yellow oil. ^{1}H NMR δ 1.20-1.33 (m, 12H), 2.45-2.80 (m, 1H), 4.08-4.20 (m, 8H), 4.45-4.60 (m, 2H), 7.30-7.42 (m, 2H), 7.83-7.98 (m, 2H), 8.90 (s, 1H). ^{13}C NMR δ 13.2, 25.3, 34.0, 65.3, 118.4, 125.9, 143.9, 151.5.

Tetraethyl-[2-(imidazol-2-yl-thio)ethyl]-bisphosphonate (3d). Yield 45%; yellow oil. ^{1}H NMR δ 1.24-1.34 (m, 12H), 3.80-3.91 (m, 1H), 4.06-4.28 (m, 8H), 4.36-4.52 (m, 2H), 6.64 (d, J=2.0, 1H), 6.87 (d, J=2.0, 1H), 11.15 (br, 1H). ^{13}C NMR: δ 16.5, 33.2, 36.5, 39.7, 42.4, 60.5, 60.7, 121.7, 122.7, 161.7.

By means of the procedure utilized, **3e** and **3f** were obtained as inseparable mixtures of regioisomers (ratio 9:1), whose structure was defined by NMR experiments carried out on derivative **4e**.

Tetraethyl-[2-(purin-9-yl)ethyl]-bisphosphonate (3e). Yield 48%; yellow oil. Main isomer: ^{1}H NMR δ 1.19-1.24 (m, 12H), 3.36-3.53 (m, 1H), 4.06-4.16 (m, 8H), 4.75-4.83 (m, 2H), 8.17 (s, 1H), 8.95 (s, 1H), 9.11 (s, 1H). ^{13}C NMR δ 13.3, 44.5, 48.7, 62.0, 133.3, 146.6, 149.6, 150.8, 168.3.

Tetraethyl-[2-(6-chloro-purin-9-yl)ethyl]-bisphosphonate (3f). Yield 50%; yellow oil. Main isomer: ^{1}H NMR δ 1.20-1.24 (m, 12H), 3.35-3.43 (m 1H), 4.01-4.15 (m, 8H), 4.73-4.84 (m, 2H), 8.0 (s, 1H), 8.22 (s, 1H), 8.71 (s, 1H). 13C NMR δ 13.0, 41.5, 44.6, 62.3, 133.3, 146.7, 149.5, 150.8, 152.7.

General Procedures for the Synthesis of Bisphosphonic acid 4a-f.

Method A. A solution of **3a-f** (0.25 mmol) in concentrated HCl (3 mL) was stirred under reflux for 3 h and the solvent evaporated in vacuo. The residual solid was recrystallized from H_2O-MeOH to give **4a-f**.

Method B. To an ice-cooled solution of **3a-f** (0.25 mmol) in CCl_4 (5 mL) was added iodotrimethylsilane (0.179 mL, 1.25 mmol) dropwise, and the resulting mixture was stirred below 5 °C for 3 h. The reaction mixture was quenched by adding MeOH (10 mL), and the precipitate was collected and recrystallized by from H_2O/MeOH to give **4a-f** as white or yellow solids.

[2-(Imidazol-1-yl)ethyl]-bisphosphonic acid (4a). Yield 90%; white solid, mp >250 °C dec. ^{1}H NMR (NaOD/D_2O) δ 1.83-1.94 (m, 1H), 4.16-4.24 (m, 2H), 6.73 (s, 1H), 7.09 (s, 1H), 7.57 (s, 1H). ^{13}C NMR (NaOD/D_2O) δ 44.3, 47.0, 120.7, 126.9, 138.8. Anal. ($C_5H_{10}N_2O_6P_2$) C, H, N.

[2-(Pyrazol-1-yl)ethyl]-bisphosphonic acid (4b). Yield 79%; white solid, mp 199-202 °C. ^{1}H NMR (NaOD/D_2O) δ 2.03-2.24 (m, 1H), 4.27-4.39 (m, 2H), 6.02-6.06 (m, 1H), 7.29 (s, 1H), 7.59 (s, 1H). ^{13}C NMR: δ 32.3, 35.5, 38.8, 44.7, 105.1, 126.6, 138.8. Anal. ($C_5H_{10}N_2O_6P_2$) C, H, N.

38

[2-(Benzoimidazol-1-yl)ethyl]-bisphosphonic acid (4c). Yield 67%; white solid, mp >250 °C dec. ^{1}H NMR (NaOD/D_2O) δ 2.20-2.35 (m, 1H), 4.45-4.58 (m, 2H), 7.35-7.42 (m, 2H), 7.83-7.98 (m, 2H), 8.72 (s, 1H). 13C NMR (NaOD/D_2O) δ 25.3, 34.0, 118.4, 125.9, 143.9, 151.5. Anal. (C9H12N2O6P2) C, H, N.

[2-(Imidazol-2-yl-thio)ethyl]-bisphosphonic acid (4d). Yield 40%. ^{1}H NMR (NaOD/D_2O) δ 2.89-2.98 (m, 1H), 3.99-4.06 (m, 2H), 7.01-7.03 (m, 2H). ^{13}C NMR: δ 35.1, 38.3, 41.1, 41.28, 121.7, 122.7, 161.9. Anal. (C5H10N2O6P2S) C, H, N, S.

[2-(Purin-9-yl)ethyl]-bisphosphonic acid (4e). Yield 55%; yellow solid. Title compound was identified by NMR study present as the main isomer (90%). ^{1}H NMR (D_2O) δ 3.05 (m, 1H), 4.95 (m, 2H), 8.97 (s, 1H), 9.30 (s, 1H), 9.42 (s, 1H). ^{13}C NMR (150.81 MHz, D_2O) δ 42.98, 38.38, 132.42, 140.56, 147.23, 153.35, 154.75.

[2-(Purin-7-yl)ethyl]-bisphosphonic acid was found as minor isomer (10%). 1H NMR (D_2O) δ2.84 (m, 1H), 4.99 (m, 2H), 9.15 (s, 1H), 9.27 (s, 1H), 9.62 (s, 1H). Anal. (C7H10N4O6P2) C, H, N.

[2-(6-Chloro-purin-9-yl)ethyl]-bisphosphonic acid (4f). Yield 59%; yellow solid. Main isomer: ^{1}H NMR (NaOD/D_2O) δ 2.16-2.32 (m, 1H), 4.32-4.42 (m, 2H), 7.93 (s, 1H), 7.97 (s, 1H). ^{13}C NMR (NaOD/D_2O) δ 41.5, 44.6, 133.3, 146.7, 149.5, 150.8, 152.7. Anal. (C7H9ClN4O6P2) C, H, N.δ

Biology.

Expansion in Vitro of γδT Cells.

Heparinized blood specimens were collected from 12 healthy volunteers (males, age range 24-46 years), all working at the Dipartimento di Biopatologia e Metodologie Biomediche, University of Palermo, upon informed consent. The study was approved by the ethical committee of the University Hospital. Peripheral blood mononuclear cells were incubated in vitro with different N-BPs or BrHPP (at the indicated final concentrations) and 20 U/mL final concentration of rIL-2, for 7 days at 37 °C. At the end of the incubation period, cells were collected and the γδ T cell

expansion factor calculated according to our previously published method.27 Expansion in vitro of γδ T cells, when the mechanism of action of different N-BPs was evaluated, was performed as indicated previously, except that the assay was carried out in the presence or absence of mevastatin or lovastatin, both used at 1 μM final concentration.

In Vivo Antitumor Activity.

In vivo antitumor activity of γδ T cells was evaluated in SCID mice, using the protocol described by Kabelitz et al., with minor modifications.19 Briefly, SCID mice (6 mice per group) were conditioned by irradiation (300 rads from a cesium source) and antiasialo-GM1 monoclonal antibody (BD Bioscience) treatment. Mice received at day 0 a single intraperitoneal injection of the breast cancer cell line BT549 (2×10^6/mouse). These high numbers of tumor cells were inoculated to allow for full-fledged tumor growth within the period before graft-vs-host reactions developed in the SCID mouse reconstituted with human lymphocytes. Mice received, concomitantly with the tumor cells, an intraperitoneal injection of human recombinant (r)IL-2 (300 ng), or **4a** (2 μg), or zoledronate (5 μg), or **4a** (2 μg) plus rIL-2 (300 ng), or zoledronate (5 μg) plus rIL-2 (300 ng). Where indicated, mice received, in addition, highly purified human γδ T cells (2×10^7/mouse). γδ T cells (2×10^7/ mouse) and zoledronate (5 μg), or **4a** (2 μg), were injected again every 15 days, while (r)IL-2 (300 ng) was given on the same day and at 3 and 6 days after each injection of γδ T cells. $*p < 0.02$ and $**p < 0.005$, when compared to all other groups.

Cytotoxicity Assays.

To evaluate the number of live and dead neoplastic cells, the cells were stained with trypan blue and counted on a hemocytometer. To determine the growth inhibitory activity of the drugs tested, 2×10^5 cells were plated into 25 mm wells (Costar, Cambridge, UK) in 1 mL of complete medium and treated with different

40

concentrations of each drug. After 48 h of incubation, the number of viable cells was determined and expressed as the percentage of control proliferation.

Clonal Assays.

To evaluate the cytotoxic effects of biphosphonates on normal hemopoietic progenitor cells, a clonal assay for CFU-GM (colony-forming units-granulocyte macrophage) was performed. Bone marrow mononucleated cells were obtained from bone marrow aspirates of five normal volunteers. Bone marrow (3-5 mL) was diluted in RPMI 1640, layered over a Ficoll-Hypaque gradient (density, 1.077), centrifuged at 400g for 30 min, and the interface mononuclear cells were collected. The interface cells were washed three times in PBS, counted, and resuspended at a concentration of 1×105 in MEM containing 0.9% methylcellulose, 30% FCS, 10-4 M _-mercaptoethanol, 5% medium conditioned by leukocytes in the presence of phytohemagglutinin (PHA-LCM) in 15 mm plastic dishes. After 7 days of culture at 37 °C in an environment of 5% CO_2 and 100% humidity, the number of CFUGM was evaluated.

Morphological Evaluation of Apoptosis and Necrosis.

Drug induced apoptosis and necrosis was determined morphologically after labeling with acridine orange and ethidium bromide. Cell (2×105) was centrifuged ($300g$) and the pellet was resuspended in 25 μL of the dye mixture. Ten μL of the mixture was examined in oil immersion with a 100× objective using a fluorescence microscope. Live cells were determined by the uptake of acridine orange (green fluorescence) and exclusion of the ethidium bromide (red fluorescence) stain. Live and dead apoptotic cells were identified by the perinuclear condensation of chromatin, stained by acridine orange (100 μg/ml) or ethidium bromide (100 μg/mL), respectively, and by the formation of apoptotic bodies. The percentage of apoptotic cells was determined after counting at least 300 cells.

Determination of Apoptosis by Annexine-V.

Cells (1 × 106) were washed with PBS and centrifuged at 200g for 5 min. Cell pellet was suspended in 100 μL of a staining solution, containing FITC-conjugated Annexine-V and propidium iodide (Annexine-V-Fluos Staining Kit, Roche Molecular Biochemicals, Mannheim, Germany) and incubated for 15 min at 20 °C. The percentage of Annexine-V-positive cells was evaluated by flow cytometry (Becton Dickinson).

Determination of Drug Interactions.

For the determination of the interactions between the drugs, the fractional product methods of Webb was applied.28 The predicted values (c) were calculated according to the equation c) $a \times b$/100, where a and b indicate cell survival values with single agents. Hence, the combination index (CI) was calculated as the ratio between the survival observed with the combinations and the predicted values. The equations CI = 1, CI < 1, and CI > 1 indicate additive effects, synergism, and antagonism, respectively.

Determination of Inhibition of FPP Synthase.

FPP synthase was purified and assayed as previously described by Kavanagh et al.29 Briefly, an expression construct encoding human FPPS (gi 61680822) as N-terminally His6-tagged fusion protein with a TEV cleavage site was expressed in *Escherichia coli* BL21(DE3). Cells were lysed using a high pressure cell disruptor, and the protein was purified to apparent homogeneity using Ni-NTA resin (Qiagen). Gel filtration chromatography was then performed using a Superdex 200 column (GE/Amersham). For analysis of inhibition, 40 ng (1 pmol) of pure FPP synthase was preincubated with N-BP in a volume of 80 μL buffer containing 50 mM Tris pH7.7, 2 mM MgCl2, 0.5 mM TCEP, 20 μg/mL BSA for 10 min. Reactions were started by the addition of 20 μL of 5× substrate (50 μM GPP and 50 μM 14C-IPP, 400 KBq/μmol) in water, bringing the inhibitor and substrate to the final desired concentrations, and allowed to proceed for an appropriate period of time at 37 °C.

Reactions were timed such that a maximum of 10% of the available substrate was used. Assays were terminated by the addition of 0.2 mL of conc HCl/methanol (1:4) and incubated for 10 min at 37 °C. The reaction mixtures were then extracted with 0.4 mL of scintillation fluid Microscint E (Perkin-Elmer). After thorough mixing, the tubes were briefly centrifuged to separate the two phases and the radioactivity was then counted directly using a Microbeta (Perkin-Elmer) scintillation counter. All data were fitted to kinetic models using Graphpad Prism.

1.12 References

1. Jung,A., Bisaz, S., Fleisch, H. *Calcif. Tissue Res.* **1973**, *11*, 296-280.

2. Rogers, M.J., Gordon, S., Benford, H.L., et al. *Cancer*, **2000**, *88 (12 Suppl)*, 2961-2978.

3. Cheng, F.; Oldfield, E. *J. Med. Chem.* **2004**, *47*, 5149–5158.

4. Green, J. R. *Cancer* **2003**, *97* (3 Suppl), 840–847. Clezardin, P.; Ebetino, F. H.; Fournier, P. G. J. *Cancer Res.* **2005**, *65*, 4971–4974.

5. Martin, M. B.; Grimley, J. S.; Lewis, J. C.; Heat, H. T.; Bailey, B. N.; Kendrick, H.; Yardley, V.; Caldera, A.; Lira, R.; Urbina, J. A.; Moreno, S. N. J.; Docampo, R.; Croft, S. L.; Oldfield, E. *J. Med. Chem.* **2001**, *44*, 909–916. Subhash, G.; Chan, J. M. W.; Lea, C. R.; Meints, G. A.; Lewis, J. C.; Tovian, Z. S.; Flessner, R. M.; Loftus, T. C.; Bruchhaus, I.; Kendrick, H.; Croft, S. L.; Kemp, R. G.; Kobayashi, S.; Nozaki, T.; Oldfield, E. *J. Med. Chem.* **2004**, *47*, 175–187. Hudock, M. P.; Sanz-Rodriguez, C. E.; Song, Y.; Chan, J. M. W.; Zhang, Y.; Odeh, S.; Kosztowski, T.; Leon-Rossell, A.; Concepcio`n, J. L.; Yardley, V.; Croft, S. L.; Urbina, J. A.; Oldfield, E. *J. Med. Chem.* **2006**, *49*, 215–223.

6. Clezardin, P.; Ebetino, F. H.; Fournier, P. G. J. *Cancer Res.* **2005**, *65*, 4971–4974.

7. Waldmann, Thomas A. *Nature Medicine.* **2003**, *9*, 269–277.

8. Keating, M.J., Cazin, B., Coutre, S., et al. *J.Clin.Oncol,* **2002**, *20*, 205-213. Hurwitz, H., Fehrenbacher, L., Novotny, W., et al. *N Engl.J.Med.* **2004**, *350*, 2335–2342. De Angelo, D., Stone, R., Durant, S., et al. *Blood*, **2003**, *102*, 100a [abstract].

9. Shipley, D.L., Spigel, D.R., Carrell, D.L., Dannaher, C., Greco, F.A., Hainsworth, J.D. *J.Clin.Onco.l* **2004**, *22*, 6519 [abstract]. Rao, A.V.,

Akabani, G., Rizzieri, D.A. *Clin Med Res,* **2005**; *3*, 157-165. Kaminski, M.S., Tuck, M., Estes, J., et al. *N.Engl.J.Med.* **2005**, *352*, 441-449.

10. Austin, C.D. et al. *Pro.Natl.Acad.Sci U S,* **2005**, *102***,** 50, 17987–17992.

11. Sheares, B. T.; White, S. S.; Molowa, D. T.; Chan, K.; Ding, V. D.; Kroon, P. A.; Bostedor, R. G.; Karkas, J. D. *Biochemistry,* **1989**, *28*, 8129–8135. Tarshis, L. C.; Yan, M.; Poulter, D.; Sacchettini, J. C. *Biochemistry,* **1994**, *33*, 10871–10877.

12. Glomset, J. A.; Gelb, M. H.; Farnsworth, C. C. *Trends Biochem.Sci.* **1990**, *15 (4)*, 139-142.

13. Kavanagh, K.L., Guo, K., Dunford, J.E., Wu, X., Knapp. S, Ebetino, F.H., Rogers, M.J., R. Russell, G.G., Oppermann, U. *Medical Sciences,* **2006**, *103 (20)*, 7829-7834.

14. Anderson, K. C.; Kyle, R. A.; Dalton, W. S.; Landowski, T.; Shain, K.; Jone, R.; Hazlehurst, L.; Berenson, J. *Hematology* **2000**, 166–179. Schultze, J. L.; Nadler, L. M. *J. Mol. Med.* **1999**, *77*, 322–331. Smyth, M. J.; Godfrey, D. I.; Trapani, J. A. *Nat. Immunol.* **2001**, *2*, 293–299. Groh, V.; Steinle, A.; Bauer, S.; Spies, T. *Science* **1998**, *279*, 1737–1740.

15. Feldman, E. J.; Brandwein, J.; Stone, R.; Kalaycio, M.; Moore, J.; O'Connor, J.; Wedel, N.; Roboz, G. J.; Miller, C.; Chopra, R.; Jurcic, J. C.; Brown, R.; Ehmann, W. C.; Schulman, P.; Frankel, S. R.; De Angelo, D.; Scheinberg, D. *J. Clin. Oncol.* **2005**, *23*, 4110–4116. Linck, D.; Lentini, G.; Tiemann, M.; Fauser, A. A.; Parwaresch, R.; Basara, N. *Leuk. Lymphoma* **2005**, *46*, 285–288.

16. Wilhelm, M., Kunzmann, V., Eckstein, S. Reimer, P., Weissinger, F., Ruediger, T., Tony. H.P. *Blood*, **2003**, *102 (1)*, 200-206.

17. Dieli, F., Gebbia, N., Poccia, F., Caccamo, N., Montesano, C., Fulfaro, F., Arcara, C., Valerio, M.R., Meraviglia, S., Di Sano, C., Sireci, G., Salerno, A. *Blood*, **2003**, *102 (6)*, 2310-2311.

18. Widler, L.; Jaeggi, K. A.; Glatt, M.; Muller, K.; Bachmann, R.; Bisping, M.; Born, A.; Cortesi, R.; Guiglia, G.; Jeker, H.; Klein, R.; Ramseier, U.; Schmid, J.; Schreiber, G.; Seltenmeyer, Y.; Green, J. R. *J. Med. Chem.* **2002**, *45*, 3721–3738.

19. Zhang, Y.; Hudock, M. P.; Krysiak, K.; Cao, R.; Bergan, K.; Yin, F.; Leon, A.; Oldfield, E. *J. Med. Chem.* **2007**, *50*, 6067–6079.

20. Kuroda, J.; Kimura, S.; Segawa, H.; Kobayashi, Y.; Yoshikawa, T.; Urasaki, Y.; Ueda, T.; Enjo, F.; Tokuda, H.; Ottmann, O. G.; Maekawa, T. *Blood* **2003**, *102*, 2229–35.

21. Kabelitz, D.; Wesch, D.; Pitters, E.; Zoller, M. *J. Immunol.* **2004**, *173*, 6767–6776.

2. Novel Stilbene derivatives as proapoptotic agents

The stilbene motif is constituted by two benzene rings link with an ethylenic bridge, exists in *cis* and *trans* configurations, and it is the core of different biologically active natural products, such as Combretastatin, Resveratrol, Arothinoids (**Figure 1**).
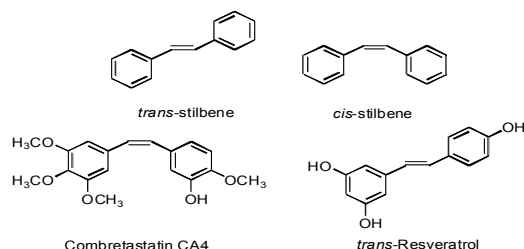

Figure 1. Examples of stilbene in nature.

It is known that in nature doesn't exist the stilbene molecule, but there are about thirty different polyhydroxy-derivatives in the Spematophytes kingdom. These compounds differs by number, positions, and eventually methylated or glycosylated hydroxyl groups. Many of these derivatives are known as Phytoalexins, compounds produced by plants under stress conditions, infections or UV irradiations; thus, in the past, they were mainly studied in botanic fields for their anti-fungal activity.

However, nowadays, after the discovery of a wide range of biologically activities on human, the attention of scientific community on stilbenes derivatives is strongly growth up.

The most important and studied natural stilbenes are Resveratrol and Combretastatin.

2.1. Apoptosis

The natural stilbenes Resveratrol and Combretastatin have in common the skill to improve apoptosis in cancer cells. Apoptosis is the process of programmed cell death that may occur in multicellular organisms; involves a series of biochemical events which leads to a variety of morphological changes, including changes to cell membranes, nuclear and chromosomal DNA fragmentation (**Figure 1**).
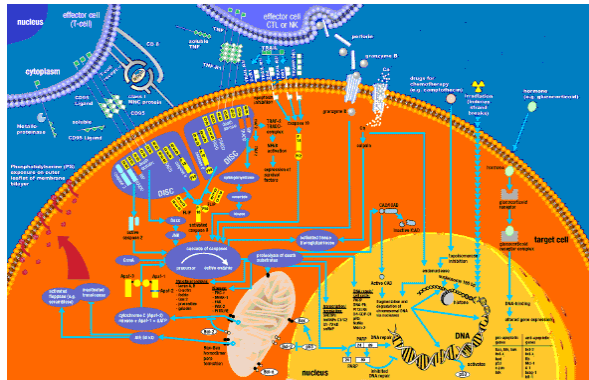

Fig 1. The complexity of Apoptosis mechanism.

In contrast to necrosis, which is a form of traumatic cell death that results from acute cellular injury, apoptosis, in general, confers advantages during an organism's life cycle. Research on apoptosis has increased substantially since the early 1990s. In addition to its importance as a biological phenomenon, defective apoptotic processes have been implicated in an extensive variety of diseases. The research to induce apoptosis is a main goal in development of drugs against cellular proliferation diseases, such cancer.

In healthy conditions, programmed cell death is a needed for proper development, such as mitosis, or to destroy cells that represent a threat to the integrity of organism,

48

such as infections, DNA damage, effectors of immune system, cancer. Upon receiving specific signals instructing the cells to undergo apoptosis a number of distinctive changes occur in the cell. A family of proteins known as caspases are typically activated in the early stages of apoptosis. These proteins breakdown or cleave key cellular components that are required for normal cellular function including structural proteins in the cytoskeleton and nuclear proteins such as DNA repair enzymes. The caspases can also activate other degradative enzymes such as DNases, which begin to cleave the DNA in the nucleus. There are a number of mechanisms through which apoptosis can be induced in cells. The sensitivity of cells to any of these stimuli can vary depending on a number of factors such as the expression of pro- and anti-apoptotic proteins (eg. the Bcl-2 proteins or the Inhibitor of Apoptosis Proteins), the severity of the stimulus and the stage of the cell cycle (**Figure 2**).
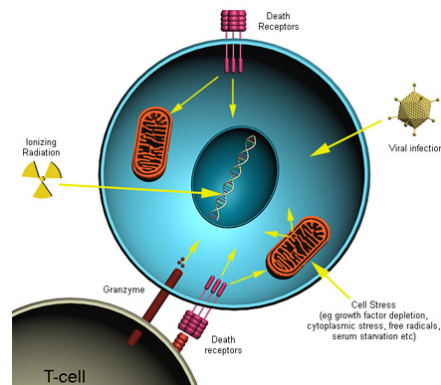

Fig 2. The main stimuli that can induce apoptosis.

Since the cancer is characterized by an abnormal cells proliferation, the induction of apoptosis is an important target for chemotherapy. Natural stilbenes resveratrol and combretastatin shows a good activity in this way, prodding us to develop novel derivatives to improve anticancer therapy.

49

2.2. Resveratrol

Resveratrol (3,4', 5 trihydroxystilbene) is a naturally occuring phytoalexin produced by some spermatophytes, such as grapevines, in response to injury. Given that it is present in grape berry skins but not in flesh, white wine contains very small amounts of resveratrol, compared to red wine. Resveratrol has been known for centuries in Asian medicine as Ko-jo-kon, in the form of the powdered root of *Polygonum cuspidatum*, as an anti-inflammatory drug. Resveratrol displays numerous properties related to very different mechanisms of action[1].

However, its interest in the field of cancer therapy is much more recent. In a pioneering study, John M. Pezzuto and his colleagues[2] reported that resveratrol was effective in blocking all three stages (i.e., initiation, promotion and progression) of carcinogenesis. Subsequent studies demonstrated that resveratrol exhibited strong chemopreventive effects in various experimentally induced tumor models[3]. The compound also inhibited proliferation and induced apoptosis of various cancerous or transformed cells, sensitized chemoresistant or radioresistant cancer cells to apoptosis, and repressed metastasis. Several recent studies reported that intratumoral, peritumoral or intraperitoneal administration of resveratrol significantly arrested tumor growth in vivo and induced apoptosis in xenografted tumors in athymic nude mice[4].

Inhibition of carcinogenic activation. Several studies have demonstrated that resveratrol impairs the carcinogenic activity of polyaromatic hydrocarbons (PAHs), which undergo metabolic activation predominantly by CYP enzymes[5]. The transactivation of CYP1A1, which encodes an enzyme frequently involved in metabolic activation of a wide spectrum of PAHs, requires the binding of activated arylhydrocarbon receptor (AhR) to the promoter segment of the gene. Resveratrol strongly inhibit 2,3,7,8-tetrachlorodibenzo-p-dioxin-(TCDD)-induced AhR DNA-binding activity in human mammary epithelial (MCF-10A) cells. Moreover, resveratrol inhibit induction of CYP1A1 expression in rat primary hepatocytes, suggesting that the compound acts as an AhR antagonist. resveratrol has been shown

to inhibit the activity of CYP1A1, CYP1B1 and CYP1A2 in murine hepatoma (Hepa1c1c7) cells, TCDDstimulated mammary epithelial (MCF-10A) cells, DMBA-treated human breast cancer (MCF-7) cells, and B[a]P-treated human hepatoma (HepG2) cells[6] . Another member of CYP family is CYP19, alternatively known as aromatase, which is a rate-limiting enzyme in the biosynthesis of estrogen. Since estrogens play a crucial role in the development of breast cancer, the inhibitory effect of resveratrol on the aromatase/CYP19 activity in MCF-7 cells[7] suggests that the chemopreventive effects of this stilbene compound on mammary carcinogenesis are attributed partly to its anti-estrogenic property.

Induction of carcinogen detoxifying/antioxidant enzymes. Resveratrol enhances the expression and/or the activity of phase II anti-oxidant/detoxification enzymes including glutathione S-transferase (GST), glutathione peroxidase (GPx), UDP glucuronosyl transferase (UGT)-1A, NADPH:quinine oxidoreductase (NQO), heme oxygenase-1 (HO-1), glutamate cysteine ligase (GCL), etc.[8]. Several recent studies also demonstrated that the compound induced the protein and mRNA expression of HO-1 in human aortic smooth muscle and rat pheochoromocytoma (PC12) cells. Moreover, resveratrol restored the cellular glutathione (GSH), which is prone to be depleted by cigarette smoke extract (CSE), by inducing GCL-catalyzed GSH synthesis in human primary small airway epithelial cells (SAEC) and human alveolar epithelial cells (A549)[9]. By upregulating GCL, resveratrol may have rescued these cells from CSE-induced oxidative stress.

Anti-inflammatory effects: implications for suppression of tumor promotion and progression. Chronic inflammation is causally linked to multistage carcinogenesis. Mediators of inflammation, such as cyclooxygenase-2 (COX-2), prostaglandins, inducible nitric oxide synthase (iNOS), NO, and pro-inflammatory cytokines have been involved in carcinogenesis, especially in the promotion and progression stages. In addition, pro-inflammatory cytokines, such as interleukin 1 (IL-1), IL-6, IL-8 and tumor necrosis factor-α (TNF-α), have also been known to be involved directly or indirectly in carcinogenesis[10]. Thus, components of the inflammatory signaling pathways are recognized as potential targets for chemoprevention. Resveratrol

51

exhibited anti-tumor promoting effects by blocking the expression of various components of pro-inflammatory signalling, diminished the COX-2 activity and reduced the production of PGE2 in peripheral blood leukocytes. The expression of pro-inflammatory cytokines appears to be differentially affected by resveratrol.

While the compound significantly decreased the expression of TNF-a mRNA in LPS-activated J774.2 macrophage cells and peripheral blood leukocytes, it failed to suppress IL-1b gene expression in J774.2 cells[11]. However, the inhibition of proliferation and induction of apoptosis in human multiple myeloma (MM) cells by resveratrol were found to be associated with its interference with signaling pathways initiated by IL-1b.

Induction of cancer cell cycle arrest. The growth of various cancer cells in culture is arrested by treatment with resveratrol at different phases of the cell cycle. The inhibition of abnormal cell proliferation via modulation of cell cycle progression is one of the important strategies for chemoprevention as well as chemotherapy. Intracellular signaling pathways, comprised of various cyclins, cyclin-dependent kinases (Cdk), Cdk inhibitors, and check point kinases (Chk 1 and Chk 2), are involved in fine-tuning of homeostatic maintenance of cell growth and differentiation. Therefore, the suppression of abnormal cell proliferation by down-regulating cyclin-Cdks and/or upregulating Cdk inhibitors may provide an ample scope to intervene in the multistage carcinogenesis by dietary phytochemicals. The anti-proliferative and growth inhibitory effects of resveratrol have been attributed to its ability to block DNA synthesis and interference with various stages of cell cycle progression.[12]

Induction of apoptosis. The induction of apoptosis selectively in cancer cells is regarded as an important strategy for cancer prevention as well as therapy. Resveratrol has been reported to induce apoptosis in various cancerous or transformed cells in culture, chemically induced mouse skin tumors, and in transplanted tumors in nude mice by activating both extrinsic and intrinsic pathways of cell death machinery. The induction of apoptosis in human promyelocytic leukemia (HL-60) and breast cancer (T47D) cells by resveratrol was mediated via

52

activation of the CD95–CD95L signaling[13]. Most notably, resveratrol did not affect the survival of normal peripheral blood lymphocytes up to 72 h, suggesting that the compound induced apoptosis selectively in cancer cells. Resveratrol inhibited mitochondrial F1F0-ATPase, an enzyme involved in cellular ATP synthesis, providing a possible explanation for resveratrol induced dysfunction of mitochondria and induction of apoptosis[14]. Resveratrol also activated caspase-2 and -8, resulting in the processing of down-stream caspases and cell death in a death receptor or mitochondria-independent manner. Although resveratrol is a well known anti-oxidant, the compound was shown to impose both redox and replication stress in cells, resulting in senescence-like growth arrest. Heiss et al.[15] demonstrated that resveratrol generated mitochondria derived ROS in HCT-116 cells and induced senescence-like growth arrest by increasing phosphorylation of p53 and elevation of the p21 level via activation of p38 MAP kinase and ATM kinase.

Inhibition of angiogenesis. The disruption of angiogenic signaling cascades appeared as a front line of attack by various anti-cancer agents. Due to increased metabolic activities and oxygen consumption by rapidly proliferating cells, solid tumors are likely to maintain an intratumoral hypoxic environment, which enforces tumor cells to adapt by inducing hypoxia responsive genes. Hypoxia inducible factor (HIF) acts as a master regulator of cellular oxygen homeostasis by regulating expression of hypoxia-responsive genes. Resveratrol has been reported to inhibit the expression of HIF-1a and VEGF in OVCAR-3 cells through multiple mechanisms, such as inhibition of Akt and MAP kinases, inhibition of protein translational regulators, and enhancement of proteasomal degradation of HIF-1a protein.[16]

Anti-invasive and anti-metastatic effects. The invasion of tumor cells through tumor-associated stroma and subsequent metastasis are the central events in neoplastic progression. One of the mediators of tumor invasion and metastasis is lysophosphatidic acid (LPA), which has been reported to enhance migration of human ovarian cancer cells through upregulation of HIF-1a and VEGF. Resveratrol significantly attenuated LPA-induced expression of HIF-1a and VEGF, and subsequent migration of ovarian cancer cells by blocking activation of upstream

ERK1/2 and p70S6 kinase. Resveratrol inibite invasion of various cancer cells by reducing the expression and activity of matrix metalloproteinase-2, and by reducing the focal adhesion kinase activity.[17]

Chemosensitizing effects. Currently, the emergence of resistance to chemotherapy is a growing challenge in reducing cancer related deaths worldwide. The use of cancer chemopreventive phytochemicals as adjuvants in combination with chemotherapeutic agents has been shown to be a pragmatic approach to sensitize chemoresistant cancer cells to apoptosis or growth arrest, while minimizing the side effects arising from the conventional therapy. As an example, resveratrol enhanced the apoptotic effects of bortezomib and thalidomide in multiple myeloma cells. Resveratrol, used as a combination therapy with etoposide, inhibited growth and induced apoptosis of human colon cancer (HT-29) cells by a ROS-dependent activation of adenosine monophosphate (AMP)-activated protein kinase (AMPK). These findings suggest that resveratrol, as an adjuvant to chemotherapy, can enhance chemosensitvity of cancer cells, while it alleviates unavoidable chemotherapy-associated adverse effects. P-Glycoprotein, a product of multi drug resistant (MDR)-1 gene, has been considered as a key player in developing chemoresistance. By actively effluxing drugs from cells, P-glycoprotein reduces intratumoral concentrations of chemotherapeutic drugs and hence lowers their efficacy. Resveratrol was shown to inhibit the P-glycoprotein function and increase accumulation of daunorubicin in multidrug resistant KB-C2 cells, thereby sensitizing these cells to apoptosis.[18]

54

2.3. Combretastatins

Isolated in the 80's from stem wood of the South African tree *Combretum caffrum* combretastatins are low molecular weight molecules containing more oxygenate groups substituted benzene rings, but with different structural nature: stilbene derivatives as combretastatins A-1 and A-4, dihydrostilbene as combretastatin B-1, phenantroquinone as C-1 or macro-lactones as combretastatin D-1(**Figure 3**).
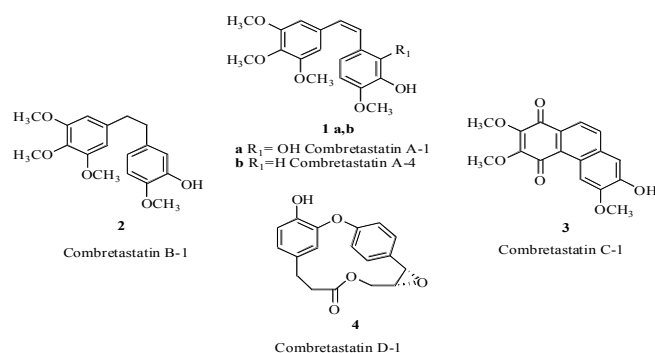

Fig 3. Natural combretastatins.

All these combretastatin are biologically active, but the best results were obtained by Combretastatin A-4 (CA-4), **1b**. Combretastatin A4 is an interesting antitumor agents and acts ac Vascular Disrupting Agents (VDAs).[19]

Vascular targeting strategies can be divided into two different approaches: an antiangiogenic approach and so called vascular disrupting approach. Angiogenesis inhibitors can be divided into two groups, monoclonal antibodies (Moabs) and small molecule tyrosine kinase inhibitors (TKIs). Bevacizumab is a humanised Moab targeting VEGF (Vascular Endothelial Growth Factor), which has shown clinical activity in combination with cytotoxic chemotherapy in metastatic colorectal cancer,

non-small cell lung cancer (NSCLC) and breast cancer. As single agent bevacizumab has demonstrated acivity in metastatic renal cell carcinoma.[20] Apart from Moabs, a large number of small-molecule VEGFR TKIs have been explored in clinical studies. Results in randomised studies in renal cell carcinoma with the broadspectrum TKIs sunitinib and sorafenib have resulted in their regulatory approval for this disease. Theoretically, it is conceivable that angiogenesis inhibitors will exert optimal activity in a situation of minimal residual disease with high angiogenic potency such as could be the case in the adjuvant setting.

Vascular disrupting agents (VDAs) target endothelial cells and pericytes of the already established tumour vasculature. Selective vascular shutdown suggests a structural difference in endothelium of tumour vessels compared to that of normal vessels. Indeed, tumour vasculature is, among others, marked by a high rate of endothelial cell proliferation, the absence of pericytes, abnormalities in the basement membrane and often an increased vascular permeability. Structurally, disorganised, tortuous, thinwalled vessels are seen that lack smooth muscle and pericyte coats and innervation (**Figure 4**).
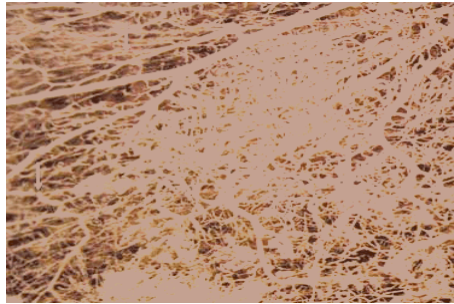

Fig 4. Architectural difference between vasculature in normal (small arrows) and tumour tissue (thick arrows).

Vessel diameters are irregular and lengths between branches are long, resulting in a high resistance to blood flow. A small decrease in perfusion pressure, which has little effect in normal tissue, therefore can be catastrophic to tumours. Finally, endothelial cells are highly dependent on tubulin cytoskeleton for their motility, invasion, attachment, alignment and proliferation.[21] Most VDAs induce changes in endothelial cell shape by disruption of the cytoskeleton and cell-to-cell junctions. This results in increased permeability to proteins and an increased interstitial fluid pressure, which might be sufficient to reduce vessel diameter. Compared to the antiangiogenic approach of both TKI and Moab, the vascular disrupting approach therefore seems to be cytotoxic rather than cytostatic. However, in preclinical models it has been observed that following exposure to a VDA, only the centre of a tumour becomes necrotic, with a viable rim (**Figure 5**) remaining in the periphery. This rim of viable tumour cells presumably survives because it derives nutritional support (most likely via diffusion) from adjacent normal blood vessels that are typically less responsive to VDAs.
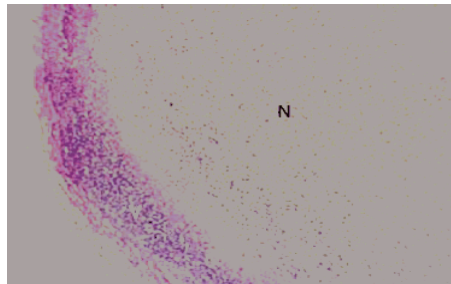

Fig 5. Typical example of a tumour with a viable rim (V) and central necrosis (N) following exposure to a vascular disrupting agent.

Vascular disrupting agents have been divided into two types, small molecule (eg Combretastatin) and ligand directed VDAs.

Small molecule VDAs can be divided into two groups; the tubulin-binding agents and the flavonoids. Tubulin-binding agents work by acting at the colchicines-binding site of the β-subunit of endothelial tubulin, resulting in depolymerisation of microtubules and disorganisation of actin and tubulin. Disruption of the endothelial cytoskeleton results in conformational changes leading to loss of blood flow. In addition to this, a recent study showed that the typical microtubule-destabilising agent combretastatin A4 phosphate (CA4P) also selectively disrupts the VE-cadherin/β-catenin complex interfering with cell–cell contact.[22]

Combretastatin A4 phosphate is a water-soluble prodrug of combretastatin A4. Following administration, CA4P is rapidly cleaved to CA4 and binds tubulin at or close to the colchicines-binding site.[23]

Loss of the cell–cell contact increases vascular permeability leading to increased interstitial pressure and additional loss of blood flow. In addition to these effects, the already mentioned loss of cell–cell contact results in the exposure of the already often abnormal basement membrane, which in turn can result in the induction of the coagulation cascade with subsequent thrombus formation. Tumour-related endothelial cells are much more sensitive to the activity of tubulin-binding agents than normal endothelial cells.[24]

Thus, these biological results make combretastatin A4 a very interesting starting point to develop novel anticancer drugs.

2.4. Novel stilbenes derivatives

The research group where I stayed during my PhD has an internationally recognized experience on the synthesis of resveratrol and combretastatin derivatives.

5

Resveratrol

1b

Combretastatin CA4
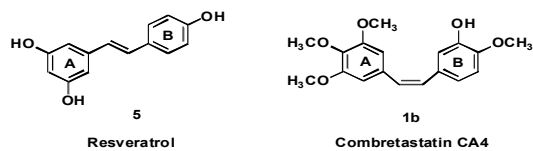
Thus, starting from our previous results, to study novel proapoptotic compounds we focused the research on two aspects: the synthesis of stilbene derivatives and their optimization, based on the substitutions of resveratrol and CA4, and the modification of the stilbene motif substituting ethylene bridge with a benzene ring, synthesizing novel terphenyl compounds.

2.4.1. Chemistry

In a previous work of my research group, it was synthesized and biologically tested a *Z* and *E* stilbene derivatives set.[25] All these compounds were assayed in vitro for cell growth inhibition and for their ability to induce apoptosis in HL60 cells (myeloblastic acute leukemia).
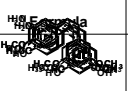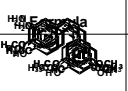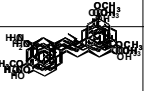
Formula	IC$_{50}$ µM	AC$_{50}$ µM	Formula	IC$_{50}$ µM	AC$_{50}$ µM
	42 ± 6.4	>200		5 ± 0.9	50 ± 8.2
	40 ± 5.3	70 ± 7		48 ± 8.8	>200
	40 ± 6.1	68 ± 5.9		80 ± 11	>200
	2 ± 0.4	5 ± 0.8		35 ± 6	70 ± 8.2
	0.03 ± 0.005	0.04 ±0.0012		4 ± 0.8	8 ± 1.5
	2.5 ± 0.2	8 ± 0.8		4 ± 0.3	15 ± 2
	0.03±0.0012	0.04 ±0.0045		0.7 ± 0.09	0.9 ± 0.1

Table 1. The antiproliferative (IC$_{50}$) and proapoptotic (AC$_{50}$) activity of *trans*-Resveratrol and their derivatives.

As shown in **Table 1**, the best result was obtained by *cis*-derivatives, especially *cis*-3'-amino-3,4',5-trimethoxystilbene and *cis*-3'-hydroxy-3,4',5-trimethoxystilbene, suggesting that introduction of 3,5 dimethoxy motif may be required for good proapoptotic action.

Starting by these results, to design new compounds we decided to maintain the best stilbene A ring (3,5- dimethoxyphenyl) and change the substituents on B ring (**Figure 1**).

60

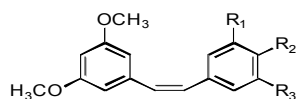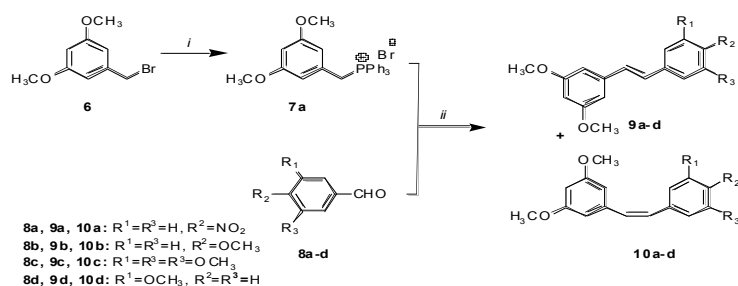**Figure.1**. Structure of new compounds

The synthesis of these derivatives is based on a Wittig reaction between the 3,5-dimethoxybenzyl-triphenylphosphonium-bromide and the appropriate aldehyde in presence of NaH with tetrahydrofuran as solvent (**Scheme 1**) giving a 40-60% yield and a 1:3 *Z/E* ratio.

8a, 9a, 10a: $R^1 = R^3 = H$, $R^2 = NO_2$
8b, 9b, 10b: $R^1 = R^3 = H$, $R^2 = OCH_3$
8c, 9c, 10c: $R^1 = R^3 = R^3 = OCH_3$
8d, 9d, 10d: $R^1 = OCH_3$, $R^2 = R^3 = H$

Scheme 1. Reagents and conditions: (*i*) triphenylphosphine, xilene, reflux; (*ii*) NaH, THF, reflux or room temperature.

For the small number of reaction steps and with the aim to develop a more fast, clean and cheap synthetic method we tried to prepare the same compounds using the solid phase synthesis (SPS).

In chemistry, solid-phase synthesis is a method in which molecules are linked on a solid support (generally polystyrene resins) and synthesized step-by-step in a reactant solution; compared with normal synthesis in a liquid state, it is easier to remove excess reactant or byproduct from the desired compound. In this method, building blocks are protected at all reactive functional groups. The two functional

61

groups that are able to participate in the desired reaction between building blocks in the solution and on the solid support can be controlled by the order of deprotection. Indeed, this method is used for the synthesis of peptides, deoxyribonucleic acids, and other molecules that need to be synthesized in a certain alignment. Recently, this method has also been used in combinatorial chemistry.

In our first approach we intended to link 3,5-dimethoxy-benzylbromide to commercial triphenylphosphine resin synthesizing the phosphonium salt on solid support. After washing (using dimethylformamide, methanol, dichloromethane and ethyl ether) and drying, the resin was suspended at room temperature for 18h in tetrahydrofuran in presence of TBD as soluble base and appropriate aldehyde giving the final *E/Z* stilbenes (**Scheme 2**).
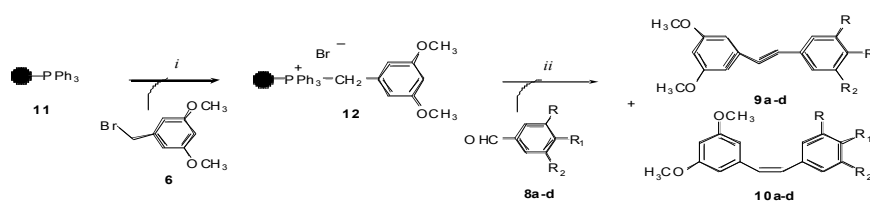
Scheme 2. Synthesis using triphenylphosphine resin. Reagents and conditions: (*i*) toluene, reflux; (*ii*) TBD, THF, reflux or room temperature.

This first approach gave similar results to traditional solution phase synthesis in terms of yields and *E/Z* ratio. Indeed, the use of triphenylphosphine on solid support permit to obtained a more clean Wittig reaction due to the absence of triphenylphosphine-oxide in solution. However, this method can't satisfy the aim to improve the synthesis of these compounds.

Thus, we thought that the best approach should be to build the entire stilbene on the resin. For this purpose, we had to synthesize the bromo-derivative directly on solid support, followed by salt formation, Wittig reaction and, finally, cleavage of the

62

resin to give the clean stilbenes. Since the linkage between 3,5-dimethoxy-benzyl bromide or alcohol and resin was difficult, firstly we used the Wang Bromo-resin (*p*-hydroxybenzyl-bromide attached on solid support) to investigate if the reaction steps occur and give the desired *p*-hydroxy-stilbenes (**Scheme 3**).
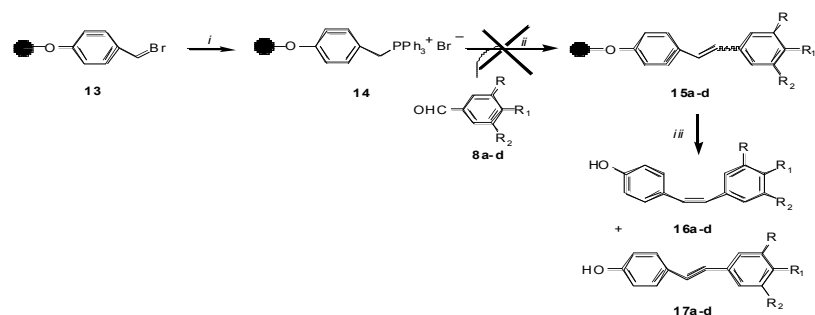
Scheme 3. Approach using Wang-Bromo resin. Reagents and conditions: (*i*) triphenylphosphine, toluene, reflux; (*ii*) TBD, THF, reflux or room temperature; (*iii*) TFA, CH$_2$Cl$_2$, room temperature.

Unexpectedly, the Wittig reaction didn't occur, when we clove the resin only *p*-hydroxybenzyl-triphenylphosphonium bromide was observed. Thus, we tried to repeat the synthesis using the Horner-Emmons reaction instead of Wittig reaction, but the results was the same (**Scheme 4**).
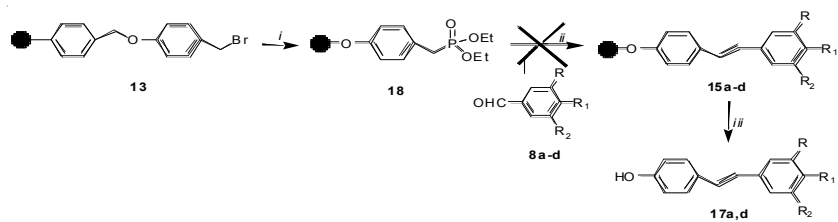
Scheme 4. The Horner-Emmons approach. Reagents and conditions: (i) triethyl phosphite, toluene, reflux; (ii) TBD, THF, reflux or room temperature; (iii) TFA, CH₂Cl₂, room temperature.

Using this method only a compound, *trans*-4-hydroxy-4'-nitro-stilbene, is observed, but in very low yield (about 15%) (**Fig.2**).
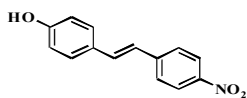
Fig.2 *trans*-4-hydroxy-4'-nitro-stilbene

Probably, this is due to more reactivity of *p*-nitro-benzaldehyde compares to the methoxylated others.

To compare the yields of solid and solution phase synthesis, we prepared two *p*-hydroxy-stilbenes in traditional way (**Scheme 5**).

64
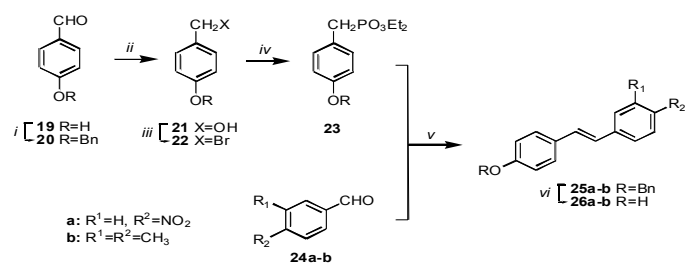
Scheme 5. Reagents and conditions: (*i*) benzyl bromide, NaH, acetonitrile, reflux; (*ii*) NaBH$_4$, CH$_2$Cl$_2$; (*iii*) CBr$_4$, triphenylphosphine, CH$_2$Cl$_2$; (*iv*) triethyl phosphite, toluene, reflux; (*v*) NaH, THF, reflux 40-50%.

Also in this case, the solution phase yields (about 50%) are better than solid phase, resulting not suitable for the preparation of stilbene derivatives libraries.

2.4.2. Biological results

In this work, we described the effect of the new stilbene set on the myeloblastic leukemia cell line HL60 cells (myeloblastic acute leukemia). Apoptosis was detected by morphological examination and confirmed by Annexin V test. In **Table 2** are reported the antiproliferative (IC50) and apoptosis-inducing (AC50) activities.
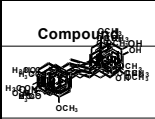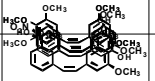
Compound	IC_{50} µM	AC_{50} µM	Compound	IC_{50} µM	AC_{50} µM
	5 ± 0.9	50 ± 8.2		42 ± 6.4	>200
	35 ± 3	68 ± 5.6		10 ± 1.8	28 ± 2.1
	2.5 ± 0.6	4 ± 2.1		0.15 ± 0.01	0.24 ± 0.017
	22 ± 3.7	42 ± 6.2		1.8 ± 0.22	2.6 ± 0.3
	37 ± 2.9	70 ± 10		2.8 ± 0.4	5.4 ± 0.4
	3.5 ± 0.2	6 ± 0.7			
	2.5 ± 0.3	4.8 ± 0.6			

Table 2. Antiproliferative and proapoptotic activities of new stilbenes.

As show the most active compounds resulted in the stilbenes **9b**, **26a**, **26b**, **10b**, **c**, **d**. Compounds **9b**, **26a**, **26b** and **10d** showed a similar antiproliferative and apoptotic-inducing activity, a little less than that of compound **10c**. Compound **9b** showed an apoptotic activity about 10–12 times higher than the natural analogues resveratrol and piceatannol, and 19 times higher than that of pterostilbene.[26] The most active compound of this series, however, was **10b**, which was about 10 and 17 times more active than compounds **10c** and **9b**. From a structure–activity relationship point of

66

view, remarkable results were obtained when the hydroxyl group of pterostilbene was changed to the methoxy derivative **9b**, having the latter about 14 times smaller IC_{50}. Analogous results were also obtained with the cis-methoxy derivative **10b** that is about 13 times more active than the corresponding 4'-hydroxy derivative. Of note, by locating the methoxy substituent at the 4'-position, as in **9b** and **10b**, we obtained compounds with significantly better activity than the corresponding 3'-methoxy derivatives **9d** and **10d**.

The effects on cell cycle of the most active cis (**10b**,**c**) and trans (**9b**, **26a**) were examined by flow cytometry after staining of cells with propidium iodide. HL60 cells were exposed to each compound at the concentrations reported in **Figure 3**.
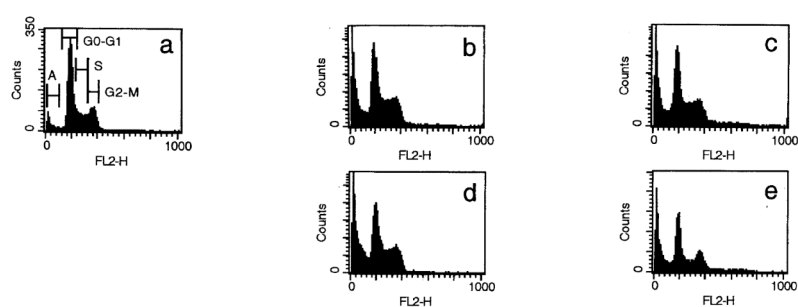
Fig 3. Flow cytometry analysis of cell cycle. HL60 cells were exposed 24 h to 3.5 μM **9b** (b), 2.5 μM **10c** (c), 4 μM **26b** (d) and 0.2 μM **10b** (e). (a) Control; A, sub-G0–G1 peak.

In previous studies, we observed that most stilbene compounds cause a block of cells in a specific phase of cell cycle, acting as phase-specific drugs; in particular many trans-stilbenes (trans-resveratrol and natural resveratrol analogues such as piceatannol) induced a prevalent block in S phase, while cis-stilbenes (such as combretastatin analogues) in G2–M phase,[27] although some trans-stilbenes can still cause a block in G2–M.[28] Similar to resveratrol, compounds **9b**, **26b** and **10c**

induced a partial block of cells in S phase and an apoptotic sub-G0–G1 peak corresponding of about 20%, suggesting that these compounds act on HL60 cells as phase-specific cytotoxic agents. In contrast, compound **10b** caused an evident sub-G0–G1 peak increase but no modification in cell cycle distribution (phases G0–G1, S, and G2–M) respect to the control.

With the aim to better understand the effect of compound **10b** on cell cycle, we expose HL60 cells to different concentration of **10b** for 24 and 48h. This stilbene caused a decrease of G0–G1, S, and G2–M peaks, and a proportional increase of the apoptotic sub-G0–G1 peak which was correlated to the time of exposure (24 or 48 h.) and to the concentration used (**Figure 4**). These data indicate that the effect of **10b** on HL60 cells is not phase-specific and suggest that **10b** could be a compound effective in cancers with different kinetics. This is particularly interesting, because it could be useful alone or in combination with other anticancer agents to decrease the percentage of minimal residual disease caused by kinetic factors.
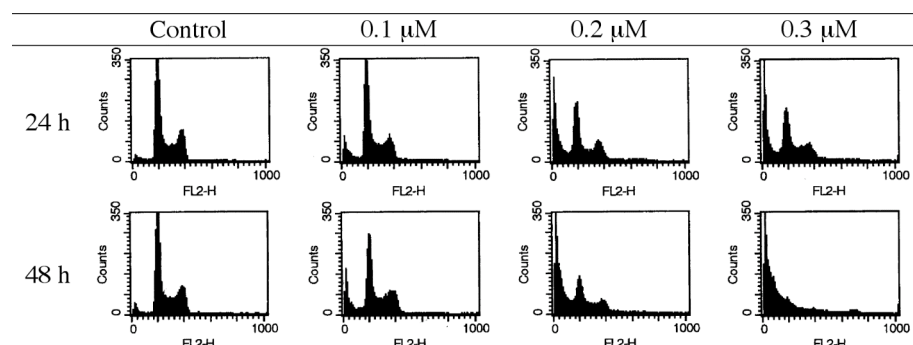
Fig 4. Flow cytometry analysis of cell cycle in HL60 cells exposed 24 and 48 h to different concentrations of compound 6b.

Thus, these results indicate that introduction of methoxy groups at the stilbene motif of resveratrol is important to confer cytotoxic and apoptotic activity to this class of compounds and, in some cases, the methoxy derivatives were more active than the

corresponding phenols. The potent apoptosis-inducing activity and the ability of **10b** to decrease the number of neoplastic cells in all phases of cell cycle make this compound of great interest for further investigations.

2.4.3. Experimental Section

Chemistry

Melting points were obtained with a Kofler apparatus and are uncorrected. Reaction courses and product mixtures were routinely monitored by thin-layer chromatography (TLC) on silica gel precoated F254 Merck plates. Nuclear magnetic resonance (1H and 13C NMR) spectra were determined in CDCl3 solution, unless otherwise indicated, with a Bruker AC-200 spectrometer, and peak positions are given in parts per million downfield from tetramethylsilane as internal standard. All drying operations were performed over anhydrous sodium sulfate. Column chromatography (medium pressure) was carried out with 60-200 mesh silica gel, using the flash technique. Microanalysis of all new final synthesized compounds agreed with calculated values within ± 0.4% of the theoretical.

3,5-Dimethoxybenzyltriphenylphosphonium bromide (7a). A solution of triphenylphosphine (1.76 g, 6.72 mmol, 1.6 equiv.) in xylene was added to a solution of 3,5-dimethoxybenzyl bromide (1 g, 4.2 mmol, 1 equiv.) in xylene and the reaction was stirred under reflux overnight. After cooling to room temperature the reaction was filtered. The solid was washed with diethyl ether and recristallyzed from methanol/diethyl ether to give white needles. Yield 95%. mp 265-267 °C.

General Procedure for the Stilbene Syntheses. To the phosphonium bromide (**7a**, 1 eq) in anhydrous tetrahydrofuran at 0°C was added NaH (1.5 eq), and the resulting yellow solution was stirred under argon for 15-30 min. A solution of the appropriate aldehyde (**8a-d**, 1.2 eq) in tetrahydrofuran was added dropwise and the mixture stirred for 2-15 h. The resulting suspension was diluted with ethyl ether and washed with water and brine. After drying on anhydrous sodium sulphate, removal of the

70

solvent in vacuo afforded a tan oil. The oil was separated by flash column chromatography (hexane/ethyl acetate). The *cis*-stilbene eluted first as a clear oil followed by the *trans* isomer as a colorless solid or oil.

3,5-Dimethoxy-4'-nitrostilbenes (9a, 10a). Obtained from 3,5-dimethoxybenzyltriphenylphosphonium bromide (**7a**, 200 mg, 0.4 mmol) and 4-nitrobenzaldehyde (**8a**, 54 mg, 0.36 mmol) with NaH (10 mg, 0.43 mmol). Purification and separation by flash chromatography (petroleum ether/diethyl ether 9:1). *Cis/trans* ratio: 1:2. Total yield 45%.

Trans (**9a**). Orange solid. M.p. = 132-135°C. ^{1}H-NMR (CDCl$_3$, 200 MHz): δ 3.84 (s, 6H), 6.46 (t, J = 2.4, 1H), 6.69 (d, J = 2.4, 2H), 7.11 (d, J = 16, 2H), 7.20 (d, J = 16, 2H), 7.63 (d, J = 9.2, 2H), 8.22 (d, J = 8.8, 2H). ^{13}C NMR (CDCl$_3$, 200 MHz): δ 55.6, 99.5, 109.5, 124.7, 126.4, 129.0, 138.3, 138.6, 143.4, 147.2, 161.9.

Cis (**10a**). Orange solid. M.p. = 70-72°C. ^{1}H-NMR (CDCl$_3$, 200 MHz): δ 3.61 (s, 6H), 6.28 (m, 3H), 6.53 (d, J = 12, 1H), 6.69 (d, J = 12, 1H), 7.34 (d, J = 8.8, 2H), 8.02 (d, J = 8.8, 2H). ^{13}C NMR (CDCl$_3$, 200 MHz): δ 55.8, 98.5, 109.8, 125.7, 127.4, 129.0, 138.3, 138.9, 145.0, 147.2, 161.8.

3,4',5-Trimethoxy stilbenes (9b, 10b). Obtained from 3,5-dimethoxybenzyltriphenylphosphonium bromide (**7a**, 200 mg, 0.4 mmol) and *p*-anisaldehyde (**8b**, 50 mg, 0.36 mmol) with NaH (10 mg, 0.43 mmol). Purification and separation by flash chromatography (petroleum ether/diethyl ether 9:1). *Cis/trans* ratio: 1.5:2. Total yield 35%.

Trans (**9b**). Light yellow solid. M.p. = 55-56°C. ^{1}H-NMR (CDCl$_3$, 200 MHz): δ 3.82 (s, 9H), 6.37 (t, J = 2.2, 1H), 6.65 (d, J = 2.2, 2H), 6.89 (d, J = 8.8, 2H), 6.89 (d, J = 16, 1H), 7.04 (d, J = 16, 1H), 7.44 (d, J = 9, 2H). ^{13}C NMR (CDCl$_3$, 200 MHz): δ 54.9, 55.6, 99.5, 109.5, 114.7, 126.4, 128.3, 129.6, 138.3, 138.6, 160.1, 161.9.

Cis (**10b**). Yellow oil. ^{1}H-NMR (CDCl$_3$, 200 MHz): δ 3.66 (s, 6H), 3.77 (s, 3H), 6.31 (t, J = 2.2, 1H), 6.43 (d, J = 2.2, 2H), 6.43 (d, J = 12.2, 1H), 6.53 (d, J = 12.2,

71

1H), 6.76 (d, J = 8.8, 2H), 7.20 (d, J = 9.2, 2H). ^{13}C NMR (CDCl$_3$, 200 MHz): δ 54.3, 55.6, 98.9, 110.1, 115.2, 126.4, 128.0, 129.2, 137.9, 159.7, 161.9.

3,3',4',5,5'-Pentamethoxy stilbenes (9c, 10c): Obtained from 3,5-dimethoxybenzyltriphenylphosphonium bromide (**7a**, 553 mg, 1.12 mmol) and 3,4,5-trimethoxybenzaldehyde (**8c**, 200 mg, 1.02 mmol) with NaH (29 mg, 1.22 mmol). Purification and separation by flash chromatography (petroleum ether/diethyl ether 8:2). *Cis/trans* ratio: 1:3. Total yield 38%.

Trans (**9c**). Light yellow solid. M.p. = 136-138°C. ^{1}H-NMR: δ 3.82 (s, 6H), 3.86 (s, 3H), 3.91 (s, 6H), 6.39 (t, J = 2.2, 1H), 6.66 (d, J = 2.2, 2H), 6.73 (s, 2H), 6.91 (d, J = 16.4, 1H), 7.02 (d, J = 16.2, 1H). ^{13}C-NMR: δ 55.4, 56.2, 61.0, 100.0, 103.7, 104.5, 128.2, 129.2, 132.9, 138.1, 139.3, 153.5, 161.1.

Cis (**10c**). Yellow oil. ^{1}H-NMR: δ 3.67 (s, 12H), 3.81 (s, 3H), 6.31 (t, J = 2.2, 1H), 6.44 (d, J = 2.4, 2H), 6.50 (s, 4H). ^{13}C-NMR: δ 55.3, 56.0, 61.0, 99.8, 106.2, 106.7, 130.0, 130.5, 139.3, 152.9, 160.7.

3,3',5-Trimethoxy stilbenes (9d, 10d): Obtained from 3,5-dimethoxybenzyltriphenylphosphonium bromide (**7a**, 200 mg, 0.4 mmol) and *m*-anisaldehyde (**8d**, 50 mg, 0.36 mmol) with NaH (10 mg, 0.43 mmol). Purification and separation by flash chromatography (petroleum ether/diethyl ether 95:5). *Cis/Trans* ratio: 1.5:2. Total yield 45%.

Trans (**9d**). Light yellow solid. M.p. 59-63°C. ^{1}H-NMR (CDCl$_3$, 200 MHz) δ 3.84 (s, 9H), 6.40 (t, J = 2.2, 1H), 6.67 (d, J = 2.2, 2H), 6.79-6.85 (m, 1H), 7.04 (s, 3H), 7.08-7.12 (m, 1H), 7.23-7.27 (m, 1H). ^{13}C-NMR (CDCl$_3$, 200 MHz): δ 55.3, 55.4, 100.1, 104.7, 111.8, 113.5, 119.4, 129.0, 129.2, 129.7, 138.6, 139.3, 160.0, 161.0.

Cis (**10d**). Yellow oil. ^{1}H-NMR (CDCl$_3$, 200 MHz): δ 3.64 (s, 6H), 3.68 (s, 3H), 6.31 (t, J = 2.2, 1H), 6.42 (d, J = 2.4, 2H), 6.52 (d, J = 12.2, 1H), 6.59 (d, J = 12.2, 1H) 6.71-6.88 (m, 3H), 7.11-7.19 (m, 1H). ^{13}C-NMR (CDCl$_3$, 200 MHz): δ 55.2, 55.3, 99.9, 106.8, 113.4, 113.9, 121.6, 129.2, 130.5, 130.6, 138.6, 139.1, 159.4, 160.6.

4-(Benzyloxy)benzyl alcohol (21): A solution of benzaldehydes **20 (**10 mmol) in THF **(**25 ml**)** was added dropwise to a well-stirred suspension of sodium borohydride **(**10 mmol) in THF **(**50 mL). The reaction mixture was stirred at room temperature for 4 h and then quenched by the dropwise addition of water **(**10 mL). The resulting reaction mixture was passed through a Celite pad. The filtrate was dried over anhydrous sodium sulphate, and the solvent was evaporated to give the corresponding alcohols **21** as white needles**.** Yield 92%: ^{1}H NMR (CDCl$_3$, 200 MHz) δ 2.70 (br s, 1H), 4.49 (s, 2H), 5.03 (s, 2H), 6.92 (d, *J*= 8.3 2H), 7.20 (*J* = 8.3 2H), 7.40 (m, 5H).

4-(Benzyloxy)benzyl bromide (22): Phosphorous tribromide (10 mmol) was added to a well-stirred solution of benzyl alcohol **21** (10 mmol) in dry methylene chloride (45 ml) at 0 °C under argon. The stirring was continued for 2 h at 0 °C and at room temperature for 1 h. The reaction mixture was poured onto ice-water (200 ml), warmed, and extracted with diethyl ether. The ether layers were combined and dried over anhydrous sodium sulphate. Evaporation of the solvent gave the respective bromides **22** as white needles**. (**yield 92%). ^{1}H NMR (CDCl$_3$, 200 MHz) δ 4.49 (s, 2H), 5.06 (s, 2H), 6.95 (d, *J* = 8.3, 2H) 7.37 (d, *J*=8.3, 2H), 7.40 (m, 5H).

Diethyl [4(benzyloxy)benzyl]phosphonate (23): Freshly distilled triethyl phosphate (2.49 g, 15 mmol) was added to the benzyl bromides **22** (10mmol) containing a catalytic amount of tetrabutylammonium iodide, and the resulting mixture was heated at 110-130 "C for 10 h. Excess triethyl phosphite was removed by heating for 3 h at 55 "C under vacuum (0.5 mmHg) to yield the resulting phosphonate esters **23** as yellow oil (yield 94%). ^{1}H NMR (CDCl$_3$, 200 MHz) δ 1.26 (t, *J* = 7.4, 6H), 3.08 (d, *J*=1.6, 2H), 3.99 (quint, J= 7.4, 4H), 5.02 (s, 2H) ,6 .89 (d, *J*= 8.3, 2H), 7.41 (d, *J*= 8.3, 2H), 7.5 (m, 5H).

General procedure for the preparation of stilbenes 25a,b: To a solution of 4-Benzyloxybenzylphosphonic acid diethyl ester (**23**, 1 equiv) in dry tetrahydrofuran, NaH (2 equiv.) and aldehyde **24a,b** (1 equiv.) were added at 0°C and the solution stirred at room temperature overnight. The reaction was quenched with water and poured into a water/ice mixture and extracted with ethyl acetate. The organic phases were collected, washed with brine and dried over anhydrous sodium sulphate. After removal of the solvent the crude material was purified by chromatography giving only *trans* isomers **25a,b**.

25a: Yield 35%. Colourless solid. M.p. = 144-147°C. ^{1}H-NMR (CDCl$_3$, 200 MHz): δ 2.27 (s, 3H), 2.29 (s, 3H), 5.09 (s, 2H), 6.93 (d, J=16.4, 1H), 6.96-6.99 (m, 2H), 7.02 (d, J=16.4, 1H), 7.11 (d, J = 8, 1H), 7.22-7.28 (m, 2H), 7.32-7.46 (m, 7H).

25b: Yield 42%. Colourless solid. ^{1}H-NMR (CDCl$_3$, 200 MHz): δ 2.16 (s, 3H), 2.24 (s, 3H), 4.98 (s, 2H), 6.64-6.67 (m, 2H), 6.92 (s, 1H), 7.03-7.17 (m, 9H), 7.40-7.44 (m, 2H).

General procedure for the cleavage of the benzyl group (Stilbenes 26a,b): *N,N*-dimethylaniline (3.0 equiv.) was added to a stirred solution of **25a,b** (1.0 equiv.) in dry methylene chloride under a argon atmosphere at 0°C. After 5 min, anhydrous AlCl$_3$ (4.0 equiv.) was added in one portion. After 2-8 h, the reaction mixture was cooled and a 5% HCl acqueous solution was added. The resulting mixture was extracted with ethyl acetate, and the combined extracts were washed with brine. Removal of solvent *in vacuo* from organic phase yielded the crude hydroxystilbene **26a,b**, which were purified by flash chromatography (petroleum ether/ethyl acetate)

26a: Yield 53%. Red solid. M.p. = 150-153°C. ^{1}H-NMR (CDCl$_3$, 200 MHz): δ 2.27 (s, 3H), 2.29 (s, 3H), 4.76 (s, 1H), 6.82 (d, J = 8.6, 2H), 6.92 (d, J = 16.4, 1H), 7.00 (d, J = 16.4, 1H), 7.10 (d, J = 8, 1H), 7.22-7.27 (m, 2H), 7.39 (d, J = 8, 2H). ^{13}C-NMR (CDCl$_3$, 200 MHz): δ 19.6, 115.6, 123.8, 126.8, 127.0, 127.6, 127.8, 130.0, 135.3.

26b: Yield 55%. Colourless solid. ^{1}H-NMR (CDCl$_3$, 200 MHz): δ 2.16 (s, 3H), 2.24 (s, 3H), 6.50 (bs, 1H), 6.63 (d, J=2.82, 2H), 6.92-7.12 (m, 5H), 7.45 (d, J=1.88, 2H).

^{13}C-NMR (CDCl$_3$, 200 MHz): δ 19.5, 115.5, 124.4, 127.8, 128.2, 130.1, 134.7, 135.0, 135.9, 136.3, 157.2.

General procedure for the preparation of the stilbenes in solid phase (triphenylphosphine resin method, Scheme 2).

To a suspension of commercial triphenylphosphine polymer bound (**11**, 1 equiv.) in dimethylformamide, 3,5-Dimethoxybenzylbromide (**7a**, 3 equiv.) was added, and the mixture was stirred at 100°C for 16 h. The reaction was filtered and the resin was washed with water, dimethylformamide, methanol, dichloromethane, diethyl ether and dried. The resulting derivatized resin was suspended in dry tetrahydrofuran (1 equiv.), TBD (3 equiv.) and aldehydes (**8a-d**, 3 equiv.) were added. The mixture was stirred under reflux for 16 h, then filtered and washed with methanol and methylene chloride. After removal of the solvent the crude material was purified by flash chromatography to give *cis* **10a-d** and *trans* **9a-d** stilbenes. Yields are calculated on loading of triphenylphosphine into the resin starting material.

Compounds **9a, 10a**: reaction of 3,5-dimethoxybenzyltriphenylphosphonium bromide polymer bound (180 mg, 0.18 mmol der., 1 equiv.) and 4-nitrobenzaldheyde (82 mg, 0.54 mmol, 3 equiv.) in presence of TBD (75 mg, 0.54 mmol, 3 equiv.). *Cis/trans* ratio: 1:3. Total yield 29%

Compounds **9b, 10b**: reaction of 3,5-dimethoxybenzyltriphenylphosphonium bromide polymer bound (400 mg, 0.4 mmol der., 1 equiv.) and *p*-anisaldehyde (163 mg, 1.2 mmol, 3 equiv.) in presence of TBD (167 mg, 1.2 mmol, 3 equiv.). *Cis/trans* ratio: 1.5:2. Total yield 15%.

Compounds **9c, 10c**: reaction of 3,5-dimethoxybenzyltriphenylphosphonium bromide polymer bound (400 mg, 0.4 mmol der., 1 equiv.) and 3,4,5-trimethoxybenzaldehyde (235 mg, 1.12 mmol, 3 equiv.) in presence of TBD (156 mg, 1.12 mmol, 3 equiv.). *Cis/trans* ratio: 1:2.5. Total yield 34%.

Compounds **9d, 10d**: reaction of 3,5-dimethoxybenzyltriphenylphosphonium bromide polymer bound (580 mg, 0.58 mmol der., 1 equiv.) and *m*-anisaldehyde

(237 mg, 1.74 mmol, 3 equiv.) in presence of TBD (242 mg, 1.74 mmol, 3 equiv.). *Cis/trans* ratio: 1.5:2. Total yield 30%.

Preparation of 4-hydroxy-stilbene 5g in solid phase (Wang-bromo resin method, Scheme 4). **4-Benzyloxybenzylphosphonic acid diethyl ester polymer bound (18)**: To a suspension of commercially available (4-Benzyloxybenzyl)-bromide polymer bound (**13**, 1 equiv.) in toluene triethyl phosphite was added (3 equiv.) and the mixture was stirred under reflux for 16 h. Then, the derivatized resin was filtered and washed with water, dimethylformamide, methanol, dichloromethane and diethyl ether and dried.

(*E*)-4-Hydroxy-4'-nitrostilbene (26a): to a suspension of (4-Benzyloxybenzyl)-phosphonic acid diethyl ester polymer bound (**18**, 1 equiv.) in dry tetrahydrofuran, TBD and *p*-nitrobenzaldehyde (**8a**) were added and the reaction was stirred at reflux for 16 h. The mixture was filtered and washed with water, dimethylformamide, methanol, dichloromethane, diethyl ether and dried. The resulting derivatised resin was stirred in a solution of trifluoroacetic acid/dichloromethane 65:35 for 3 h at room temperature. After filtration, the resin was washed with methanol and methylene chloride and the solvent was evaporated in *vacuo*. The resulting crude material was purified by chromatography on silica gel.

Purification by flash chromatography (petroleum ether/ethyl acetate 9:1). Yield 50 % of red solid.

Biology

Cells. Continuous neoplastic cells HL60 (myeloblastic acute leukemia) were grown in RPMI 1640 (Gibco Grand Island, NY, USA) containing 10% FCS (Gibco), 100 U/mL penicillin (Gibco), 100 µg/ml streptomycin (Gibco), and 2mM L-glutamine (Sigma Chemical Co, St Louis, MO) in a 5% CO_2 atmosphere at 37 °C.

Cytotoxicity assays. To evaluate the number of live and dead neoplastic cells, the cells were stained with trypan blue and counted on a hemocytometer. To determine the growth inhibitory activity of the drugs tested, $2x10^5$ cells were plated into 25 mm wells (Costar, Cambridge, UK) in 1 mL of complete medium and treated with different concentrations of each drug. After 48 h of incubation, the number of viable cells was determined and expressed as percent of control proliferation.

Morphological evaluation of apoptosis and necrosis. Drug induced apoptosis and necrosis was determined morphologically after labelling with acridine orange and ethidium bromide. Cells ($2x10^5$) were centrifuged (300 g) and the pellet was resuspended in 25 µL of the dye mixture. Ten µL of the mixture was examined in oil immersion with a 100x objective using a fluorescence microscope. Live cells were determined by the uptake of acridine orange (green fluorescence) and exclusion of ethidium bromide (red fluorescence) stain. Live and dead apoptotic cells were identified by perinuclear condensation of chromatin stained by acridine orange (100 µg/mL) or ethidium bromide (100 µg/mL), respectively, and by the formation of apoptotic bodies. The percentage of apoptotic cells was determined after counting at least 300 cells.

Determination of apoptosis by Annexine V. Cells ($1x10^6$) were washed with PBS and centrifuged at 200 g for 5 minutes. Cell pellets were suspended in 100 µL of staining solution containing FITC-conjugated Annexine-V and propidium iodide (Annexine-

V-Fluos Staining Kit, Roche Molecular Biochemicals, Mannheim, Germany) and incubated for 15 minutes at 20 C°: Annexine V positive cells was evaluated by flow cytometry Becton Dickinson, San Jose, CA).

Flow cytometry analysis of cell cycle and apoptosis. Cells were washed once in ice-cold PBS and resuspended at concentration of $1x10^6$/mL in a hypotonic fluorochrome solution containing propidium iodide (Sigma) 50 µg/mL in 0.1% sodium citrate plus 0.03% (v/v) nonidet P-40 (Sigma). After 30 minutes of incubation, the fluorescence of each sample was analysed as single-parameter frequency histograms by using a FACScan flow cytometer (Becton Dickinson). The distribution of cells in the cell cycle was analysed with the ModFit LT program (Verity Software House, Inc) and apoptosis was determined by evaluating the percentage of hypoploid nuclei accumulated in the sub-G_0-G_1 peak after labeling with propidium iodide.

2.5. Development of stilbenes optimization

In this PhD thesis and in previous works of my research group are described different series of stilbene derivatives with proapoptotic activity. The best results were obtained by *cis*-3,4′,5-trimethoxy-3′-aminostilbene (**27**, and in previous works called **5c**, Figure **4**).

27 (5c)
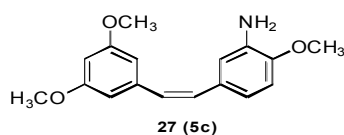
Figure 4. *cis*-3,4′,5-trimethoxy-3′-aminostilbene: the best candidate for optimization

This compound shows a proapoptotic activity and is a colchicine site microtubule inhibitor,[25] is highly potent against various tumor cells and blocks cell cycle progression in G2-M phase; is tolerated in mice up to 100 mg/kg, and no major organ toxicity was observed. In particular, there was no bone marrow toxicity, and the ability of bone marrow engraftment was not affected by stilbene **5c** treatment.[29] Stilbene **5c** can selectively suppress tumor vascular perfusion without damaging normal vascular perfusion in a DCE-MRI study. Most importantly, mice treated with 5 daily injection of stilbene **5c** did not show any compromise in heart function, suggesting that stilbene **5c** may be superior to existing VDAs by it low cardiac toxicity. Thus, we selected this derivative as lead compound to optimize for further investigations.

In this purpose, we tried to improve two aspects of our lead, the biological activity and water solubility. In our previous study[29], stilbene **5c** was made as an HCl salt form to enhance water solubility, which was sufficient to carry out animal experiment but it is still an issue for drug formulation.

We used two approach to optimize the stilbene **5c**: the first was computer-based drug design and synthesis of other derivatives; the second was to make prodrugs as it was done in ZD6126 and CA4P. Both of them are attached to a phosphate group to make a prodrug to enhance their water solubility, and the added phosphate group could be activated by removing the phosphate group.[30] Prodrugs are pharmacologically inactive drug derivatives that must undergo a chemical or biochemical transformation in order to be active in the body and exert the desired pharmacological effect of the parent drugs. Conversion to the active drugs can occur before, during or after absorption, or at any specific site in the body. The major goal in designing prodrugs is to overcome the various physicochemical and pharmacokinetic limitations of the parent drugs which compromise their clinical application.

2.5.1. The first approach: computer-based drug design

With the aim to design the new derivatives we started by docking model of stilbene **5c** into tubulin, observing that there is enough space in the colchicine binding pocket to accommodate a molecular design in the neighbor of the amino group. Thus, We converted the amino group and the methoxyl groups of the phenyl ring into a 5-atom ring structure to make into a pyrrole or imidazole ring. Combined with the existing benzyl ring, they will make a structure of indole or benzimidazole. The advantage of this modification is to remove the methoxy group that is highly hydrophobic. The added nitrogen allows formation of a hydrogen bond withVal-315 of tubulin (**Fig. 5**), which may potentially enhance the binding affinity and improve water solubility. We also added a methyl group to the nitrogen of the indole or benzimidazole to recapitulate the methoxy group and compare their biological activity with their parent molecules without methyl group. If the addition of methyl group lead to a better biological activity, it would suggest that the hydrophobic interaction in this pocket is absolutely essential.
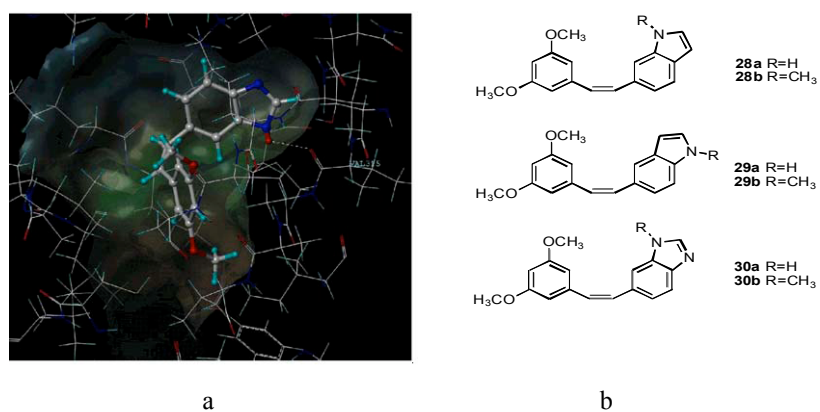

a   b

Fig. 5. **a** Computer based design and synthesis of stilbene derivatives. **b** Structures of the six new derivatives.

These compounds were synthesized by classical Wittig reaction (**Scheme 3**):

a: R=H, X=C, Y=CHO, Q=H
b: R=CH₃, X=C, Y=CHO, Q=H
c: R=H, X=C, Y=H, Q=CHO
d: R=CH₃, X=C, Y=H, Q=CHO
e: R=H, X=N, Y=CHO, Q=H
f: R=CH₃, X=N, Y=CHO, Q=H
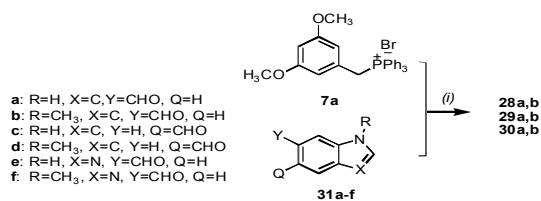
Scheme 3. Synthesis of optimized compounds.

Thus, we tested the new compounds in UCI-101 ovarian cancer cells, MDAMB231 ovarian cancer cells and MiaPaCa2 pancreatic cancer cells. IC_{50} of each compound was determined using Alamar Blue staining and the results were very similar among the three cells.
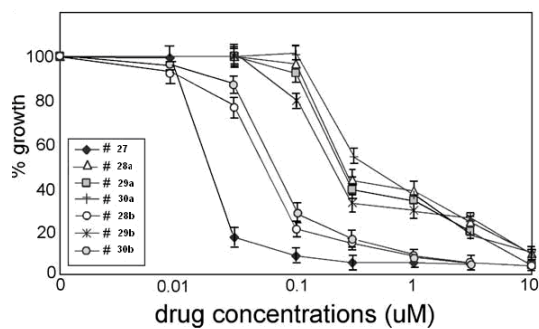
Fig.6

Compound	IC_{50} (nM)	Compound	IC_{50} (nM)	Compound	IC_{50} (nM)
28a	250	**29a**	250	**30a**	260
28b	60	**29b**	200	**30b**	80

Table 3. IC_{50} against UCI-101 ovarian cancer cells.

The compounds with a methyl group exhibited a better biological activity compared with those without methyl group (**Table 3**). The compound with the methyl group at the *cis* side of the molecule has a better cytotoxic activity compared with that with methyl group at the *trans* location. Addition of second nitrogen to make into benzimidazole rather than indole does not change the biological activity. Similar studies were performed in other cell lines, including MDA-MB231 breast cancer cells, MiaPaCa2 pancreatic cancer cells and A549 non-small cell lung cancer cells and the results are similar. However, water solubility of compounds with or without a methyl group turns out to be worse than stilbene **5c** and not optimal for further development.

2.5.2. The second approach: synthesis of prodrugs

With the aim to improve water solubility of stilbene **5c** we choose to synthesize some its prodrug derivatives. This was the strategy used to solve the water solubility problem of CA4 and ZD6126 by adding a phosphate group. Different water soluble side chains were added through two different linkages with the free amino group of stilbene **5c**. The side chains used for enhancing water solubility are a morpholino group linked to the amino group by either carbamate (**PD7**) or urea (**PD6**) linker, and a triethylene glycol linked by carbamate linker (**PD5**) (**Fig. 7**).
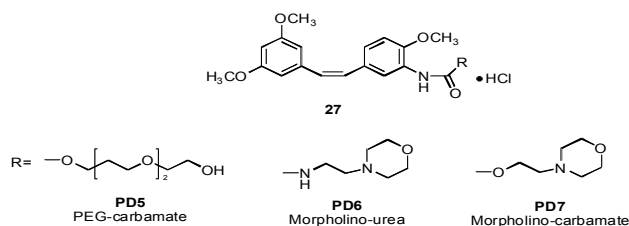
Fig 7 Structure of synthesized prodrugs derivatives

The synthesis of these new compounds was conducted as shown in **Scheme 4**. Stilbene **5c** was firstly reacted with one equivalent of trichloroethyl chloroformate in dioxane at 60°C for 3 h to give a crude isocyanate. To the latter crude isocyanate solubilized in dry dioxane, the appropriate nocleophile was added portionwise. The reaction was heated at 60°C for 12 h. After cooling down to room temperature, the mixture was concentrated in vacuo and the residue was purified by flash chromatography on silica gel to afford expected derivative.
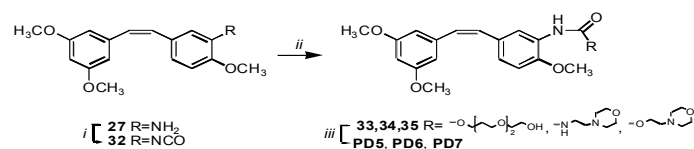
Scheme 4. Reagents and conditions: (*i*) Trichloromethyl chloroformate, dioxane, 60°C, (*ii*) triethylen glycol or 4-aminoethyl-morpholine or 4-hydroxyethyl-morpholine, dioxano, 60°C, (*iii*) HCl/Ethyl acetate or HCl/Methanol or HCl 10% in aqueous solution.

Then, to hydrochloride formation, the free bases were treated with a solution of chloridric acid in ethyl acetate or methanol to prevent the carbamate or urea hydrolysis; however, the derivatives stability was maintain also using an aqueous solution.

These three prodrugs were tested in UCI-101 cells for their IC50 in vitro. Only **PD7** was active in suppressing growth of tumor cells at a concentration of 3 μM, which is 100 times higher than the active form stilbene **5c**. Both **PD5** and **PD6** were not able to induce significant killing even at concentration up to 3 μM, suggesting that their activity is inferior compared with **PD7** (**Fig. 8**).
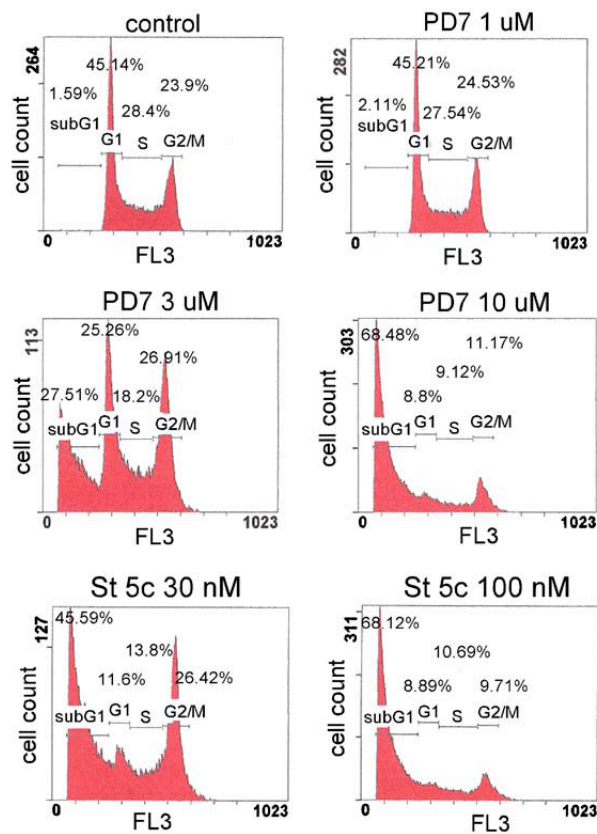
Fig 8. Cell cycle effect of PD7 on UCI-101 cells.

This could be due to the fact that prodrugs may not be converted into the active form stilbene **5c** in tissue culture condition, and the intact prodrugs could never be fit into the colchicine-binding pocket due to their bulky side chains added for improving water solubility. Incubation of the three prodrugs with serum for 1 h followed by addition into the culture cells was not able to enhance their activity, suggesting that the prodrug conversion is dependent on the presence of cells.

86

With these results in hand, we decided to perform further studies on **PD7**. In order to test whether **PD7** induces cell death through the same mechanism as its active form stilbene **5c**, cell cycle analysis in UCI101 cells was done after cells are treated with stilbene **5c** or **PD7**. At 1 μM **PD7** had no effect in cells cycle progression. At 3 μM (IC50), **PD7** induced significant G2/M arrest and a subG1 population that represents cell death. Further increase of **PD7** concentration to 10 μM leads to near complete cell death. These findings are very similar to what we observed with stilbene **5c** except that higher concentrations (100 folds higher than stilbene **5c**) of **PD7** were required (**Fig. 9**).
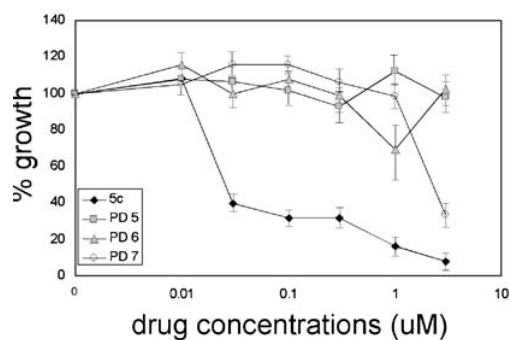
Fig.9 Suppression of tumor growth by prodrugs.

To get a better assessment of mitotic arrest by either agent, cells treated with either stilbene **5c** or **PD7** were stained with phospho-histone 3b, a mitotic marker. The result showed an increase in the positive stained cells after either treatment (**Fig. 10**), confirming the mitotic arrest shown in cell cycle analysis.

Same studies was done in other tumor cells including A549 lung cancer, MDA-MB231 breast cancer, HCT116 colon cancer cells with similar IC_{50}.
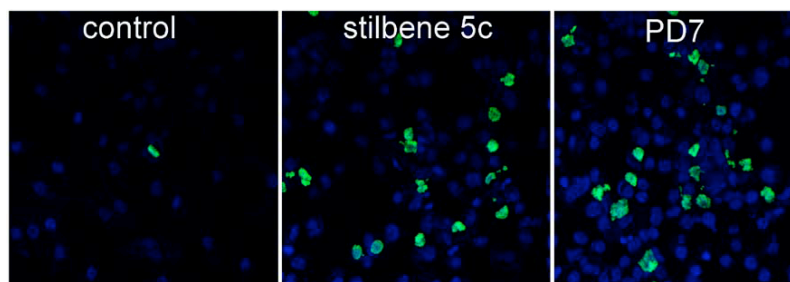
Fig.10 Immunofluorescence staining of mitotic cells**.**

After these tests, we investigate the effects of our prodrug on microtubule pattern. Because UCI-101 cells have scant cytoplasm and not ideal for examination of tubulin, MDAMB231 breast cancer cells were used instead and treated with vincristine, stilbene **5c**, **CA4** or **PD7**. Microtubule in cells treated with all microtubule inhibitors exhibited a disrupted pattern compared with a fine reticular network in control cells (**Fig. 11**).
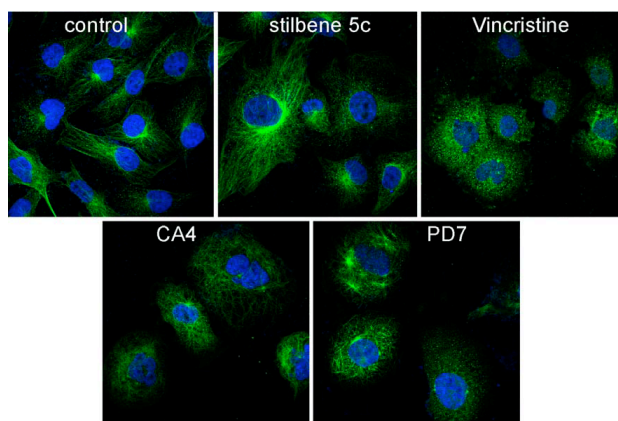
Fig 11. Disruption of microtubule

Thus, both **PD7** and stilbene **5c** are tubulin inhibitors, and are expected to disrupt mitotic spindle formation and stop cell cycle progression in the G2/M stage, as shown in flow cytometry studies. It is interesting that when cells was treated with **PD7** showed multiple microtubule organization centre, which was not seen in cells treated with other microtubule-interfering agents, probably due to prodrug nature of this compound and a slow release of active drug.

To carry on our study, we investigate the signalling pathway in cells after **PD7** treatment analyzing cell lysates by western blotting using antibodies against various kinases. UCI-101 cells were treated with stilbene **5c** (100 nM), **PD7** (3 μM) or **CA4** (10 nM) and harvested at a time course (0, 4, 8, 16, and 36 h) for this study. Phosphorylation of Cdc2, a kinases controlling cell cycle progression, was significantly suppressed after incubation with **PD7** for 36 h (**Fig. 12**).

Fig.12. Signaling events induced by various anti-mitotic agents

The total Cdc2 protein level also decreased at 36 h, but not as prominent. This finding is consistent with the cell cycle arrest in mitotic phase after treatment (**Figure 2b**). Similar finding was seen in cells treated with stilbene **5c** and **CA4**. The phosphorylation status of MAPK, Chk1 and Chk2 was investigated next. Phosphorylation of Chk2 appears to increase after cells were treated with any of the three agents, and the effect of **PD7** appears most prominent. No significant difference was detected in total protein or phos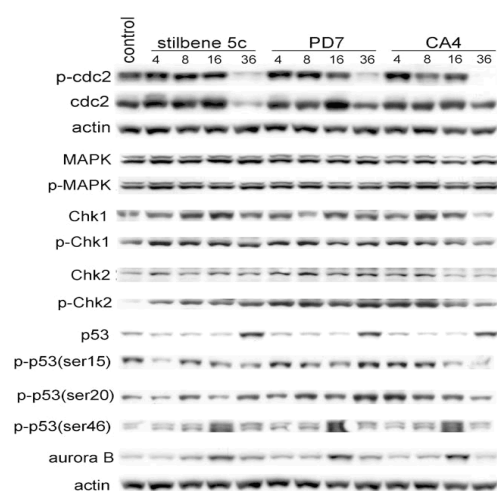phorylation status of MAPK and Chk1. Total protein level of p53 did not change in the first 16 h after treatment but increased dramatically at 36 h. Examination of phosphorylation of ser15, ser20, and ser46 in p53 showed that ser46 exhibited a transient increase at 16 h but then back to baseline at 36 h. Finally the total amount of aurora B kinase has a same transient increase at 16 h as phosphorylation of p53 at ser 46.

Thus, with the aim to confirm the conversion of **PD7** in **5c**, we started a set of in vivo tests. Firstly, we injected **PD7** (100 mg/kg) intravenously into BALB/c mice, collected blood in three different time points, and, after separation and analysis by LC/MS/MS, we saw that the improvement of concentrations ratio of **5c** versus **PD7** was about 4.7% during the time, confirming the prodrug nature of **PD7**. Thus, we investigated its tolerability in mice. Since **PD7** is fully water soluble, it was dissolved in normal saline and injected intravenously into BALB/c mice at the same dose of 100 mg/kg. Mice tolerated the same dose well without any evidence of toxicity. When the dose of **PD7** was increased to 330 mg/kg, mice died at 3rd day, indicating that the maximal tolerated dose is in the 100–330 mg/kg range.

The in vivo efficacy of **PD7** was then investigated using nude mice with tumor xenograft derived from UCI-101 cells. Mice with tumor xenografts were treated with stilbene **5c**, **PD5** or **PD7** at 25 mg/kg by intraperitoneal injection three times a week for total 7 doses and compared with control group treated with normal saline. Tumor sizes were calculated by the long and short axes. Mouse weight and behavior did not suggest any sign of toxicity. Neither stilbene **5c** nor **PD5** showed any tumor growth suppression when mice were treated by a schedule of three times a week. There was 20–30% tumor growth suppression in mice treated with **PD7** (**Fig 12**).
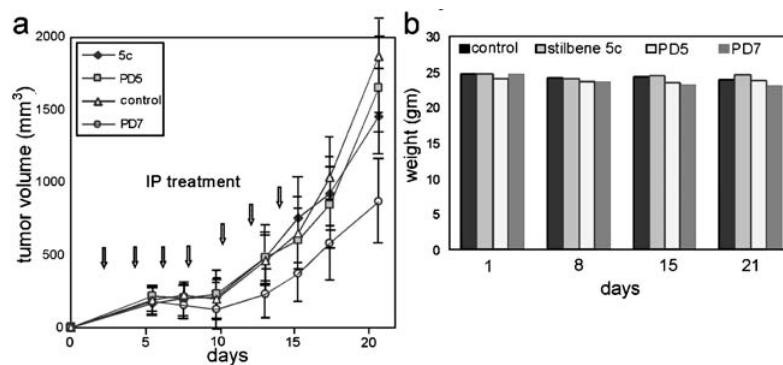
Fig.12. **a**) Suppression of tumor growth by single agent. **b**) No weight change after treatment.

With these results in hand we can assert that this derivative had a marginal benefit in therapy used a singlet agent. Thus, we started to study the its biological activity in association with other drugs. At this purpose we chose Bevacizumab (monoclonal antibody, a VEGF) as ideal candidate; in fact, this strategy has previously been successfully with stilbene **5c** and is based based on the rationale that VDAs induce tumor hypoxia and release of VEGF to mobilize bone marrow endothelial progenitor cells for repair. Addition of a VEGF inhibitor could potentially prevent the effect due to the surge of VEGF after VDAs treatment. Mice were treated with **PD7** intraperitoneally at 25 mg/kg per day 5 days a week with or without bevacizumab intravenously at 10 mg/kg twice a week. Each group had 8 mice for statistical analysis. Treatment was continued for 2 weeks. Tumor growth was evaluated by measuring the long and short axes to calculate the volume. In this set of experiment, **PD7** by itself had a very weak effect compared with the control group and show minimal benefit in suppressing tumor growth. Mice treated with bevacizumab along showed a tumor growth suppression of about 60%. Mice treated with combination of **PD7** and bevacizumab showed a robust tumor growth suppression up to 80%, indicating that **PD7** have a synergistic effect with bevacizumab similar to stilbene **5c** (**Fig. 13**).
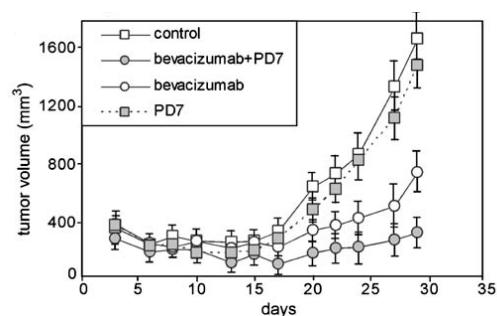
Fig. 13. Synergistic effect of PD7 and bevacizumab.

Thus, in this thesis work, we developed an optimization of a stilbene derivative with strong activity, but low solubility and some undesired effect. We used two different approaches, the first was based on computer design, and the elimination of a methoxyl group enhance the water solubility, decreasing, however, the biological activity. The second approach was based on the preparation of prodrugs derivatives, a successful strategy for CA4P and ZD6126. In these cases the addition of phosphate group enhance the solubility and lead these drugs to finish the phase I clinical trials, rendering the CA4P and ZD6126 the most advanced agents in clinical development as VDAs for cancer therapy.

Here, instead of phosphate group, we chose an urea and two carbamates linkages, and the best results was obtained by a morpholino-carbamate group that solve completely the problem of solubility. The product **PD7** is completely water soluble, which will greatly help drug formulation. The carbamate can be hydrolyzed to release the morpholino group in a cell-dependent manner because incubation with serum for 1 h before adding to tissue culture cells did not change the biological activity of **PD7**. The biological activity of **PD7** was 100 folds less effective in vitro but has a similar potency compared to stilbene **5c** in tumor xenografts. We also confirmed that **PD7** can be converted into stilbene **5c**, although the ratio between stilbene **5c** and **PD7** is about 5%. **PD7** may have another advantage in slower release of active stilbene **5c** to further minimize any potential side effect. The carbamate

92

linkage can be hydrolyzed in circulation without enzymatic reaction, the byproduct morpholino group is a small molecule and is expected to be excreted in kidney in a short period of time.

The cell cycle analysis and microtubule staining assays proved that **PD7** and stilbene **5c** have similar mechanism of action in disrupting microtubule. We did notice a minor difference in one of the **PD7** treated cells, which shows multiple microtubule organizing centers. The significance of this finding is not clear, perhaps it is due to lower activity in inducing microtubule depolymerization without affecting the proliferation of organization centers. Several cell signalling mediators are all similar in their changes after treatment with **5c** and its prodrug. These findings support that the effect of **PD7** is mediated by its conversion into active stilbene **5c** to suppress mitotic spindle formation.

The biological activity of **PD7** by itself is not very active similar to stilbene **5c** in barely suppressing tumor growth. However, similar to the situation of stilbene **5c**, the effect is much more robust when combined with the VEGF inhibitor bevacizumab. The reason for the synergistic effect between **PD7** and bevacizumab should be similar to that of stilbene **5c**. **PD7**/stilbene **5c** induces tumor hypoxia by damaging tumor vasculature. The hypoxia environment in tumor lead to production of VEGF to induce proliferation and mobilization of bone marrow endothelial progenitor cells, which will be responsible to home in tumor vessels that are stripped off endothelial cells to reestablish tumor vasculature. Blocking the effect of VEGF will prevent the surge of endothelial progenitor cells immediately after **PD7**/stilbene **5c** administration and enhance the therapeutic efficacy of **PD7**/stilbene **5c**.

Finally, The fact that **PD7** is not active by itself could a potential benefit of **PD7** in cardiac toxicity noted in many other VDAs. Although animal study of stilbene **5c** did not reveal any compromise in cardiac function after daily IP injection for 5 days[31], stilbene **5c** is still a potent cell death inducer of human umbilical vein endothelial cells (HUVECs). This means that stilbene **5c** in circulation could still have the potential to induce normal endothelial damage.

93

Thus, the prodrug **PD7** in a soluble form and slow conversion, could strongly decrease the undesired side effects of stilbene **5c**, improving their activity. Hence, **PD7** can be a very attractive candidate for further clinical and pre-clinical investigations in cancer therapy.

General procedure for the synthesis of stilbenes 28-30a,b and trans isomers.

To a solution of opportune aldehyde (**31a-f**, 2 mmol) in 10 mL of anhydrous THF, the appropriate phosphonium salt **7a** (2,2 mmol) was added in one portion. The suspension was cooled in an ice bath and NaH was added (50% in mineral suspension, 2.2 mmol). The reaction mixture was then stirred at room temperature for 24 h, filtered on a Celite bed and washed with THF. After solvent evaporation, the residue was solubilized with methylene chloride (15 mL) and washed with water (5 mL) and brine (5 mL), then dried and evaporated again. The residue was purified and the mixture of Z and E isomers separated by flash chromatography on silica gel.

(Z)-6-[2-(3,5-Dimethoxyphenyl)-ethenyl]-1H-indole (28a). Eluent: Diethyl ether–light petroleum 3:7; Yield 29%. ^{1}H NMR (CDCl$_3$, 400 MHz) δ: 3.61 (s, 6H), 6.31 (t, J=2.4, 1H), 6.47–6.51 (m, 4H), 6.72 (d, J=12.4, 1H), 7.08 (dd, J=1.6, J=8.0 1H), 7.17–7.18 (m, 1H), 7.32 (s, 1H), 7.49 (d, J=8.0 1H), 8.05 (br, 1H). ^{13}C NMR (CDCl$_3$, 400 MHz) δ: 55.3, 99.8, 102.7, 106.8, 111.4, 120.3, 121.6, 124.9, 127.3, 128.7, 131.8, 139.9, 160.6. Anal. Calcd for C$_{18}$H$_{17}$NO$_2$: C, 77.40; H, 6.13; N, 5.01. Found: C, 77.24; H, 6.12; N, 4.99.

(Z)-6-[2-(3,5-Dimethoxyphenyl)-ethenyl]-1-methylindole (28b). Oil, 270 mg. Yield 30% ^{1}H NMR (CDCl$_3$, 400 MHz) δ: 3.62 (s, 6H), 3.68 (s, 3H), 6.33 (t, J=2.2, 1H), 6.41 (d, J=3.2, 1H), 6.45 (d, J=3.2, 1H), 6.50–6.54 (m, 3H), 6.74 (d, J=12.0, 1H), 7.02 (d, J=3.2, 1H), 7.09 (d, J=8.4, 1H), 7.46 (d, J=8.4, 1H). ^{13}C NMR (CDCl$_3$, 400 MHz) δ: 32.7, 55.3, 99.8, 100.0, 101.0, 106.8, 109.8, 120.3, 121.0, 128.6, 129.5, 131.9, 139.9, 160.6. Anal. Calcd for C$_{19}$H$_{19}$NO$_2$: C, 77.79; H, 6.53; N, 4.77. Found: C, 77.93; H, 6.55; N, 4.76.

(Z)-5-[2-(3,5-Dimethoxyphenyl)-ethenyl]-1H-indole (29a). Eluent: Diethyl ether–light petroleum 3:7; Yield 27%. ^{1}H NMR (CDCl$_3$, 400 MHz) δ: 3.61 (s, 6H), 6.31 (t, J=2.4, 1H), 6.43–6.49 (m, 3H), 6.73 (d, J=12.2, 1H), 7.13–7.18 (m, 3H), 7.24 (d, J=8.8 1H), 7.60 (s, 1H), 8.10 (br, 1H). ^{13}C NMR (CDCl$_3$, 400 MHz) δ: 55.2, 99.7,

102.9, 106.8, 110.6, 121.5, 123.5, 124.5, 127.9, 128.1, 128.8, 132.0, 135.1, 139.8, 160.5. Anal. Calcd for $C_{18}H_{17}NO_2$: C, 77.40; H, 6.13; N, 5.01. Found: C, 77.15; H, 6.13; N, 5.00.

(Z)-5-[2-(3,5-Dimethoxyphenyl)-ethenyl]-1-methylindole (29b). Oil, 274 mg. Yield 28%. ^{1}H NMR (CDCl$_3$, 400 MHz) δ: 3.63 (s, 6H), 3.76 (s, 3H), 6.32 (t, J=2.2, 1H), 6.40–6.43 (m, 2H), 6.46–6.52 (m, 2H), 7.73 (d, J=12.2, 1H), 7.0 (d, J=2.2, 1H), 7.17–7.19 (m, 2H), 7.58–7.59 (m, 1H). ^{13}C NMR (CDCl$_3$, 400 MHz) δ: 33.0, 55.4, 99.7, 101.3, 104.7, 106.7, 108.8, 121.7, 123.0, 127.8, 129.1, 132.0, 139.9, 160.5. Anal. Calcd for $C_{19}H_{19}NO_2$: C, 77.79; H, 6.53; N, 4.77. Found: C, 77.95; H, 6.50; N, 4.76.

(Z)-5-[2-(3,5-Dimethoxyphenyl)-ethenyl]-1H-benzoimidazole (30a). Eluent: Diethyl ether–light petroleum 3:7; Yield 25% ^{1}H NMR (CDCl$_3$, 400 MHz) δ: 3.04 (br, 1H), 3.61 (s, 6H), 6.31 (t, J=2.2, 1H), 6.41 (d, J=2.2, 2H), 6.54 (d, J=12.2, 1H), 6.73 (d, J=12.2, 1H), 7.25–7.29 (m, 1H), 7.53–7.56 (m, 2H), 8.20 (s, 1H). Anal. Calcd for $C_{17}H_{16}N_2O_2$: C, 72.84; H, 5.75; N, 9.99. Found: C, 72.66; H, 5.76; N, 9.95.

(Z)-5-[2-(3,5-Dimethoxyphenyl)-ethenyl]-1methylbenzoimidazole (30b). Eluent: Diethyl ether–light petroleum 3:7; Yield 28% ^{1}H NMR (CDCl$_3$, 400 MHz) δ: 3.06 (br, 1H), 3.65 (s, 6H), 3,81 (s, 3H), 6.35 (t, J=2.2, 1H), 6.40 (d, J=2.2, 2H), 6.59 (d, J=12.2, 1H), 6.83 (d, J=12.2, 1H), 7.27–7.31 (m, 1H), 7.51–7.55 (m, 2H), 8.22 (s, 1H). Anal. Calcd for $C_{17}H_{16}N_2O_2$: C, 72.84; H, 5.75; N, 9.99. Found: C, 72.66; H, 5.76; N, 9.95.

Synthesis of isocyanate intermediate (32). To a mixture of amino stilbene **27**, free base (1.8 mmol, 519 mg) solubilized in dry dioxane (15 mL), trichloromethyl chloroformate (0.84 mmol, 105μl), was added in one portion. The mixture was heated at 60°C for 2 h. After cooling down to room temperature the mixture was concentrated in vacuo and the crude residue was used for the next reaction without any purification.

96

(Z)-{5-[2-(3,5-Dimethoxyphenyl)-ethenyl]-2-methoxyphenyl}carbamic acid 2-[2-(2-hydroxyethoxy)ethoxy]ethyl ester (PD5). To solution of triethylene glycol (TEG, 5 mmol, 0.67 ml) in dry dioxane (5 ml) the crude isocyanate **32** (0.49 mmol, 160 mg) dissolved in dry dioxane (3 ml) was added in one portion. The reaction mixture was heated at 60°C for 48 h. After cooling down to room temperature, the mixture was concentrated in vacuo and the residue was purified by flash chromatography (3% methanol/ dichloromethane) on silica gel to afford the expected compound 8c. Oil, 200 mg; Yield 89%. ^{1}H NMR (CDCl$_3$, 400 MHz) δ: 2.55 br, (1H), 3.61–3.76 (m, 16H), 3.81 (s, 3H), 4.29–4.34 (m, 2H), 6.30 (t, *J*=2.2, 1H), 6.43 (d, *J*=12.0, 1H), 6.44 (d, *J*=2.2, 2H), 6.53 (d, *J*=12.0, 1H), 6.56 (d, *J*=8.4, 1H), 6.92 (d, *J*=2.2, *J*=8.4, 1H), 7.93 (s, 1H), 8.02 (d, *J*=2.2, 1H). ^{13}C NMR (CDCl$_3$, 400 MHz) δ: 55.3, 55.8, 61.8, 64.0, 69.5, 70.4, 70.6, 72.5, 99.8, 106.7, 109.7, 119.3, 123.5, 127.3, 129.1, 130.1, 130.5, 139.4, 146.9, 153.2, 160.5. Anal. Calcd for C$_{24}$H$_{31}$NO$_8$: C, 62.46; H, 6.77; N, 3.04. Found: C, 62.67; H, 6.79; N, 3.05.

(Z)-1-{5-[2-(3,5-Dimethoxyphenyl)-ethenyl]-2-methoxyphenyl}-3-(2-morpholin 4-yl-ethyl)-urea hydrochloride salt (PD6). To a solution of crude isocyanate **32** (0.61 mmol, 200 mg) solubilised in dry dioxane (5 ml) 4-(2-aminoethyl) morpholine, (0.67 mmol, 88 mg) was added portionwise. The mixture was heated at 60°C for 12 h. After cooling down to room temperature, the mixture was concentrated in vacuo and the crude residue was purified by flash chromatography (3% methanol/dichloromethane) on silica gel to afford 105 mg of the expected title morpholine derivative. The compound (0.5 mmol, 220 mg) was dissolved in ethyl acetate and a slight excess of 0.1 N hydrochloride solution was added at 0°C. The mixture was stirred about 30 min at room temperature. The solvent was evaporated in vacuo and the solid residue was washed twice with few ml of diethyl ether to give 205 mg of title compound. Yield 70%. ^{1}H NMR (CDCl$_3$, 400 MHz) δ: 2.83–3.02 (m, 2H), 3.15–3.30 (m, 2H), 3.46–3.66 (m, 8H), 3.67–3.78 (m, 2H), 3.81 (s, 3H), 3.94–4.10 (m, 2H), 4.16–4.35 (m, 2H), 6.26 (t, *J*=2.4, 1H), 6.40 (d, *J*=12.6, 1H), 6.42 (d, *J*=2.4, 2H), 6.52 (d, *J*=12.6, 1H), 6.63, 6.67 (m, 1H), 6.90 (dd, *J*=1.6, *J*=8.4,

1H), 7.39 (s, 1H), 8.0 (s, 1H). ^{13}C NMR (CDCl$_3$, 400 MHz) δ: 36.0, 53.8, 55.8, 56.5, 60.2, 65.2, 100.8, 108.0, 111.4, 121.8, 125.1, 129.3, 130.4, 131.4, 131.7, 140.8, 149.5, 159.4, 162.2. Anal. Calcd for C$_{24}$H$_{32}$ClN$_3$O$_5$: C, 60.31; H, 6.75; Cl, 7.42; N, 8.79. Found: C, 60.18; H, 6.74; Cl, 7.40; N, 5.80.

(Z)-{5-[2-(3,5-Dimethoxyphenyl)-ethenyl]-2-methoxyphenyl} carbamic acid 2-morpholin-4-yl-ethyl ester, hydrochloride (PD7). To a solution of the crude isocyanate **32** (0.59 mmol, 180 mg) solubilised in dry dioxane (5 mL) the 4-(2-hydroxylethyl)morpholine, (0.6 mmol, 74 µl) was added portionwise. The mixture was heated at 60°C for 12 h. After cooling down to room temperature the mixture was concentrated in vacuo and the crude residue was purified by flash chromatography (3% methanol/dichloromethane) on silica gel to afford 117 mg of the expected desired carbamate. The compound (0.5 mmol, 220 mg) was dissolved in tetrahydrofuran (THF, 7 ml) and mixed with 0.1 N hydrochloride acid solution (a slight excess) in THF (5 ml). The hydrochloride salt **PD7** separates as a colorless solid that was filtrated and washed with 10 ml of THF to give 212 mg. Yield 75%. Mp 152–154°C. ^{1}H NMR (CDCl$_3$, 400 MHz) δ: 2.86–3.0 (m, 2H), 3.28–3.35 (m, 2H), 3.49 3.55 (m, 2H), 3.67 (s, 6H), 3.82 (s, 3H), 3.92–4.06 (m, 2H), 4.28–4.44 (m, 2H), 4.67–4.72 (m, 2H), 6.30 (t, J=2.2, 1H), 6.41 (d, J=2.2, 2H), 6.45 (d, J=12.0, 1H), 6.54 (d, J=12.0, 1H), 6.70 (d, J=8.2, 1H), 6.97 (dd, J=2.2, J=8.2, 1H), 7.42 (s, 1H), 7.92 (s, 1H), 13.45 (br, 1H). ^{13}C NMR (CDCl$_3$, 400 MHz) δ: 52.5, 55.3, 55.8, 56.6, 58.5, 63.6, 99.7, 106.7, 109.9, 119.4, 124.3, 126.5, 129.3, 129.9, 130.2, 139.3, 147.2, 152.1, 160.5. Anal. Calcd for C$_{24}$H$_{31}$ClN$_2$O$_6$: C, 60.18; H, 6.52; Cl, 7.40; N, 5.85. Found: C, 60.05; H, 6.53; Cl, 7.42; N, 5.84.

98

2.6. Terphenyl Derivatives

The research goal in the field of stilbene derivatives is to develop novel, potent and low toxic pro-apoptotic agents. The group where I stay during my PhD thesis has a strong experience in this field, and another approach to modify the stilbene motif to improve its potency is act on ethylenic-bridge. The substitution of this double bond with another phenyl moiety was saw to be often advantageous. Terphenyl structure is reported as part also of other interesting analogues of natural compounds active on cell cycle, such as resveratrol. Hence, we discovered that some terphenyl derivatives (**Fig.1**) led to a growth rate enhancement in the tested cell population with respect to control. Confirmation of such protective behaviour was found by testing these compounds on HL60 cells cultured with serum-free medium and, moreover, on neuronal cells exposed to proapoptotic agents.[32]
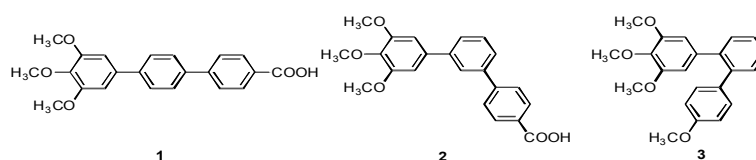
Fig.1. Known terphenyl derivatives endowed with cell growth-supporting activity.

To continue the search for structural modifications needed for new drugs active on cell cycle we therefore planned further modifications on the terphenyl backbone, present in the most active derivatives found in previous studies.

Starting from the previous active terphenyl derivatives (**Fig.1**) we decided three synthetic strategies: the substitution of trimethoxy-moiety with an 3-adamantyl-4-hydroxyphenyl group; the change of central phenyl ring with another heteroaromatic ring; the substitution of the carboxylic group with an amino one.

2.6.1. Chemistry

For the synthesis of these new terphenyl derivatives we decided to substitute the trimethoxy-moiety with an adamantanyl one, a substitution set recurring in known compound CD43714[33] and in more recent derivatives[34] that regulate the mechanisms promoting differentiation and/or apoptosis in several cancer cell lines. Moreover, we previously found that derivatives bearing such substitution are endowed with either agonistic or antagonistic behavior toward apoptotic induction.[35]

From a synthetic point of view, the preparation of these compounds is based on two Suzuki reactions as shown in **Scheme 1**.
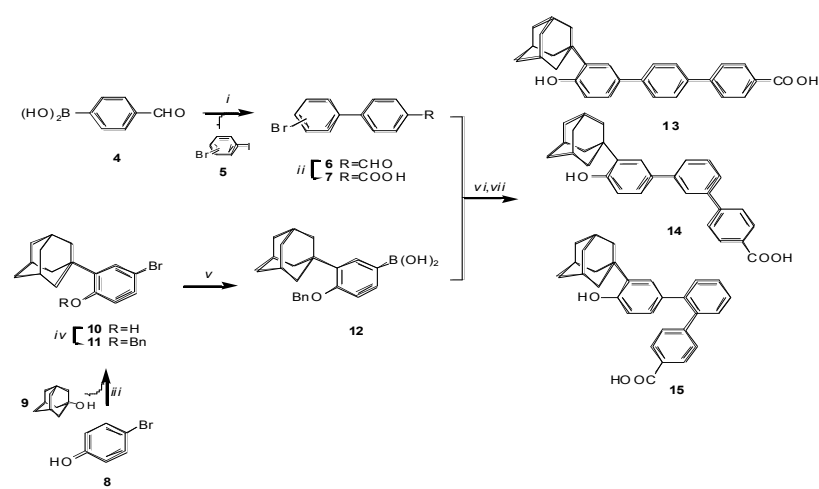
Scheme 1. Regents and conditions: (i) Pd(Ph₃P)₄, aq. Na₂CO₃, toluene/EtOH, (ii) aq. KMnO₄, (iii) H₂SO₄ conc., CH₂Cl₂, (iv) Benzyl bromide, K₂CO₃, CH₃CN, (v) BuLi, B(OiPr)₃, THF, (vi) Pd(Ph₃P)₄, aq. Na₂CO₃, CH₃CN, (vii) H₂, 5% Pd/C, EtOH.

The desired 2′-, 3′-, or 4′-bromobiphenyl carboxylic acids were prepare with a first Suzuki reaction between boronic acid **4** and 2′-, 3′-, or 4′-bromo-iodobenzene. After oxidation by potassium permanganate, a second Suzuki coupling with the adamantanyl boronic acid **12** occurs, to give, previous deprotection, the desired triphenyl derivatives in good yields. Compound **12** was prepare starting to *p*-bromo-phenol, which after a Friedel-Craft alkylation with 1-adamantan-ol, and benzyl protection, reacted with triisopropyl borane in presence of butyllhythium at -78°C to give the appropriate boronic acid.

With the aim to substitute the central phenyl ring with an heteroatomic one, we synthesized the isoxazolines and isoxazoles as described in **Scheme 2**.
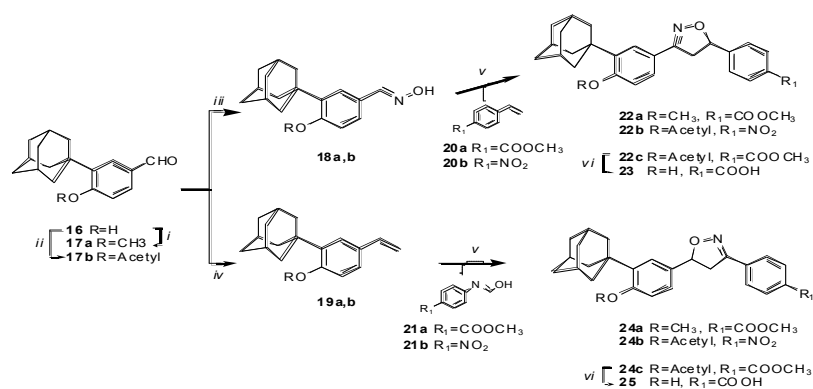
Scheme 2. Synthesis of isoxazolines. Reagents and conditions: (i) MeI, KOH, DMSO, (ii) Ac$_2$O, reflux, (iii) NH$_2$OHxHCl, NaHCO$_3$, MeOH, (iv) MeP(Ph)$_3$Br, NaH, THF, (v) NCS, CHCl$_3$, TEA, (vi) LiOH, H$_2$O/MeOH.
.

Starting from the aldehyde 16 and after classical methylation or acetylation, 17a and b reacted with hydroxylamine hydrochloride to give oximes 18a,b, or with methyl-triphenylphosphonium bromide in a Wittig reaction to give alkenes compounds

19a,b in good yields. Then, the nitrile oxides generated from oximes **18a,b** following Torssell's procedure[36] underwent a [3 + 2] regioselective cycloaddition with alkenes **20a,b** to produce isoxazolines **22a-c** in good yields. In the same manner, isoxazolines **24a-c** were obtained from nitrile oxides generated from oximes **21a,b**, and alkenes **19a,b**. Alkaline hydrolysis of compounds **22c** and **24c** gave the corresponding carboxylic acids **23** and **25**.

To prepare the isoxalozes we oxidize the isoxazoline ring using *N*-bromosuccinimide-triethylamine in methylene chloride (**Scheme 3**).
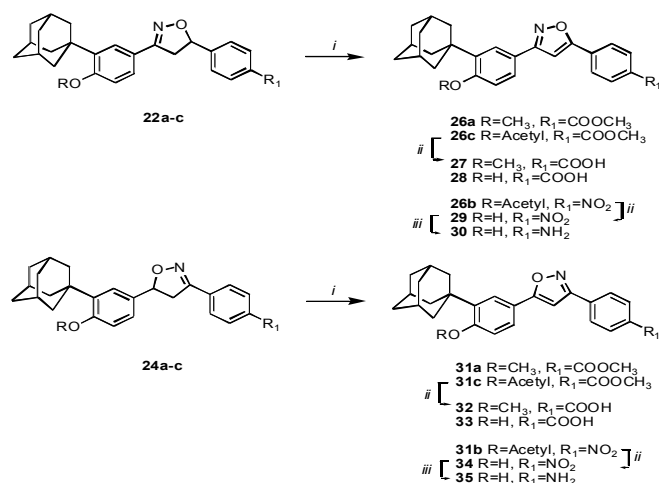
Scheme 3. Synthesis of isoxazoles. Reagents and conditions: (i) NBS, CCl$_4$, reflux, (ii) LiOH, H$_2$O/MeOH, (iii) Zn, AcOH.

Thus, isoxazoles **27-29**, **32-34** were obtained by alkaline hydrolysis of the respective methyl esters; and, in order to prepare amino derivatives instead of carboxylic acids, compounds **30** and **35** were synthesized by reduction of nitro group of **29** and **30**.

102

2.6.2. Biological results

To valuated the biological activity of this new set of terphenyl compunds, we tested their different concentrations on HL60 cells growth (**Fig.2**)
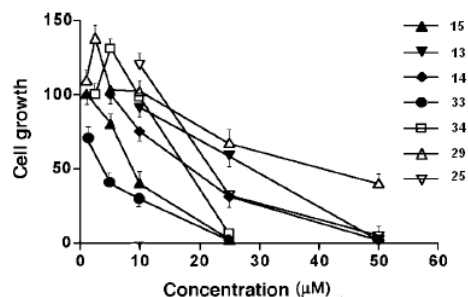
Fig.2 Effects of novel terphenyl, diarylisoxazole, and diarylisoxazoline derivatives on HL60 cell growth.

All compounds caused a cell growth inhibition when used at concentrations higher than 10 μM. Compounds **15** and **33** were the most active antiproliferative agents, showing an IC50 of 8 and 3 μM, respectively.

Surprisingly, compounds **29**, **34**, and **25** caused an increase of cell growth when used at low (<10 μM) concentration. In particular, we observed that compound 29 was at the concentration of 2.5 μM was the most active in improving cell growth; it was able to increase the percentage of cells in S and G2-M phases of the cell cycle with a decrease in the percentage of cells in G0-G1 phase (**Fig.3**). This observation suggests that compound **29** might stimulate cell growth by promoting the G1-S transition.

103
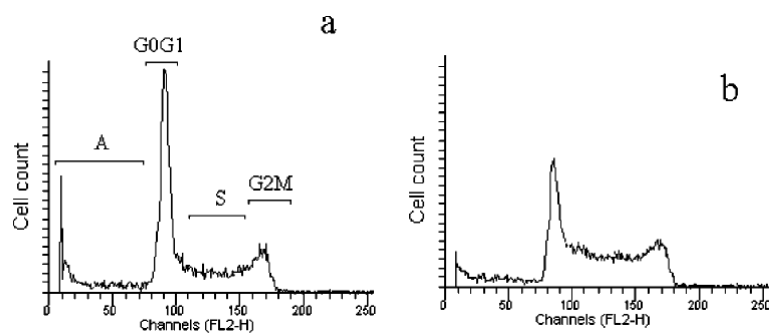
Fig.3 Cell cycle distribution of HL60 cells (a) and HL60 cells exposed 24 h to 2.5 μM compound **29** (b).

Thus, excited by this unexpected finding, we conducted further test to prove our hypothesis. Hence, we evaluated whether compounds **29**, **34**, and **25** were able to support growth and to avoid death of cells cultured in a serum-free medium. As is well-known, serum is an essential constituent of a cell culture medium to support the in vitro growth of continuous cell lines. Accordingly, HL60 cells were washed twice with PBS and suspended in a serum-free medium constituted by only RPMI 1640. After 72 h, cells were harvested and the number of living cells was determined. As reported in Fig.4, cells cultured 72 h in serum-free medium showed a cell growth inhibition of 70% compared to cells growing in a complete medium.
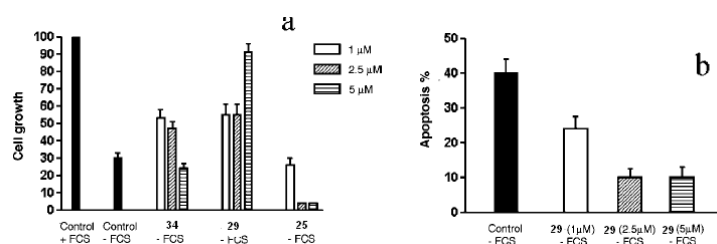
Fig. 4 (a) Effects of compounds **34**, **29**, and **25** on cell growth of HL60 cells growing in serum-free medium (-FCS). (b) Effects of compound **29** on apoptosis induced by serum deprivation. Bars represent ± SE of three independent experiments.

Compound **29** was able to support growth of cells cultured in serum-free medium especially when used at the concentration of 5 μM (**Figure 4a**). Compound **34** was less effective than **29**, although it was able to support in part cell growth when used at 1 and 2.5 μM concentrations. In contrast, compound **25** (1 μM) did not show any cell growth stimulating activity in serum free medium and, at 2.5 and 5 μM concentrations, it caused instead a potent cell growth inhibition. Moreover, compound **29** was also able to inhibit apoptosis of cells cultured in serum-free medium. As shown in **Figure 4b**, serum deprivation induced apoptosis in about 40% of HL60 control cells (evaluation after 72 h of culture), whereas addition with 2.5 or 5 μM of **29**, reduced the percentage of apoptosis to only 10%. Compounds **2** and **3** were able to decrease the percentage of apoptosis of HL60 from about 40% to 18% and 17%,[9] resulting in being less active than **29** as antiapoptotic agent.

Thus, also these new data demonstrated that terphenyl derivative **29** acts as a proliferative stimulating and antiapoptotic agent. To better verify this latter property, we tested the ability of **29** to inhibit the apoptotic activity of daunorubicin, a chemotherapic agent that potently induces apoptosis in HL60 cells. After 48 h of exposure to increasing concentrations of daunorubicin alone or in combination with 2.5 μM of **30**, HL60 cells were harvested and the percentage of apoptosis was determined. As reported in **Figure 5**, **29** was able to halve the percentage of apoptosis induced by daunorubicin.
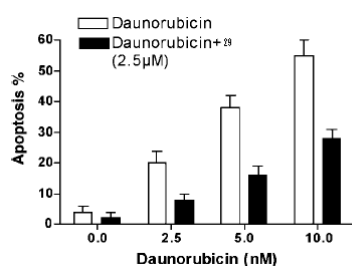
Fig. 5. Percentage of apoptosis of HL60 cells after 48 h exposure to different concentrations of daunorubicin in combination or not with compound **29**. Bars represent ± SE of three independent experiments.

105

The daunorubicin is an anthracycline (daunorubicin, idarubicin, epirubicin, and doxorubicin), widely used cytotoxic drugs in the treatment of haematological malignancies and solid tumors. These agents are especially prone to causing severe tissue damage on extravasation by inducing apoptosis in skin cells. Accidental extravasation has been estimated to occur in 0.5-6% of all patients receiving chemotherapy.[21–23] The local toxicity is characterized by immediate pain, erythema, and swelling at the extravasation site. The ulceration may not appear for several days or even weeks and may continue to worsen for months, probably because of drug diffusion into adjacent tissue. Indeed, it has been demonstrated that doxorubicin can persist in the tissue for at least a month. Whereas small ulcerations may heal, large ulcerations require surgical excision. The ability of **29** to inhibit apoptosis induced by daunorubicin suggests that a topical use of this compound could be useful for the treatment of tissue damage caused by extravasation of anthracyclines.

2.6.3. Conclusions

In this part of research, we studied a further modification on stilbene motif to synthesize novel compounds with pro-apoptotic activity. In previous work of my research group was reported the activity of some terphenyl derivatives, where the double bond of stilbene was replace by another phenyl ring. Thus, the goal was prepare others compounds with further substitutions on terphenyl core.

Hence, we achieve three different kind of structural modifications: the replacement of trimethoxyl-moiety with an adamantnyl-group; the central phenyl ring with an heteroaromatic other; and the carboxylic acid with an amino group.

Thus, we tested these new compounds on HL60 cells to evaluate their apoptotic activity. Surprisingly, these structural modifications lead to derivatives with opposite activity toward cell growth. In fact, we observed that some derivatives act as inductors of growth cells and as antiapoptotic agents at low concentrations. Among compounds with carboxylic acid function at ring C, only isoxazolinic **25** has shown a small growth enhancing property, but not in serum-free conditions. None of the amino compounds were found of interest but, unexpectedly, their nitro precursors **29** and **34** showed interesting cell growth promoting and antiapoptotic activities. In particular, compound **29** was able to support effectively the cell growth of HL60 cultured in serum-free medium, preventing apoptosis induced by serum deprivation. The apoptosis inhibitory effect of **29** was still observed when cells were exposed to the potent apoptotic inducing factor daunorubicin.

This activity is very interesting because high apoptosis level causes different disease, especially in central nervous system. In fact inappropriate apoptosis in the brain leads to permanent neurological deficits. Disregulated apoptosis has

been implicated in several neurodegenerative disorders. Moreover, this is the cause of local toxicity of some antineoplastic agents, as anthracyclines, which can lead to several skin maligniances.

In conclusion, our data indicate that compound **29** is a potent cell growth agent endowed with antiapoptotic activity, and could be involved in therapy to inhibit undesired effects of a widely used traditional chemotherapy. Therefore, further studies on terphenyl derivatives could improve the research of cell growth inducing agents, in the field of neurological deficits and neurodegenerative disorders.

2.6.4. Experimental Section

Chemistry

Melting points were obtained with a Kofler apparatus and are uncorrected. Reaction courses and product mixtures were routinely monitored by thin-layer chromatography (TLC) on silica gel precoated F254 Merck plates. Nuclear magnetic resonance (1H and 13C NMR) spectra were determined in CDCl3 solution, unless otherwise indicated, with a Bruker AC-200 spectrometer, and peak positions are given in parts per million downfield from tetramethylsilane as internal standard. All drying operations were performed over anhydrous sodium sulfate. Column chromatography (medium pressure) was carried out with 60-200 mesh silica gel, using the flash technique. Microanalysis of all new final synthesized compounds agreed with calculated values within ± 0.4% of the theoretical.

General Procedure for Biphenylcarbaldehyde Synthesis (6). To a solution of *o*-, *m*-, or *p*-iodobromobenzene (120 mg, 0.42 mmol) in 1 ml of toluene is added a catalytic amount (3-5% mol) of tetrakis-triphenylphosphine palladium and 0.3 ml of aqueous 2 M Na_2CO_3. A solution of 4-formylbenzeneboronic acid (**4**, 100 mg, 0.66 mmol) in 1 ml of ethanol is then added, and the mixture is heated to reflux for 3 h in an argon atmosphere. After cooling, the mixture is extracted three times with dichloromethane and the joined organic phases are washed with water and brine, dried, and evaporated under vacuum. The residue is purified by chromatography, giving the bromodiphenylaldehyde derivative.

2'-Bromobiphenyl-4-carbaldehyde (6a).[36] Oil. Yield 30%. ^{1}H NMR (CDCl$_3$, 200 MHz) δ: 7.26-7.41 (m, 3H), 7.60 (d, *J*=8.1, 2H), 7.71 (d, *J*=8, 1H), 7.97 (d, *J*=8.3 2H), 10.09 (s, 1H).

3'-Bromobiphenyl-4-carbaldehyde (6b).[37] Oil. Yield 50%. ^{1}H NMR(CDCl$_3$, 200 MHz) δ: 7.37,(J=7.7, 1H), 7.57 (m, 2H), 7.72 (d, J=9.2, 2H), 7.77 (m, 1H), 7.96 (d, J =9, 2H), 10.07 (s, 1H).

4'-Bromobiphenyl-4-carbaldehyde (6c).[38] Solid. Mp 135- 140°C. Yield 62%. ^{1}H NMR (CDCl$_3$, 200 MHz) δ: 7.50 (d, J=8.8, 2H), 7.62 (d, J=8.8, 2H), 7.72 (d, J=8, 2H), 7.96 (d, J=8.6, 2H), 10.06 (s, 1H).

General Procedure for Oxidation to Biphenylcarboxylic Acid (7a-c). To a gently boiling solution of bromobiphenylcarbaldehyde (**6a-c**, 100 mg) in sodium carbonate (5 mL) is added potassium permanganate (70 mg in 1 mL of water), and reflux is maintained for 3 h. After cooling, the solution is acidified with concentrated hydrochloric acid and extracted three or more times with diethyl ether. The residue is used in the next reaction with no further purification.

2'-Bromobiphenyl-4-carboxylic Acid (7a).[39] Yield 99%. Mp 237-241 °C. ^{1}H NMR (DMSO-d6, 200 MHz): δ 7.40-7.70 (m, 5H), 8.00-8.10 (m, 3H).

3'-Bromobiphenyl-4-carboxylic Acid (7b).[39] Yield 99%. Mp 250-253 °C. ^{1}H NMR (DMSO-d6, 200 MHz): δ 7.40-7.85 (m, 6H), 8.11 (d, J =8.4, 2H).

4'-Bromobiphenyl-4-carboxylic Acid (7c).[39,40] Yield 98%. Mp >300 °C. ^{1}H NMR: (DMSO-d6, 200 MHz): δ 7.50 (d, J=8.8, 2H), 7.59-7.68 (m, 4H), 8.16 (d, J =8.6, 2H).

General Procedure for Terphenyl Synthesis. To a solution of bromobiphenyl acid (**7a-c**, 1 eq) and 4-Benzyloxy-3-tricyclo[3.3.1.10,0]dec-1-yl-boronic acid (**12**, 1 eq) in 0.4 M aqueous sodium carbonate (5 ml) and acetonitrile (5 ml) is added a catalytic amount (5% mole) of tetrakis-triphenylphosphine palladium, and the mixture is heated to reflux under argon atmosphere for 3 h. The suspension is cooled, filtered, and washed with dichloromethane. The water

110

phase is then acidified and extracted with diethyl ether. Purification of the residue of ether extracts gave the O-protected terphenyl products.

General Procedure for Removal of the Benzyl-Protection Group. To a solution of the appropriate benzyl protected derivative (0.11 mmol) in abs EtOH (15 mL) was added Pd/C 5% (catalytic amount). The reaction was stirred in hydrogen atmosphere for 15 h. The mixture was filtered over celite and the solution evaporated. The residue was chromatographed on silica gel (light petroleum-ethyl acetate).

4-Hydroxy-3-tricyclo[3.3.1.1^{0,0}]dec-1-yl-[1,1´;4´,1˝]terphenyl-4˝-carboxylic Acid (13). Yield 40%; mp 300 °C (dec.). ^{1}H NMR (DMSO-$d6$, 200 MHz): δ 1.71 (s, 6H), 2.01 (s, 9H), 5.76 (s, 1H), 7.46-7.52 (m, 4H), 7.72-7.82 (m, 5H), 8.01 (d, J=8.2, 2H), 12.96 (br, 1H). ^{13}C NMR (DMSO-$d6$, 200 MHz): δ 28.1, 37.1, 43.1, 44.1, 121.0, 126.1, 127.5, 128.7, 130.5, 131.6, 134.3, 140.8, 141.0, 142.4, 143.1, 162.4, 167.2.

4-Hydroxy-3-tricyclo[3.3.1.1^{0,0}]dec-1-yl-[1,1´;3´,1˝]terphenyl-4˝-carboxylic acid (14). Yield 35%; mp 263-265 °C. ^{1}H NMR (DMSO-$d6$, 200 MHz): δ 1.80 (s, 6H), 2.11 (s, 3H), 2.19 (s, 6H), 5.12 (s, 1H), 6.76 (d, J=8.0, 1H), 7.34 (dd, J=8.0, J=1.8, 1H), 7.48-7.60 (m, 4H), 7.73-7.77 (m, 3H), 8.20 (d, J=8.0, 2H), 12.47 (br, 1H). ^{13}C NMR (DMSO-$d6$, 200 MHz): δ 28.1, 37.1, 43.1, 44.1, 120.4, 127.3, 129.8, 132.1, 135.5, 136.8, 139.1, 141.6, 142.5, 143.6, 162.4, 167.2.

4-Hydroxy-3-tricyclo[3.3.1.1^{0,0}]dec-1-yl-[1,1´;2´,1˝]terphenyl-4˝-carboxylic Acid (15). Yield 47%; mp 179-181 °C. ^{1}H NMR (CD$_3$OD, 200 MHz) δ 1.86 (s, 6H), 1.92 (s, 9H), 5.49 (s, 1H), 6.60 (d, J=8.1, 1H), 6.70 (d, J=2.1, 1H), 6.86 (dd, J=8.1, J=2.1, 1H), 7.09 (d, J=8.1, 2H), 7.35-7.40 (m, 4H), 7.86 (d, J=8.1, 2H), 12.3 (br, 1H). ^{1}H NMR (CD$_3$OD, 200 MHz) δ 28.1, 37.1, 43.1,

44.1, 121.5, 123.7, 125.1, 127.5, 130.9, 133.8, 136.7, 139.3, 139.6, 141.2, 141.5, 142.7, 161.7, 167.2.

2- tricyclo[3.3.1.10,0]dec-1-yl -4-bromo-phenol (10). To a suspension of 4-bromo-phenol **8** (0,011 mmol) and adamant-1-ol **9** in dichloromethane (15-20 ml) were added dropwise H$_2$SO$_4$ conc After complete dissolution, the reaction was poured into water, neutralized with bicarbonate satured solution and extracted with dichloromethane. The organic layers were collected, dried on anhydrous sodium sulphate, filtered and evaporated in vacuo. The crude material was purified by chromatography (petroleum ether/ethyl ether) to give product **10** (yield 65%). ^{1}H NMR(CDCl$_3$, 200 MHz) δ: 1.77 (s, 6H), 2.09 (s, 9H), 4.86 (s, 1H), 6.56 (d, 1H, *J*=8.24), 7.13-7.17 (m, 1H), 7.26-7.30 (m, 1H).

3-tricyclo[3.3.1.10,0]dec-1-yl-4-benzyloxyphenyl   bromide   (11).   To   a suspension of potassium carbonate in acetonitrile was added hydroxyl-derivative **10** and the reaction was stirred at reflux for 4h. After cooling to room temperature, the solid was filtered off and the solvent concentrated in vacuo. The crude material was then crystallized by hexane giving the desired product **11**. (yield 88%). ^{1}H NMR(CDCl$_3$, 200 MHz) δ: 1.75 (s, 6H), 2.05 (s, 9H), 4.93 (s, 2H), 6.56 (d, 1H, *J*=8.23), 7.10-7.17 (m, 6H), 7.30-7.34 (m, 1H).

3-tricyclo[3.3.1.10,0]dec-1-yl-4-benzyloxyphenylboronic Acid (12). To a solution of 3-tricyclo[3.3.1.10,0]dec-1-yl-4-benzyloxyphenyl bromide **11** (2.00 g, 5.04 mmol) in THF (7 ml) at -78 °C (dry ice/acetone bath) under argon was added in one
portion 1.6 M *n*-BuLi (7.56 mmol) in hexane (4.7 ml). The mixture was stirred at -78 °C for 15 min, (*i*-PrO)$_3$B (3.5 ml, 15.1 mmol) was added, and the resulting solution was stirred at -78 °C for 20 min and then at room temperature overnight.

112

The mixture was quenched with 0.1 N HCl (30 ml) and extracted with EtOAc. The extracts were washed with brine and dried over anhydrous sodium sulphate. After filtration and evaporation of the solvent, the crude product was used without further purifications.

4-Methoxy-3-tricyclo[3.3.1.10,0]dec-1-yl-benzaldehyde (17a). To a suspension of KOH pulverized (450 mg, 7.9 mmol) in DMSO (10 ml) that was stirred for 15 min was added **16** (500 mg, 1.96 mmol) and then iodomethane (0.25 ml, 3.9 mmol). After stirring for 2 h at room temperature, dichloromethane (30 ml) was added and the mixture was poured into ice-water and extracted three times with dichloromethane. The combined organic extracts were washed with water, brine, dried, and evaporated, and the residue was chromatographed on silica gel (light petroleum-ethyl acetate 9/1) to give compound 17a (oil, 380 mg, yield 73%). ^{1}H NMR(CDCl$_3$, 200 MHz) δ: 1.79 (s, 6H); 2.11 (s, 9H); 6.97 (d, J=8.4, 1H), 7.70-7.79 (m, 2H,); 9.89 (s, 1H).

Acetic Acid 4-Formyl-2-tricyclo[3.3.1.10,0]dec-1-yl-phenyl Ester (17b). A solution of **16** (4.3 g, 17 mmol) in acetic anhydride (20 ml) was refluxed for 1 h. After evaporation, diethyl ether (30 ml) was added to the residue and washed with 5% NaHCO$_3$ (15 ml), water, and brine, dried over Na$_2$SO$_4$, and evaporated. The residue was purified by chromatography to give compound **17b** (oil, 4.28 g, yield 85%). ^{1}H NMR(CDCl$_3$, 200 MHz) δ: 1.77 (s, 6H), 2.12 (s, 9H), 2.40 (s, 3H), 7.17 (d, J=8.1, 1H) 7.75 (dd, J=8.1, J) 1, 1H), 7.90 (d, 1H), 9.97 (s, 1H).

General Procedure for Oximes. To a solution of hydroxylamine hydrochloride (250 mg, 3.7 mmol) dissolved in water (7 ml), NaHCO$_3$ (470 mg, 5.6 mmol) was added portionwise at 0 °C, and the mixture stirred for 30 min at room temperature. The appropriate aldehyde (**17a,b**, 3.1 mmol), dissolved in methanol (5 ml), was

then added to the solution and stirring was continued for additional 6 h. Methanol was evaporated in vacuo and the residue extracted with diethyl ether. The organic extracts were washed with brine, dried, and evaporated under reduced pressure. The residue was chromatographed on silica gel (diethyl ether-light petroleum).

4-Methoxy-3-tricyclo[3.3.1.1⁰,⁰]dec-1-yl-benzaldehyde Oxime (18a). Yield 75%; mp 158-160 °C. ^{1}H NMR(CDCl$_3$, 200 MHz) δ: 1.77 (s, 6H), 2.09 (s,9H), 3.86 (s, 3H), 6.87 (d, J=8.3, 1H), 7.33-7.38 (m, 2H), 7.48 (s, 1H), 8.09 (s, 1H).

Acetic Acid 4-(Hydroxyimino-methyl)-2-tricyclo[3.3.1.1⁰,⁰]dec- 1-yl-phenyl Ester (18b). Yield 98%, oil. ^{1}H NMR(CDCl$_3$, 200 MHz) δ: 1.77 (s, 6H), 2.02 (s, 9H), 2.37 (s, 3H), 7.02 (d, J=8.1, 1H), 7.42 (dd, J=8.1, 2, 1H), 7.58 (d, 1H), 8.12 (s, 2H).

4-(Hydroxyiminomethyl)benzoic Acid Methyl Ester (21a). Yield 80%; mp 119-122 °C. ^{1}H NMR(CDCl$_3$, 200 MHz) δ: 3.9 (s, 3H); 7.27 (s, 1H); 7.69 (d, J=8.4, 2H); 8.06 (d, J) 8.3, 2H); 8.17 (s, 1H).

General Procedure for Olefins. NaH (1.2 eq), was added to a stirred suspension of methyltriphenylphosphonium bromide (1.07 g, 3 mmol) in dry THF (15 ml) containing the appropriate aldehyde (**17a,b**, 3 mmol). After stirring for 5 h at room temperature, diethyl ether (30 ml) was added and the mixture was poured into ice-water and extracted with Et$_2$O. The combined organic extracts were dried and evaporated, and the residue was chromatographed on silica gel (diethyl ether-light petroleum).

1-(2-Methoxy-5-vinyl-phenyl)-tricyclo[3.3.1.1⁰,0]decane (19a). Yield 65%; oil. ^{1}H NMR(CDCl$_3$, 200 MHz) δ: 1.78 (s, 6H), 2.11 (s, 9H), 3.83 (s, 3H), 5.12 (d, J=11.1, 1H), 5.61 (d, J=17.6, 1H), 6.68 (dd, J=17.6, J=11.1, 1H), 6.84 (d, J=8.4, 1H), 7.22-7.30 (m, 2H).

114

Acetic Acid 2-Tricyclo[3.3.1.1⁰,⁰]dec-1-yl-4-vinyl-phenyl Ester (19b). Yield 79%; oil. ^{1}H NMR(CDCl$_3$, 200 MHz) δ: 1.79 (s, 6H), 2.03 (s, 9H), 2.36 (s, 3H), 5.23 (dd, J=11.1, J=0.6, 1H), 5.70 (dd, J=17.0, J=0.6, 1H), 6.71 (dd, J=17.1, J=11.1, 1H), 6.96 (d, J=8.2, 1H), 7.29 (dd, J=8.2, J=2.1, 1H), 7.31 (d, J=2.1, 1H).

4-Vinylbenzoic Acid Methyl Ester (20a). Yield 60%; oil. IR (neat) 1724, 1608, 1436, 1278, 1107, 782. ^{1}H NMR(CDCl$_3$, 200 MHz) δ: 3.91 (s, 3H), 5.38 (d, J=10, 1H), 5.96 (d, J=17.6, 1H), 6.75 (dd, J=17.6, J=10, 1H), 7.46 (d, J=8, 2H), 7.99 (d, J=8, 2H).

General Procedure for Isoxazolines. A mixture of *N*-chlorosuccinimide (174 mg, 1.3 mmol), pyridine (2 drops) and oxime (1.3 mmol) in anhydrous CHCl$_3$ (15 ml) was stirred for 1 h at 50-60°C. Olefin (1.4 mmol) was then added followed by triethylamine (0.27 ml, 1.95 mmol) in CHCl$_3$ (5 ml). After stirring at 25 °C for 20 min, water was added and the organic phase was washed with 2.5% HCl and water, then dried and evaporated under reduced pressure. The residue was chromatographed on silica gel (ethyl acetate-light petroleum).

4-[3-(4-Methoxy-3-tricyclo[3.3.1.1⁰,⁰]dec-1-yl-phenyl)-4,5-dihydro-isoxazol-5-yl]-benzoic Acid Methyl Ester (22a). Yield 80%. ^{1}H NMR(CDCl$_3$, 200 MHz) δ: 1.76 (s, 6H), 2.09 (s, 9H), 3.30 (dd, J=16.1, J=7.9, 1H), 3.76-3.93 (m, 7H), 5.75 (dd, J=11.2, J=7.9, 1H), 6.87 (d, J=8.4, 1H), 7.42-7.49 (m, 3H), 7.62 (s, 1H), 7.65 (d, J=6.6, 2H), 8.04 (dd, J=8.2, J=1.8, 2H).

Acetic Acid 4-[5-(4-Nitro-phenyl)-4,5-dihydro-isoxazol-3-yl]-2-tricyclo[3.3.1.1⁰,⁰]dec-1-yl-phenyl Ester (22b). Yield 42%. ^{1}H NMR(CDCl$_3$, 200 MHz) δ: 1.78 (s, 6H), 2.01 (s, 6H), 2.09 (s, 3H), 2.37 (s, 3H), 3.29 (dd, J=16.4, J=7.2, 1H), 3.88 (dd, J=16.8, J=11.2, 1H), 5.83 (dd, J=10.8, J=7.2, 1H), 7.04 (d, J=8.4, 1H), 7.46 (dd, J=8.4, J=2.0, 1H), 7.55-7.58 (m, 2H), 7.74 (d, J=2.0, 2H), 8.22-8.25 (m, 2H).

4-[3-(4-Acetoxy-3-tricyclo[3.3.1.1⁰,⁰]dec-1-yl-phenyl)-4,5-dihydroisoxazol-5-yl]-benzoic Acid Methyl Ester (22c). Yield 82%. ^{1}H NMR(CDCl₃, 200 MHz) δ: 1.77 (s, 6H), 2.02 (s, 9H), 2.37 (s, 3H), 3.30 (dd, *J*=16.3, 1H), 3.83 (dd, *J*=16.5, *J*=11, 1H), 3.92 (s, 3H), 5.79 (dd, *J*=11.1, *J*=7.6, 1H), 7.04 (d, *J*=8.3, 1H), 7.43-7.50 (m, 3H), 7.55 (d, *J*=2, 1H), 8.05 (d, *J*=8.2, 2H).

4-[5-(4-Methoxy-3-tricyclo[3.3.1.1⁰,⁰]dec-1-yl-phenyl)-4,5-dihydro-isoxazol-3-yl]-benzoic Acid Methyl Ester (24a). Yield 53%. ^{1}H NMR(CDCl₃, 200 MHz) δ: 1.76 (s, 6H), 2.07 (s, 9H), 3.36 (dd, *J*=16.4, *J*=8.6, 1H), 3.65-3.83 (m, 4 H), 3.93 (s, 3H), 5.72 (dd, *J*=11,2, *J*=8.6, 1H), 6.86 (d, *J*=8.8, 1H), 7.19-7.24 (m, 2H), 7.77 (d, *J*=8.1, 2H), 8.07 (d, *J*=8.2, 2H).

Acetic Acid 4-[3-(4-Nitro-phenyl)-4,5-dihydro-isoxazol-5-yl]-2-tricyclo[3.3.1.1⁰,⁰]dec-1-yl-phenyl Ester (24b). Yield 45%. ^{1}H NMR(CDCl₃, 200 MHz) δ: 1.76 (s, 6H), 2.0 (s, 6H), 2.08 (s, 3H), 2.35 (s, 3H), 3.44 (dd, *J*=17.0, *J*=8.0, 1H), 3.78 (dd, *J*=17.0, *J*=11.0, 1H), 5.80 (dd, *J*=11.0, *J*=8.0, 1H), 7.0 (d, *J*=8.4, 1H), 7.22 (dd, *J*=8.2, *J*=1.1, 1H), 7.85 (d, *J*=9.0, 2H), 8.27 (d, *J*=9.0, 2H).

4-[5-(4-Acetoxy-3-tricyclo[3.3.1.1⁰,⁰]dec-1-yl-phenyl)-4,5-dihydroisoxazol-3-yl]-benzoic Acid Methyl Ester (24c). Yield 44%. ^{1}H NMR(CDCl₃, 200 MHz) δ: 1.76 (s, 6H), 2.01 (s, 9H), 2.35 (s, 3H), 3.37 (dd, *J*=16.7, *J*=8.6, 1H), 3.76 (dd, *J*=16.7, *J*=11.1, 1H), 3.93 (s, 3H), 5.76 (dd, *J*=11.2, *J*=8.6, 1H), 7.01 (d, *J*=8.2, 1H), 7.24 (dd, *J*=8.2, *J*=2.1, 1H), 7.36 (d, *J*=2.1, 1H), 7.65 (d, *J*=6.6, 2H), 8.07 (d, *J*=6.7, 2H).

General Procedure for Isoxazoles. To a solution of the isoxazoline (0.25 mmol) in carbon tetrachloride (10 ml), *N*-bromosuccinimide (66 mg, 0.37 mmol) was added and the mixture was gently refluxed for 3 h. Hydrogen bromide was slowly liberated. The cooled solution was filtered from the precipitated succinimide, washed with 5% aqueous sodium hydroxide and then with water until the organic phase became clear. The organic layer was dried and the solvent removed in vacuo. The residue was chromatographed on silica gel (ethyl acetate-light petroleum).

4-[3-(4-Methoxy-3-tricyclo[3.3.1.10,0]dec-1-yl-phenyl)-isoxazol-5-yl]-benzoic Acid Methyl Ester (26a). Yield 81%. ^{1}H NMR(CDCl$_3$, 200 MHz) δ: 1.80 (s, 6H), 2.15 (s, 9H), 3.90 (s, 3H), 3.96 (s, 3H), 6.90 (s, 1H), 6.97 (d, J=8.2, 1H), 7.66-7.75 (m, 2H), 7.92 (d, J=8.4, 2H) 8.16 (d, J=8.4, 2H).

Acetic Acid 4-[5-(4-Nitro-phenyl)-isoxazol-3-yl]-2-tricyclo-[3.3.1.10,0]dec-1-yl-phenyl Ester (26b). Yield 54%. ^{1}H NMR(CDCl$_3$, 200 MHz) δ: 1.72 (s, 6H), 2.02 (s, 9H), 2.33 (s, 3H), 6.92 (s, 1H), 7.07 (d, J=8.4, 1H), 7.62 (dd, J=8.4, J=2.2, 1H), 7.82 (d, J=2.2, 1H), 7.93-7.97 (m, 2H), 8.28-8.33 (m, 2H).

4-[3-(4-Acetoxy-3-tricyclo[3.3.1.10,0]dec-1-yl-phenyl)-isoxazol-5-yl]-benzoic Acid Methyl Ester (26c). Yield 81%. ^{1}H NMR(CDCl$_3$, 200 MHz) δ: 1.80 (s, 6H), 2.15 (s, 9H), 3.90 (s, 3H), 3.96 (s, 3H), 6.90 (s, 1H), 6.97 (d, J=8.2, 1H), 7.66-7.75 (m, 2H), 7.92 (d, J=8.4, 2H) 8.16 (d, J=8.4, 2H).

4-[5-(4-Methoxy-3-tricyclo[3.3.1.10,0]dec-1-yl-phenyl)-isoxazol-3-yl]-benzoic Acid Methyl Ester (31a). Yield 62%. ^{1}H NMR(CDCl$_3$, 200 MHz) δ: 1.80 (s, 6H), 2.14 (s, 9H), 3.89 (s, 3H), 3.95 (s, 3H), 6.75 (s, 1H), 6.96 (d, J=8.4, 1H), 7.65-7.70 (m, 2H), 7.95 (d, J=8.4 Hz, 2H), 8.15 (d, J=8.4, 2H).

Acetic Acid 4-[3-(4-Nitro-phenyl)-isoxazol-5-yl]-2-tricyclo-[3.3.1.10,0]dec-1-yl-phenyl Ester (31b). Yield 81%. ^{1}H NMR(CDCl$_3$, 200 MHz) δ: 1.81 (s, 6H), 2.07 (s, 6H), 2.14 (s, 3H), 2.40 (s, 3H), 6.86 (s, 1H), 7.14 (dd, J=8.0, J=2.0, 1H), 7.84 (d, J=2.0, 1H), 8.05-8.07 (m, 2H), 8.34-8.37 (m, 2H).

4-[5-(4-Acetoxy-3-tricyclo[3.3.1.10,0]dec-1-yl-phenyl)-isoxazol-3-yl]-benzoic Acid Methyl Ester (31c). Yield 65%. ^{1}H NMR(CDCl$_3$, 200 MHz) δ: 1.61 (s, 6H), 2.08 (s, 9H), 2.40 (s, 3H), 3.96 (s, 3H), 6.84 (s, 1H), 7.13 (d, J=8.4, 1H), 7.69 (dd, J=8.4, J=2.1, 1H), 7.84 (d, J=2.1, 1H), 7.95 (d, J=8.3, 2H), 8.15 (d, J=8.3, 2H).

General Procedure for Ester Hydrolysis. A mixture of ester (1 mmol), methanol (10 ml), water (6-7 ml), and lithium hydroxide (40 mg, 1.5 mmol or double amount for acetyl derivatives) was allowed to stand at 50-60°C for 24 h. The solution was concentrated in vacuo to remove methanol, and the remaining aqueous solution was

extracted with diethyl ether to separate trace amounts of unreacted ester. The aqueous solution was acidified with 1 M hydrochloric acid and extracted with three portions of ethyl acetate. The combined organic extracts were washed with saturated aqueous sodium chloride and dried. Removal of the solvent under reduced pressure afforded a residue, which was chromatographed on silica gel (eluent: ethyl acetate-light petroleum).

4-[3-(4-Hydroxy-3-tricyclo[3.3.1.1^{0,0}]dec-1-yl-phenyl)-4,5-dihydro-isoxazol-5-yl]-benzoic Acid (23). Yield 90%; mp 251-253 °C (dec). ^{1}H NMR(DMSO, 200 MHz) δ: 1.72 (s, 6H), 2.06 (s, 9H), 3.27-3.39 (m, 1H), 3.86 (dd, J=17.1, J=11.1, 1H), 5.75 (dd, J=10.7, J=7.4, 1H), 6.82 (d, J=8.4, 1H), 7.34 (d, J=8.4, 1H), 7.44-7.51 (m, 3H), 7.95 (d, J=8.0, 2H), 9.86 (s, 1H), 12.98 (br, 1H). ^{13}C NMR(DMSO, 200 MHz) δ: 28.1, 37.1, 43.1, 44.1, 45.2, 81.1, 116.6, 128.7, 129.1, 129.6, 131.1, 131.8, 132.7, 137.1, 158.1, 162.1, 167.2.

4-[5-(4-Hydroxy-3-tricyclo[3.3.1.1^{0,0}]dec-1-yl-phenyl)-4,5-dihydro-isoxazol-3-yl]-benzoic Acid (25). Yield 94%; mp 240-242 °C (dec). 1H NMR (DMSO-d_6) δ 1.71 (s, 6H), 2.05 (s, 9H), 3.38-3.46 (m, 1H), 3.79 (dd, J=16.4, J=11.2, 1H), 5.63 (dd, J=11.2, J=8.3, 1H), 6.77 (d, J=8.1, 1H), 7.03-7.10 (m, 2H), 7.82 (d, J=8.3, 2H), 8.0 (d, J=8.3, 2H), 9.43 (s, 1H), 12.90 (br, 1H). ^{13}C NMR(DMSO-d_6, 200 MHz) δ: 28.1, 37.1, 43.2, 44.1, 45.2, 82.7, 118.8, 122.1, 126.1, 127.6, 129.6, 130.2, 133.6, 134.3, 157.0, 158.9, 167.2.

4-[3-(4-Methoxy-3-tricyclo[3.3.1.1^{0,0}]dec-1-yl-phenyl)-isoxazol-5-yl]-benzoic Acid (27). Yield 98%; mp 230 °C (dec). ^{1}H NMR(DMSO-d_6, 200 MHz) δ: 1.75 (s, 6H), 2.09 (s, 9H), 3.87 (s, 3H), 7.14 (d, J=8.4, 1H), 7.70-7.77 (m, 3H), 8.02-8.09 (m, 4H), 13.15 (br, 1H). ^{13}C NMR(DMSO-d_6, 200 MHz) δ: 28.1, 37.1, 43.1, 43.8, 55.1, 95.1, 115.8, 126.3, 129.8, 130.5, 132.3, 132.7, 133.9, 158.5, 160.7, 163.5, 167.2.

4-[5-(4-Methoxy-3-tricyclo[3.3.1.1^{0,0}]dec-1-yl-phenyl)-isoxazol-3-yl]-benzoic Acid (32). Yield 95%; mp 230 °C (dec). ^{1}H NMR(DMSO-d_6, 200 MHz) δ: 1.76 (s, 6H), 2.09 (s, 9H), 3.88 (s, 3H), 7.16 (d, J=8.8, 1H), 7.62 (s, 1H), 7.68 (d, J=1.8,

118

1H), 7.76 (d, *J*=8.8, *J*=1.8, 1H), 8.03-8.10 (m, 4H), 13.15 (br, 1H). ^{13}C NMR(DMSO-d_6, 200 MHz) δ: 28.1, 35.7, 37.1, 43.1, 55.1, 95.1, 116.4, 128.9, 129.0, 129.5, 130.2, 129., 133.3, 133.9, 157.5, 160.7, 164.9, 167.2.

4-[3-(4-Hydroxy-3-tricyclo[3.3.1.10,0]dec-1-yl-phenyl)-isoxazol-5-yl]-benzoic Acid (28). Yield 95%; mp 251-253 °C (dec). ^{1}H NMR(DMSO-d_6, 200 MHz) δ: 1.75 (s, 6H), 2.10 (s, 9H), 6.91 (d, *J*=8.1, 1H), 7.57-7.70 (m, 3H), 8.01-8.12 (m, 4H), 9.88 (s, 1H), 13.25 (br, 1H). ^{13}C NMR(DMSO-d_6, 200 MHz) δ: 28.1, 37.1, 43.1, 44.1, 95.1, 117.1, 128.4, 129.8, 130.5, 132.3, 134.1, 135.0, 158.5, 162.4, 163.5, 167.2.

4-[5-(4-Hydroxy-3-tricyclo[3.3.1.10,0]dec-1-yl-phenyl)-isoxazol-3-yl]-benzoic Acid (33). Yield 95%; mp 241 °C (dec). ^{1}H NMR(DMSO-d_6, 200 MHz) δ: 1.75 (s, 6H), 2.06 (s, 9H), 6.93 (d, *J*=8.1, 1H), 7.51 (s, 1H), 7.59 (d, *J*=8.4, 2H), 8.04-8.09 (m, 4H), 10.06 (s, 1H), 13.20 (br, 1H). ^{13}C NMR(DMSO-d_6, 200 MHz) δ: 28.1, 36.0, 37.1, 43.1, 95.1, 116.9, 127.6, 128.6, 129.5, 130.2, 130.5, 132.1, 133.9, 157.5, 161.1, 164.9, 167.2.

4-[5-(4-Nitro-phenyl)-isoxazol-3-yl]-2-tricyclo[3.3.1.10,0]dec-1-ylphenol (29). Yield 85%; mp 246-248 °C. ^{1}H NMR(DMSO-d_6, 200 MHz) δ: 1.80 (s, 6H), 2.16 (s, 9H), 6.82 (d, *J*) 8.0, 1H), 6.95 (s, 1H), 7.56 (dd, *J*) 8.0, *J*) 2.0, 1H), 7.72 (d, *J*) 2.0, 1H), 8.01 (d, *J*) 9.2, 2H), 8.34 (d, *J*) 9.2, 2H). ^{13}C NMR(DMSO-d_6, 200 MHz) δ: 20.7, 29.0, 29.8, 37.1, 38.0, 40.2, 40.5, 46.9, 100.1, 110.3, 117.4, 120.8, 124.5, 125.6, 126.1, 126.6, 133.1, 156.7, 167.5.

4-[3-(4-Nitro-phenyl)-isoxazol-5-yl]-2-tricyclo[3.3.1.10,0]dec-1-ylphenol (34). Yield 84%; mp 250-253 °C. ^{1}H NMR(DMSO-d_6, 200 MHz) δ: 1.81 (s, 6H), 2.13-2.16 (m, 9H), 6.76 (s, 1H), 6.77 (d, *J*=8.4, 1H), 7.57 (dd, *J*=8.4, *J*=2.0, 1H), 7.70 (d, *J*=2.0, 1H), 8.03-8.07 (m, 2H), 8.32-8.37 (m, 2H). ^{13}C NMR(DMSO-d_6, 200 MHz) δ: 28.1, 36.0, 37.1, 43.1, 95.1, 116.8, 126.6, 126.9, 128.6, 130.5, 132.0, 148.1, 157.5, 161.2, 164.9.

General Procedure for Reduction of Nitro Compounds. To a solution of nitro compound 29 or 34 (1 mmol, 415 mg) in acetic acid (15 mL) is added Zn powder (100 mmol, 6.5 g). The suspension is stirred for 2 h at room temperature. The reaction mixture is filtered over Celite and concentrated. The crude material is dissolved in ethyl acetate (15 mL) and washed with sodium bicarbonate 5% (5 mL), brine (5 mL), dried (Na2SO4), and concentrated to afford the crude amino compound which is chromatographed on silica gel.

4-[5-(4-Amino-phenyl)-isoxazol-3-yl]-2-tricyclo[3.3.1.10,0]dec-1-yl-phenol, Hydrochloride (30). Yield 72%; mp 189-191 °C. ^{1}H NMR(DMSO-d_6, 200 MHz) δ: 1.83 (s, 6H), 2.07 (s, 3H), 2.20 (s, 6H), 6.83 (d, J) 8.2, 1H), 7.25 (s, 1H), 7.50-7.56 (m, 3H), 7.68 (d, J) 2.2, 2H), 8.04 (d. J) 8.6, 2H). ^{13}C NMR (CD$_3$OD, 200 MHz) δ: 30.6, 38.0, 38.2, 41.4, 53.6, 99.3, 117.7, 120.7, 123.7, 126.4, 126.6, 128.0, 138.2, 159.9, 165.2, 170.0.

4-[3-(4-Amino-phenyl)-isoxazol-5-yl]-2-tricyclo[3.3.1.10,0]dec-1-yl-phenol, Hydrochloride (35). Yield 80%; mp 149-152 °C. ^{1}H NMR (CD3OD, 200 MHz) δ: 1.83 (s, 6H), 2.08 (s, 3H), 2.20 (s, 6H), 6.84 (d, J) 8.4, 1H), 7.01 (s, 1H), 7.48-7.66 (m, 4H), 8.05 (d, J) 8.6, 2H). ^{13}C NMR (CD$_3$OD, 200 MHz) δ: 29.4, 36.9, 37.0, 40.1, 95.3, 116.6, 118.5, 123.3, 124.5, 124.6, 128.4, 128.8, 128.9, 130.0, 131.8, 132.0, 132.6, 133.1, 137.2, 159.0, 172.3.

Cell Culture and Culture Conditions. HL60 cells were obtained from the American Type Culture Collection (Rockville, MD). Cells were grown in RPMI 1640 (Gibco Grand Island, NY) containing 10% FCS (Gibco), 100 U/mL penicillin (Gibco), 100 mg/mL streptomycin (Gibco), and 2 mM L-glutamine (Sigma Chemical Co., St. Louis, MO) in a 5% CO_2 atmosphere at 37 °C. The employed serum-free medium is constituted by RPMI 1640 and ITS+1 liquid media supplement (Sigma). ITS+1 liquid media supplement contains 0.5% delipidated bovine serum albumin, 10 g/mL insulin, 5.5 g/mL transferrin, 4.7 g/mL linoleic acid, and 2 mM L-glutamine (Sigma).

Cytotoxicity Assays. To evaluate the number of live and dead cells, cells were stained with trypan blue and counted on a hemocytometer. Cells that showed trypan blue uptake were interpreted as nonviable.

Morphological Evaluation of Apoptosis and Necrosis. Drugs effects on apoptosis and necrosis were determined morphologically by fluorescence microscopy after labeling with acridine orange and ethidium bromide. Cells (2×10^5) were centrifuged ($300g$), and the pellet was resuspended in 25 L of the dye mixture. An amount of 10 μL of the mixture was placed on a microscope slide, covered with a 22 mm^2 coverslip, and examined in oil immersion with a 100× objective using a fluorescence microscope. Live cells were determined by the uptake of acridine orange (green fluorescence) and exclusion of ethidium bromide (red fluorescence) stain. Live and dead apoptotic cells were identified by perinuclear condensation of chromatin stained by acridine orange or ethidium bromide, respectively, and by the formation of apoptotic bodies. Necrotic cells were identified by uniform labeling with ethidium bromide.

Determination of Apoptosis by Annexine V. Cells (1 × 106) were washed with PBS and centrifugated at 200g for 5 min. The cell pellet was suspended in 100 μL of staining solution containing annexine-V-fluorescein labeling reagent (Annexine-V-Fluos Staining Kit, Roche Molecular Biochemicals, Mannheim, Germany) and incubated for 15 min at 20 °C. Annexine V positive cells were evaluated by fluorescence microscopy and flow cytometry.

Flow Cytometric Analysis of Cell Cycle Distribution. The effects of the most active compounds of the series on cell cycle distribution were studied on K562 cells (myeloblastic leukemia) by flow cytometric analysis after staining with propidium iodide. Cells were exposed 24 h to each compound. After treatment cells were washed once in ice-cold phosphate buffered saline medium (PBS, Sigma) and resuspended at 1 × 106 mL in a hypotonic fluorochrome solution containing propidium iodide (Sigma, St Louis, MO) 50 μg/mL in 0.1% sodium citrate plus 0.03% (v/v) nonidet P-40 (Sigma). After 30 min of incubation, the fluorescence of each sample was analyzed as single-parameter frequency histograms by using a FACScan flow cytometer (Becton Dickinson, San Jose, CA). The distribution of cells in the cell cycle was analyzed with the ModFit LT3 program (Verity Software House, Inc.).

2.7. References

1. Kundu, J.K., Surh, Y.-J. *Mutat. Res.* **2004**, *555*, 65–80. Baur, J.A., Sinclair, D.A. *Nat. Rev. Drug Discov.* **2006**, *5*, 493–506.

2. Jang, M., Cai, L., Udeani, G.O., Slowing, K.V., Thomas, C.F., Beecher, C.W., Fong, H.H., Farnsworth, N.R.., Kinghorn, A.D., Mehta, R.G., Moon, R.C., Pezzuto, J.M. *Science,* 1997, *275,* 218–220.

3. Kundu, J.K., Surh, Y.-J. *Mutat. Res*., **2004**, *555*, 65–80.

4. Garvin, S., Ollinger, K., Dabrosin, C., *Cancer Lett.* **2006,** *231*, 113–122. Zhou, H.B., Chen, J.J., Wang, W.X., Cai, J.T., Du, Q. *World J.Gastroenterol.* **2005**, 11, 280–284.

5. Chen, Z.H., Hurh, Y.J., Na, H.K., Kim, J.H., Chun, Y.J., Kim, D.H., Kang, K.S., Cho, M.H., Surh, Y.J. *Carcinogenesis.* **2004,** *25*, 2005–2013.

6. Ciolino, H.P., Yeh, G.C. *Mol. Pharmacol.* **1999**, *56*, 760–767.

7. Wang, Y., Lee, K.W., Chan, F.L., Chen, S., Leung, L.K. *Toxicol. Sci.* **2006,** *92*, 71–77.

8. Chen, C.Y., Jang, J.H., Li, M.H., Surh, Y.J. *Biochem.Biophys.Res.Commun.* **2005,** *331*, 993–1000. Hebbar, V., Shen, G., Hu, R., Kim, B.R., Chen, C., Korytko, P.J., Crowell, J.A., Levine, B.S., Kong, A.N. *Life Sci.* **2005,** 76, 2299–2314. Juan, S.H., Cheng, T.H., Lin, H.C., Chu, Y.L., Lee, W.S. *Biochem. Pharmacol.* **2005**, *69*, 41–48.

9. Kode, A., Rajendrasozhan, S., Caito, S., Yang, S.R., Megson, I.L., Rahman, I. *Am.J.Physiol.LungCellMol.Physiol.* **2008**, *294*, L478–L488.

10. Perwez Hussain, S., Harris, C.C. *Int. J. Cancer.* **2007**, *121*, 2373–2380.

11. Martinez, J., Moreno, J.J. *Biochem.Pharmacol.* **2000,** *59*, 865–870. Murakami, A., Matsumoto, K., Koshimizu, K., Ohigashi, H. *Cancer Lett.* **2003**, *195*, 17–25. Kundu, J.K., Shin, Y.K., Kim, S.H., Surh, Y.-J. *Carcinogenesis* **2006,** *27*, 1465–1474.

12. Fontecave, M., Lepoivre, M., Elleingand, E., Gerez, C., Guittet, O. *FEBS Lett.* **1998**, *421*, 277–279. Gusman, J., Malonne, H., Atassi, G. *Carcinogenesis* **2001**, *22*, 1111–1117.

13. Clement, M.V., Hirpara, J.L., Chawdhury, S.H., Pervaiz, S. *Blood* **1998**, *92*, 996–1002.

14. Gledhill, J.R., Montgomery, M.G., Leslie, A.G., Walker, J.E. *Proc.Natl.Acad.Sci.* **2007,** *104*, 13632–13637.

15. Heiss, E.H., Schilder, Y.D., Dirsch, V.M. *J.Biol.Chem.* **2007**, *282*, 26759–26766.

16. Cao, Z., Fang, J., Xia, C., Shi, X., Jiang, B.H. *Clin.CancerRes.* **2004,** 10, 5253–5263

17. Miura, D., Miura, Y., Yagasaki, K. *Clin. Exp. Metastasis,* **2004,** *21*, 445–451. Azios, N.G., Dharmawardhane, S.F. *Neoplasia* **2005**, *7*, 128–140.

18. Nabekura, T., Kamiyama, S., Kitagawa, S. *Biochem.Biophys.Res. Commun.* **2005**, *327*, 866–870.

19. Hinnen1, P. Eskens, F. *Brit.J.Cancer* **2007**, *96*, 1159 – 1165.

20. Yang, J.C., Haworth, L., Sherry, R.M., Hwu, P., Schwartzentruber, D.J., Topalian, S.L., Steinberg, S.M., Chen, H.X., Rosenberg, S.A. *N.Engl.J. Med.* **2003**, *349*, 427 –434.

21. Denekamp, J. *Br.J.Cancer* **1982,** *45*, 136–139.

22. Vincent, L., Kermani, P., Young, L.M., Cheng, J., Zhang, F., Shido, K., Lam, G., Bompais-Vincent, H., Zhu, Z., Hicklin, D.J., Bohlen, P., Chaplin, D.J., May, C., Rafii, S. *J.Clin.Investigation.* **2005,** *115*, 2992–3006.

23. McGown, A.T., Fox, B.W. *AntiCancer.Drud.Des.* **1989**, *3*, 249–254.

24. Chaplin, D.J., Dougherty, G.J. *Br.J.Cancer.* **1999**, *80(Suppl 1)*, 57–64.

25. Roberti, M., Pizzirani, D., Simoni, D., Rondanin, R., Baruchello, R., Bonora, C., Buscemi, F., Grimaudo, S., Tolomeo, M. *J.Med.Chem.* **2003,** *46,* 3546-3554.

26. Tolomeo, M., Grimaudo, S., Di Cristina, A., Roberti, M., Pizzirani, D., Meli, M., Dusonchet, L., Gebbia, N., Abbadessa,V., Crosta, L., Baruchello, R., Grisolia, G., Invidiata, G.P., Simoni, D. *Int.J.Biochem.Cell Biol.* **2005**, *37*, 1709.

27. Nam, N.H. *Curr.Med.Chem.* **2003**, *10*, 1697. Gaukroger, K., Hadfield, J. A., Lawrence, N. J., Nolan, S., McGown, A.T. *Org.Biomol.Chem.* **2003**, *1*, 3033.

28. Cushman, M., Nagarathnam, D., Gopal, D., He, H. M., Lin, C.M., Hamel, E. *J.Med.Chem.* **1992**, *35*, 2293.

29. Cao, T.M. et al. *Am.J.Hematol.* **2008,** *83(5)*, 390–397.

30. Tozer, G.M. et al. *Cancer Res.* **1999,** *59(7)*, 1626–1634. Malcontenti-Wilson, C. et al. *Clin.Cancer.Res* **2001**, *7(4),* 1052–1060.

31. Durrant, D. et al. *Cancer Chemother.Pharmacol* **2008. DOI 10.1007/s00280-008-0726-6**

32. Simoni, D., Giannini, G., Roberti, M., Rondanin, R., Baruchello, R., Rossi, M., Grisolia, G., Invidiata, F. P., Aiello, S., Marino, S., Cavallini, S., Siniscalchi, A., Gebbia, N., Crosta, L., Grimaudo, S., Abbadessa, V., Di Cristina, A., Tolomeo, M. *J.Med.Chem.* **2005,** *48*, 4293-4299.

33. Charpentier, B., Bernardon, J. M., Eustache, J., Millois, C., Martin, B., Michel, S., Shroot, B. *J.Med.Chem.* **1995**, *38*, 4993–5006.

34. Cincinelli, R., Dallavalle, S., Nannei, R., Carella, S., De Zani, D., Merlini, L., Penco, S., Garattini, E., Giannini, G., Pisano, C., Vesci, L., Carminati, P., Zuco, V., Zanchi, C., Zunino, F. *J.Med.Chem.* **2005**, *48*, 4931–4946. Dawson, M. I., Xia, Z., Liu, G., Fontana, J. A., Farhana, L., Patel, B. B., Arumugarajah, S., Bhuiyan, M., Zhang, X.-K., Han, Y.-H., Stallcup, W. B., Fukushi, J., I Mustelin, T., Tautz, L., Su, Y., Harris, D. L., Waleh, N., Hobbs, P. D., Jong, L., Chao, W., Schiff, L. J.; Sani, B. P. *J. Med. Chem.* **2007**, *50*, 2622–2639.

35. Garattini, E., Parrella, E., Diomede, L., Gianni, M., Kalac, Y., Merlini, L., Simoni, D., Zanier, R., Fosca Ferrara, F., Chiarucci, I., Carminati, P., Terao, M., Pisano, C. *Blood,* **2004**, *103*, 194–207.

36. Larsen, K. E., Torssell, K. B. G. *Tetrahedron,* **1984**, *40*, 2985–2988.